

PHYTOALEXIN AND BIOMARKER PEPTIDE DETECTION USING MASS
SPECTROMETRY



A Dissertation Submitted in Partial Fulfillment of the Requirements
for the Degree of Doctor of Philosophy in Biotechnology

Common Course

FACULTY OF SCIENCE

Chulalongkorn University

Academic Year 2020

Copyright of Chulalongkorn University

การตรวจหาสารไฟโตเอเล็กซินและสารเปปไทด์บ่งชี้ทางชีวภาพโดยใช้แมสสเปกโตรเมตรี



วิทยานิพนธ์นี้เป็นส่วนหนึ่งของการศึกษาตามหลักสูตรปริญญาวิทยาศาสตรดุษฎีบัณฑิต

สาขาวิชาเทคโนโลยีชีวภาพ ไม่สังกัดภาควิชา/เทียบเท่า

คณะวิทยาศาสตร์ จุฬาลงกรณ์มหาวิทยาลัย

ปีการศึกษา 2563

ลิขสิทธิ์ของจุฬาลงกรณ์มหาวิทยาลัย

Thesis Title	PHYTOALEXIN AND BIOMARKER PEPTIDE DETECTION USING MASS SPECTROMETRY
By	Miss Sasikarn Komkleow
Field of Study	Biotechnology
Thesis Advisor	Professor Dr. POLKIT SANGVANICH
Thesis Co Advisor	Dr. Chantragan Phiphobmongkol

Accepted by the FACULTY OF SCIENCE, Chulalongkorn University in Partial Fulfillment
of the Requirement for the Doctor of Philosophy

----- Dean of the FACULTY OF SCIENCE
(Professor Dr. POLKIT SANGVANICH)

DISSERTATION COMMITTEE

----- Chairman
(Dr. SUPAWIN WATCHARAMUL)

----- Thesis Advisor
(Professor Dr. POLKIT SANGVANICH)

----- Thesis Co-Advisor
(Dr. Chantragan Phiphobmongkol)

----- Examiner
(Associate Professor Dr. SUCHADA CHANPRATEEP
NAPATHORN)

----- Examiner
(Associate Professor Dr. SEHANAT PRASONGSUK)

----- External Examiner
(Emeritus Professor Dr. Prakitsin Sihanonth)

ศศิกานต์ กลมเกลียว : การตรวจหาสารไฟโตเอเล็กซินและสารเปปไทด์บ่งชี้ทางชีวภาพโดยใช้แมสสเปกโตรเมตรี. (PHYTOALEXIN AND BIOMARKER PEPTIDE DETECTION USING MASS SPECTROMETRY) อ.ที่ปรึกษาหลัก : ศ. ดร.พลกฤษณ์ แสงวณิช, อ.ที่ปรึกษาร่วม : ดร.จันทรกานต์ พิภพมงคล

แมสสเปกโตรเมตรี (MS) เป็นหนึ่งในเทคนิคทางวิทยาศาสตร์ที่ถูกใช้อย่างกว้างขวางในหลายสาขาวิชา งานวิจัยนี้มีวัตถุประสงค์เพื่อศึกษาบทบาทของเทคนิคแมสสเปกโตรเมตรีในการวิเคราะห์ทางชีววิทยา โดยเนื้อหาในงานวิจัยแบ่งออกเป็น 2 ส่วนหลัก ส่วนที่หนึ่งมีการใช้เทคนิคแมสสเปกโตรเมตรีอิมเมจจิง เพื่อศึกษาสารเมตาบอไลต์โดยตรงจากเนื้อเยื่อพืช โดยนำพันธุ์ข้าวไทยมาศึกษาการผลิตและการกระจายตัวของสารไดเทอร์พินอยด์ไฟโตเอเล็กซินด้วยเทคนิคแมลดี-แมสสเปกโตรเมตรีอิมเมจจิง (MALDI-MSI) การศึกษานี้ประสบความสำเร็จโดยสามารถตรวจพบสารไดเทอร์พินอยด์ไฟโตเอเล็กซินในเนื้อเยื่อของใบข้าวพันธุ์ กข6 จำนวน 5 ชนิด คือ momilactone-A (m/z 353.17), momilactone-B (m/z 369.16), phytocassane-A/D/E (m/z 355.18), phytocassane-B (m/z 373.19) และ phytocassane-C (m/z 357.20) ส่วนที่สองของงานวิจัยใช้เทคนิคแมสสเปกโตรเมตรี เพื่อศึกษาผลของการใช้นิโคตินเป็นเวลานานต่อความสามารถในการรุกรานของเซลล์มะเร็งปอด A549 ด้วยเทคนิค label-free quantitative proteomic การศึกษาการเปลี่ยนแปลงการแสดงออกของโปรตีนทำใน 2 ระบบคือ ระบบ monolayer และ ระบบ invasion ผลการทดลองพบว่าเมื่อเซลล์มะเร็งถูกเลี้ยงในนิโคตินเป็นเวลานาน จะเกิดการเปลี่ยนแปลงการแสดงออกของโปรตีนต่าง ๆ โดยพบการเปลี่ยนแปลงในระบบ monolayer จำนวน 55 โปรตีน และในระบบ invasion จำนวน 100 โปรตีน จากนั้นเลือกโปรตีนที่สนใจมาตรวจสอบการแสดงออกของโปรตีนอีกครั้งด้วยเทคนิค western blot ผลการทดลองชี้ให้เห็นว่าการใช้นิโคตินเป็นเวลานาน ส่งเสริมให้เกิดการรุกรานของเซลล์ A549 ที่น่าสนใจคือพบการแสดงออกเพิ่มขึ้นของโปรตีน legumain, heat shock protein HSP 90-alpha, heat shock related 70 kDa protein 2, protein disulfide isomerase A3 และ profilin-1 อันเป็นผลมาจากการใช้นิโคตินเป็นเวลานาน งานวิจัยนี้แสดงให้เห็นถึงบทบาทของเทคนิคแมสสเปกโตรเมตรีในการใช้ตรวจวิเคราะห์สารชีวโมเลกุล และชี้ให้เห็นว่าเทคนิคนี้สามารถนำไปสู่การค้นพบข้อมูลใหม่ ๆ ในอนาคต

สาขาวิชา เทคโนโลยีชีวภาพ
ปีการศึกษา 2563

ลายมือชื่อนิสิต
ลายมือชื่อ อ.ที่ปรึกษาหลัก
ลายมือชื่อ อ.ที่ปรึกษาร่วม

5872826023 : MAJOR BIOTECHNOLOGY

KEYWORD: mass spectrometry, MALDI-MSI, phytoalexins, nicotine, lung cancer, label-free quantitative proteomic

Sasikarn Komkleow : PHYTOALEXIN AND BIOMARKER PEPTIDE DETECTION USING MASS SPECTROMETRY . Advisor: Prof. Dr. POLKIT SANGVANICH Co-advisor: Dr. Chantragan Phiphobmongkol

Mass spectrometry (MS) has been one of the scientific techniques most commonly used in different areas. Therefore, the current research was carried out in order to investigate the role of MS in biological analysis. This study is divided into two main parts. The first part used MS imaging to reveal the ability of the technique for imaging metabolites directly from plant tissue. Thai rice varieties were used to investigate the production and distribution of diterpenoid phytoalexins using matrix-assisted laser desorption/ionization mass spectrometry imaging (MALDI-MSI). Results revealed the successful detection of 5 types of diterpenoid phytoalexins on RD6 rice leaf tissue, including momilactone-A (m/z 353.17), momilactone-B (m/z 369.16), phytocassane-A/D/E (m/z 355.18), phytocassane-B (m/z 373.19) and phytocassane-C (m/z 357.20). In the second part, MS technique was used to assess the consequence of prolonged nicotine treatment on the invasion of A549 non-small cell lung cancer cell line by label-free quantitative proteomic analysis. Proteins were collected from both the monolayer and the invasion systems to investigate the alteration in protein expression. Fifty five proteins from the monolayer system and 100 proteins from the invasion system were identified with a change in expression level after prolonged nicotine treatment. Western blotting was then employed to validate the candidate proteins. The results indicated that prolonged exposure of nicotine promoted invasion on A549 cells. Interestingly, legumain, heat shock protein HSP 90-alpha, heat shock related 70 kDa protein 2, protein disulfide isomerase A3 and profilin-1 were found to show higher expression in A549 cells after prolonged exposure to nicotine. These findings testify to the power of mass spectrometry in biological molecule detection, allowing the discovery of novel information in the future.

Field of Study: Biotechnology

Student's Signature

Academic Year: 2020

Advisor's Signature

Co-advisor's Signature

ACKNOWLEDGEMENTS

It would not have been possible to write this thesis without the help and support of the kind people around me. First of all, I wish to express my greatest appreciation towards my advisor Professor Dr. Polkit Sangvanich and my co-advisor Dr. Chantragan Srisomsap for the continuous support of my Ph.D study and research, for their patience, motivation and immense knowledge.

This work cannot be completed without kindness and helps of many people. It is a pleasure to thank Dr. Ploypat Niyomploy, Miss Daranee Chokchaichamnankit and Mrs. Papada Chaisuriya for their valuable suggestions. The thank also expressed to Program in Biotechnology, Faculty of Science, Chulalongkorn University and the Laboratory of Biochemistry, Chulabhorn Research Institute for providing facilities in my work.

I wish to acknowledge the Scholarship from the Graduate School, The 100th Anniversary Chulalongkorn University Fund for Doctoral Scholarship and The 90th Anniversary of Chulalongkorn University Fund (Ratchadaphiseksomphot Endowment Fund) for financial support.

Finally, the greatest gratitude is expressed to my parents, my sister, my boyfriend (Mr. Joonho Kim) and my best friend (Miss Saowanee Wongsawad) for providing me with unfailing support and continuous encouragement throughout my years of study.



Sasikarn Komkleow

TABLE OF CONTENTS

	Page
ABSTRACT (THAI)	iii
ABSTRACT (ENGLISH).....	iv
ACKNOWLEDGEMENTS	v
TABLE OF CONTENTS.....	vi
LIST OF TABLES	ix
LIST OF FIGURES	x
LIST OF ABBREVIATIONS.....	xiii
CHAPTER 1 INTRODUCTION	1
CHAPTER 2 LITERATURE REVIEWS	2
2.1 Principle and basic components of mass spectrometer.....	2
2.1.1 Ion source	2
2.1.2 Mass analyzer	5
2.2 Mass spectrometry imaging (MSI)	7
2.3 Applications of mass spectrometry for biological research.....	13
2.4 Background of the study for the first part of thesis (Chapter 3: MALDI-mass spectrometry imaging for phytoalexins detection in Thai rice).....	16
2.4.1 Importance of rice and blast disease.....	16
2.4.2 Phytoalexins: role in disease resistance in rice plants	18
2.5 Background of the study for the second part of thesis (Chapter 4: Global analysis of protein expression of A549 cells after prolonged nicotine exposure by using label-free quantification).....	19
2.5.1 Lung cancer	19
2.5.2 Nicotine	22
2.5.3 Metastasis	24
CHAPTER 3 MALDI-Mass Spectrometry Imaging for Phytoalexins Detection in Thai Rice	27

3.1 Materials and Chemicals.....	29
3.2 Equipments	29
3.3 Methods	30
3.3.1 Plant materials	30
3.3.2 Blast fungus optimizing medium	30
3.3.3 Blast fungus cultivation.....	31
3.3.4 Blast fungus inoculation.....	31
3.3.5 Analysis of phytoalexins on rice leaf tissues by MALDI-MSI	31
3.3.6 Analysis of phytoalexins in rice leaves by liquid extraction.....	32
3.4 Results.....	33
3.4.1 Optimization of medium for spore production of blast fungus	33
3.4.2 Observation of rice leaves infection by blast fungus at 7 days post- infection.....	36
3.4.3 Determination of phytoalexin production and distribution on a fractured rice leaf by MALDI-MSI	37
3.4.4 Structural analysis of phytoalexins by tandem mass spectrometry	42
3.5 Discussion.....	45
CHAPTER 4 Global Analysis of Protein Expression of A549 Cells after Prolonged Nicotine Exposure by using Label-Free Quantification	48
4.1 Materials and Chemicals.....	50
4.2 Equipments	51
4.3 Methods	53
4.3.1 Cell culture	53
4.3.2 Cytotoxicity assay	53
4.3.3 Cell invasion assay	53
4.3.4 Prolonged nicotine exposure of A549 cells.....	54
4.3.5 Prolonged nicotine exposure on motile A549 cells.....	54
4.3.6 Protein preparation for label free proteomic analysis	55
4.3.7 Label free LC-MS/MS analysis.....	55
4.3.9 Bioinformatics	57

4.3.10 Statistical analysis	57
4.4 Results.....	57
4.4.1 Cytotoxic effect of nicotine on A549 lung cancer cells	57
4.4.2 Nicotine induces invasion of A549 lung cancer cells	58
4.4.3 Prolonged nicotine exposure enhances the invasive capability of A549 lung cancer cells	59
4.4.4 Label free quantitative proteomic analysis of untreated and nicotine treated A549 cells	61
4.4.5 Functional and interaction analysis	70
4.4.6 Validation of differential protein expression in untreated and nicotine treated A549 cells using western blot analysis.....	71
4.4.7 Label free quantitative proteomic analysis of untreated and nicotine treated A549 cells in invasion system	72
4.4.8 Validation of the identified proteins from LC-MS/MS from invasion system.....	85
4.5 Discussion.....	86
CHAPTER 5 CONCLUSIONS	93
REFERENCES	95
APPENDICES	112
APPENDIX A MALDI-MS Images of Infected RD6 Rice Leaf Section	113
APPENDIX B MALDI Mass Spectra of Rice Leaf Extract	115
APPENDIX C Fungal Media Compositions from Chapter 3	117
APPENDIX D Western Blot Analysis.....	120
APPENDIX E Recipes of All Reagents from Chapter 4	122
VITA.....	127

LIST OF TABLES

	Page
Table 2.1 List of ion sources used for MSI. Information about lateral resolutions, preparation steps required for MSI, sample considerations, and applications.....	12
Table 2.2 Summary the common applications of mass spectrometry in various study fields in biological research	13
Table 3.1 Growth of fungus after 14 days of culture on various media	34
Table 3.2 Observation of spore production of blast fungus on various media under microscope	35
Table 4.1 List of up-regulated proteins from the monolayer system.....	63
Table 4.2 List of down-regulated proteins from the monolayer system	67
Table 4.3 List of up-regulated proteins from the invasion system	74
Table 4.4 List of down-regulated proteins from the invasion system.....	77

LIST OF FIGURES

	Page
Figure 2.1 Components of mass spectrometers	2
Figure 2.2 MALDI ionization process	3
Figure 2.3 MALDI matrices	4
Figure 2.4 Schematic diagram of the electrospray ionization process.....	5
Figure 2.5 General representation for TOF analyzer	6
Figure 2.6 General representation for QIT analyzer	7
Figure 2.7 Number of publications per year from an ISI Web of Science search of the topic “mass spectrometry imaging”	8
Figure 2.8 Experimental workflow for the MSI analysis (modified from the image of Dong et al. (10)).....	9
Figure 2.9 Rice blast disease caused by Magnaporthe oryzae. (A) Lesion on the leaf. (B) Conidia of M. oryzae under light microscope. (C) Blast disease cycle (24).....	17
Figure 2.10 Diterpenoid phytoalexins in rice (34).....	19
Figure 2.11 Global cancer burden of new cases and deaths as reported by IARC in December 2020	21
Figure 2.12 The main types of lung cancer under microscope	21
Figure 2.13 Structure of nicotine or 3-(1-methyl-2-pyrrolidinyl) pyridine.	22
Figure 2.14 Overview key events in the metastatic cascade (71)	26
Figure 3.1 Steps of the modified fracturing method	33
Figure 3.2 Colony morphology of blast fungus on different media after 14 days of incubation.....	34
Figure 3.3 Infected rice leaves after 7 days of inoculation	36
Figure 3.4 Stereo microscope images of rice leaf surface. (A, B) Surface of leaf tissue before fracture. (C, D) Surface of leaf tissue after fracture.	38
Figure 3.5 SEM images of rice leaf surface. (A, B) Surface of leaf tissue before using a modified fracturing method. (C, D) Surface of leaf tissue after using a modified fracturing method.....	38

- Figure 3.6 MALDI-MS images of uninfected rice leaf section. (A) An optical image of the rice leaf. MALDI-MS images of (B) disaccharide, most likely, sucrose (m/z 381.21) and (C) MGDG (m/z 813.74). Both compounds were detected as potassiated ions ($[M + K]^+$).40
- Figure 3.7 MALDI-MS images of infected rice leaf section. (A) An optical image of the rice leaf with a black circle representing the infected area. MALDI-MS images of (B) momilactone-A (m/z 353.17), (C) phytocassane-A, D, or E (m/z 355.18), (D) phytocassane-C (m/z 357.20), (E) momilactone-B (m/z 369.16), and (F) phytocassane-B (m/z 373.19). All compounds were detected as potassiated ions ($[M + K]^+$). (G) MALDI mass spectrum of diterpenoid phytoalexins from infected rice leaf section.41
- Figure 3.8 MALDI mass spectra obtained from RD6 rice leaf extract. (A) Uninfected rice leaf extract. (B) Infected rice leaf extract. Both mass spectra are shown, highlighting the m/z values of interest. All compounds were detected as potassiated ions ($[M + K]^+$).43
- Figure 3.9 MALDI-MS/MS spectra obtained from rice leaf extract. (A) Momilactone-A. (B) Phytocassane-A/D/E. (C) Phytocassane-C. (D) Sucrose. The MS/MS spectra match the standard analysis of isolated diterpenes from rice leaves.44
- Figure 4.1 The cytotoxic effects of nicotine on A549 lung cancer cells by MTT assay. The results were expressed as mean \pm SD of three independent experiments.....58
- Figure 4.2 Nicotine induces invasion of A549 lung cancer cells. (A) Representative images of invasion assay from A549 cells treated with 0.1, 1.0, 5 and 10 nM of nicotine for 24 h. Scale bar, 200 μ m. (B) Bar graph represents the relative invasion of A549 cells after treated with various concentrations of nicotine. Data points represent the mean \pm SD. (* $P < 0.05$, *** $P < 0.001$, **** $P < 0.0001$).....59
- Figure 4.3 Experimental scheme of A549 cells continuous exposure to 5 nM nicotine. Samples were divided into 2 main groups, monolayer and invasion system. Each sample groups were subdivided into 2 conditions, control and nicotine treatment.60
- Figure 4.4 Prolonged nicotine exposure enhances the invasive capability of A549 lung cancer cells. Representative images of invasion assay from five sublines of A549 cells untreated (A) and treated (B) with 5 nM of nicotine. Scale bar, 200 μ m. Bar graphs represent the relative invasion of sublines with (D) and without (C) nicotine treatment. Data points represent the mean \pm SD. (* $P < 0.05$, ** $P < 0.01$).....61
- Figure 4.5 The differentially expressed proteins from the monolayer system were analyzed based on biological process.70

Figure 4.6 Nicotine induces differential protein expression in the A549 cells from monolayer culture (flask). The differentially expressed proteins were used to search the STRING database to predict their protein-protein interactions.	71
Figure 4.7 The expression levels of the dysregulated proteins from monolayer system were verified by western blot analysis. Western blot showing the expression of selected proteins in untreated and nicotine treated A549 cells.	72
Figure 4.8 The differentially expressed proteins from invasion system were analyzed based for biological process.	85
Figure 4.9 The expression levels of the dysregulated proteins from invasion system were verified by western blot analysis. Western blot showing the expression of selected proteins in untreated A549-L5 and nicotine treated A549-L5 cells.	86
Figure A.1 MALDI-MS images of infected RD6 rice leaf section (2nd repeated experiment). (A) momilactone-A (m/z 353.24), (B) phytocassane-A, D, or E (m/z 355.24), (C) phytocassane-C (m/z 357.25), (D) sucrose (m/z 381.23) All compounds were detected as potassiated ions ($[M + K]^+$). The overlapping images between phytoalexins and infected leaf sections have been included to highlight that the phytoalexins were found at the infected areas only. (E) overlapping image of momilactone-A, (F) overlapping image of phytocassane-A, D, or E, (G) overlapping image of phytocassane-C, (H) overlapping image of sucrose.	113
Figure A.2 MALDI-MS images of infected RD6 rice leaf section (3rd repeated experiment). (A) momilactone-A (m/z 353.41), (B) phytocassane-A, D, or E (m/z 355.41), (C) phytocassane-C (m/z 357.40), (D) momilactone-B (m/z 369.34), (E) phytocassane-B (m/z 373.33), (F) sucrose (m/z 381.35). All compounds were detected as potassiated ions ($[M + K]^+$).	114
Figure B.1 MALDI mass spectra obtained from uninfected rice leaf extract. (A) Uninfected rice leaf extract of RD31. (B) Uninfected rice leaf extract of RD41. (C) Uninfected rice leaf extract of RD57. (D) Uninfected rice leaf extract of Pathumthani1.	115
Figure B.2 MALDI mass spectra obtained from infected rice leaf extract. (A) Infected rice leaf extract of RD31. (B) Infected rice leaf extract of RD41. (C) Infected rice leaf extract of RD57. (D) Infected rice leaf extract of Pathumthani1.	116
Figure D.1 Western blot showing the expression of selected proteins in untreated and nicotine treated A549 cells. (2nd repeated experiment).	120
Figure D.2 Western blot showing the expression of selected proteins in untreated and nicotine treated A549 cells. (3rd repeated experiment).	121

LIST OF ABBREVIATIONS

%	percentage
°C	degree Celsius
µg	microgram
µl	microliter
µm	micrometer
µM	micromolar
µmol	micromole
cm	centimeter
Da	dalton
g	gram
h	hour
Hz	hertz
kg	kilogram
kV	kilovolt
l	liter
M	molar
min	minute
mg	milligram
ml	milliliter
mm	millimeter
mM	millimolar
m/z	mass-to-charge ratio
ng	nanogram
nm	nanometer
nM	nanomolar
ns	nanosecond
psi	pound per square inch

s second
w/v weight by volume



จุฬาลงกรณ์มหาวิทยาลัย
CHULALONGKORN UNIVERSITY

CHAPTER 1

INTRODUCTION

Mass spectrometry (MS) is one of the most widely used analytical techniques within multiple fields, such as food analysis, pharmaceutical, medical science, and plant science research. The first mass spectrometer was built in 1912 and it has developed to becoming an effective analytical tool for both quantitative and qualitative applications (1).

Mass spectrometry is based on the principle that the ions are produced from either inorganic or organic compounds using any suitable technique, their mass-to-charge ratios (m/z) were separated and detected by their respective m/z and abundance (2). This analysis could provide valuable data for the research, including structure, purity, and composition of analytes.

Due to a large number of MS applications to biology, the current investigations were therefore undertaken to examine the role of MS technique in biological analysis. This study is divided into two main parts. The first part (Chapter 3) used MS imaging to reveal the ability of the technique for imaging metabolites directly from plant tissue. Thai rice varieties were used to investigate the production and distribution of diterpenoid phytoalexins using MALDI-MSI. Results obtained from MALDI-MSI were also confirmed by liquid extraction analysis. In the second part (Chapter 4), MS technique was used to analyze multiple protein changes in human non-small cell lung cancer cell line A549 after prolonged nicotine treatment. After getting results of dysregulation proteins from label-free quantitative mass spectrometry analysis, the potential targeted proteins were chosen and validated by immunoblot.

CHAPTER 2

LITERATURE REVIEWS

2.1 Principle and basic components of mass spectrometer

A mass spectrometer consists of three main components: an ion source, a mass analyzer, and a detector (Fig. 2.1)

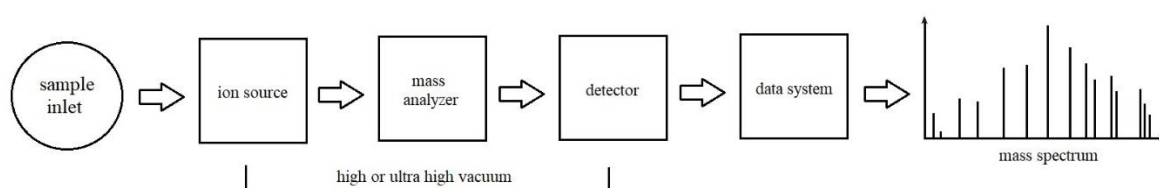


Figure 2.1 Components of mass spectrometers

The ion source is responsible for introducing molecules into the mass spectrometer and convert them to ionized form. After the ions are produced in the source, they are accelerated to the mass analyzer where they have been segregated by mass and charge under high vacuum conditions using electric and/or magnetic fields. Lastly, the ions are sent to an ion detector that generates an electrical current which is amplified and detected (1).

2.1.1 Ion source

Many methods of ionization are currently being used for example, electron ionization (EI), chemical ionization (CI), fast atom bombardment (FAB), liquid secondary ion mass spectrometry (LSIMS), matrix-assisted laser desorption ionization (MALDI), and electrospray ionization (ESI). However, this thesis will only mention about the last two ionization techniques which were used in the research.

Matrix-Assisted Laser Desorption Ionization (MALDI)

In MALDI, the analyte is dissolved in an appropriate solvent first and then mixed with an excess amount of matrix compound that absorbs at the laser

wavelength. It is subsequently spotted on a MALDI target plate and dried by air. The analyte is co-crystallized with the matrix in these conditions. The irradiated spot is rapidly heated and becomes vibrationally excited after a very brief laser pulse. The matrix molecules are energetically vaporized from the surface of the sample, capture the laser energy, and bring the analytical molecules into the gas phase as well. The analyte molecules are typically ionized by protonation or deprotonation with the adjacent matrix molecules during the ablation process. The most common format for MALDI ionization is to carry a single positive charge for analyzing molecule. Figure 2.2 illustrates the ionization process which are formed during MALDI-MS.

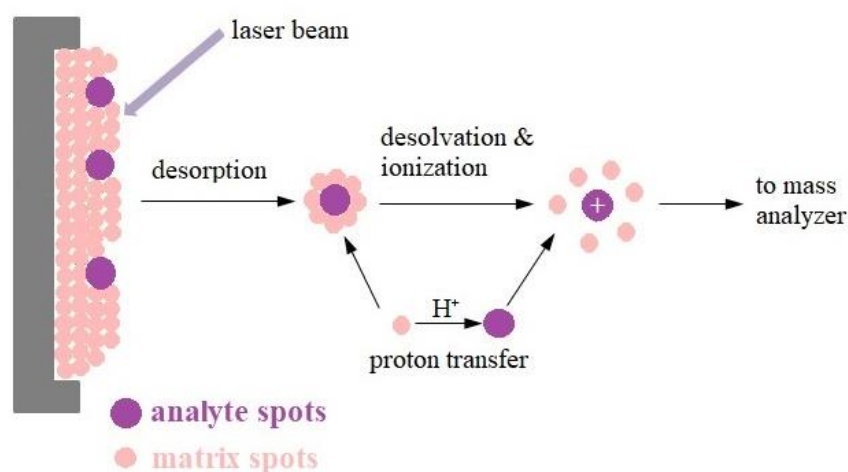


Figure 2.2 MALDI ionization process

At the beginning, MALDI was performed under vacuum. However, atmospheric pressure (AP) MALDI was established in 2000 (3). This establishment has lowered costs and made the operations simpler. The ion formation processes in MALDI are not yet fully understood and a matrix chosen is mostly experimental. However, choosing the correct matrix is crucial to the success in MALDI. Currently, the commonly used matrices consisting of nicotinic acid, 2,5-dihydroxybenzoic acid, sinapinic acid and α -cyano-4-hydroxycinnamic acid (Fig 2.3).

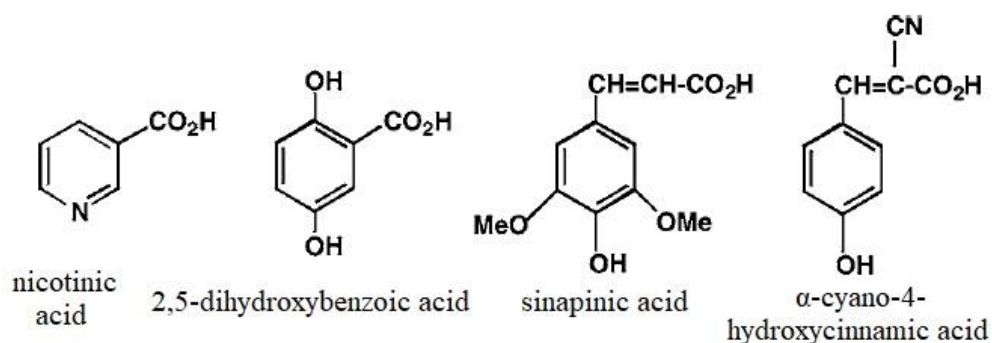


Figure 2.3 MALDI matrices

Electrospray Ionization-Mass Spectrometry (ESI-MS)

The first conception of ESI was introduced in the late 1960s by Malcolm Dole (4) and improved in the late 1980s with the experiments by John Fenn and coworkers. Currently, ESI-MS is being used to carry out a qualitative and quantitative analysis for complex biological structures as well as a broad range of nonvolatile and thermally labile simple inorganic chemicals (5).

Figure 2.4 demonstrates the ionization process which are formed during ESI-MS. In this technique, the sample should be dissolved in a polar solvent (e.g., methanol, acetonitrile, water, etc.) that can be injected into the ionization source through a thin needle under atmospheric pressure. When the sample is continuously sprayed, a high electrical potential is given to the needle which results in the formation of highly charged droplets. The droplets are then electrically driven and vaporized by a warm neutral gas. As the droplets evaporate, the size of the droplets decreases until it reaches the point (Rayleigh limit) where Coulombic repulsive forces between the ions on the surface droplets can overcome surface tension of the solvent, resulting in “Coulomb explosion” or “Coulomb fission”. This Coulomb fission process produces tiny offspring droplets from the parent droplet. The solvent evaporation process and Coulomb fission is repeatedly performed to produce smaller progeny droplets. Finally, naked charge analytes are formed which are passed through mass analyzer and detected (6).

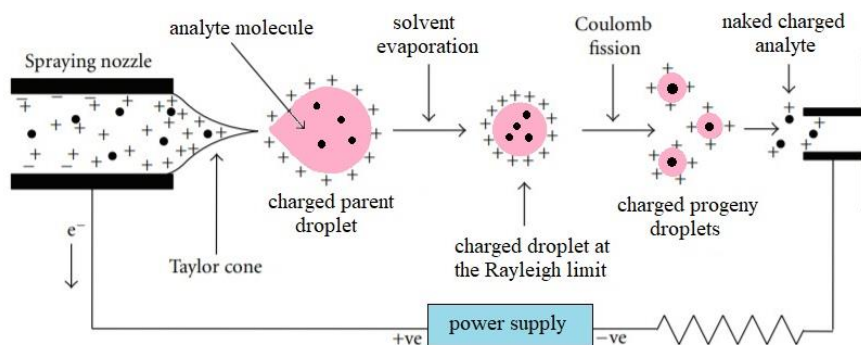


Figure 2.4 Schematic diagram of the electrospray ionization process

2.1.2 Mass analyzer

After the ions have been produced and introduced into a mass spectrometer, a mass analyzer separates ions based on their mass-to-charge ratio by applying electric and magnetic fields. There are several mass analyzers including time-of-flight (TOF), magnetic sector (B), quadrupole (Q), quadrupole ion trap (QIT), fourier transform-ion cyclotron resonance (FT-ICR), orbitrap, etc. However, this section will only mention about TOF and QIT.

Time-of-Flight (TOF) Analyzer

In 1946, the W. E. Stephens developed the first TOF analyzer (7). The principal of TOF is shown in Figure 2.5. As the name “time-of-flight”, TOF analyzer separate ions and measure their mass to charge ratio (m/z) from how long they take to travel from ionizer to detector. Typically, the flight tube is 1-2 m in length and neither the electric nor magnetic fields are the basis for separation. The ions are separated in the flight tube which is recognized as the field-free region before entering the detector. The lighter ions would arrive earlier than the heavier ions to the detector. The main advantages of TOF analyzer are the ability to detect unlimited the m/z range, a very high mass spectral acquisition rate, and high sensitivity (8).

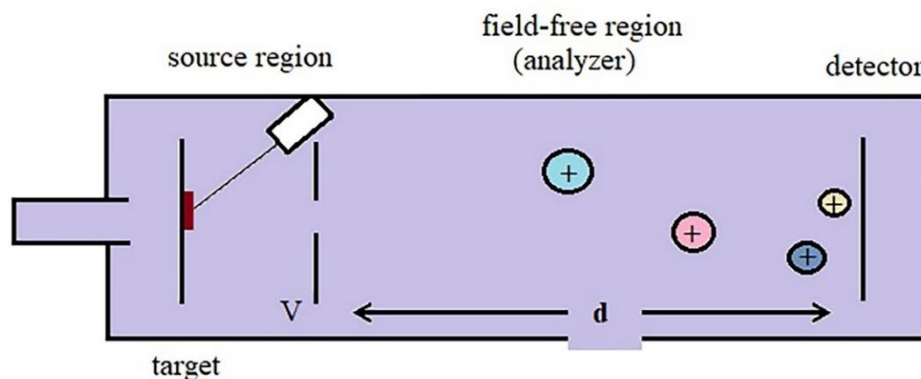


Figure 2.5 General representation for TOF analyzer

Quadrupole Ion Trap (QIT) Analyzer

Quadrupole ion trap (QIT) also known as ion trap (IT) is a mass analyzer which have similar operating principles to the standard quadrupole mass analyzer. It traps and store ions in an orbital motion within the ion trap and ejects ions for detection. QIT consists of three hyperbolic electrodes: donut-shaped ring electrode, an entrance endcap electrode, and the exit endcap electrode (Fig. 2.6). In this cavity of electrodes, the ions are trapped and analyzed. Each of the endcap electrodes have a hole which enables the ions to pass through, and the ring electrode is located in the middle of the two endcap electrodes. The QIT working concept is based on the creation of stable trajectories for ions of a certain m/z or m/z range while eliminating undesirable ions by letting them to collide with walls or by axial ejection from the trap as a result of their unstable trajectories (8).

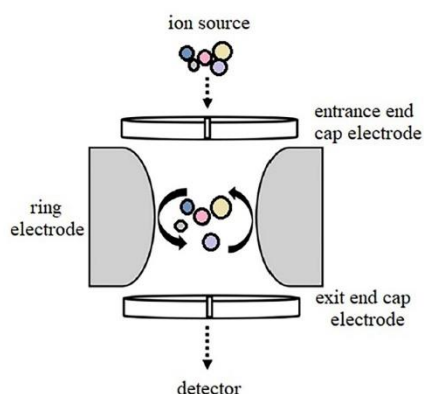


Figure 2.6 General representation for QIT analyzer

After the ions enter the quadrupole ion trap via the entrance endcap electrode, they are trapped in the cavity between electrodes by DC and AC electric fields. Different voltages are given to the electrodes to trap and eject ions depending on their m/z . The ring electrode RF potential generates a 3D quadrupolar trapping potential field in the trapping cell that traps ions in a stable oscillating trajectory. Trapping potential and the m/z values of the ions can decide the precise nature of the trajectory. To generate instability in the ion trajectories, the electrode system potentials are then changed, allowing the ions to be axially ejected in order of increasing the m/z value and focused by the exit lens before detection (9).

2.2 Mass spectrometry imaging (MSI)

In recent years, mass spectrometry imaging (MSI) has been recognized as an excellent tool for imaging diverse compounds in a variety of samples. It is a powerful technique that provides spatial distribution of analytes directly from tissue samples without any labeling or staining agents (10). The integration of data gained from mass spectrometry and visualization of spatial distributions in thin specimen sections allows this a useful technique for the study of biological samples. Figure 2.7 shows the number of publications during 2001-2020 from an ISI Web of Science search of the topics “mass

spectrometry imaging”. It shows that the published articles have gradually increased in the last 20 years.

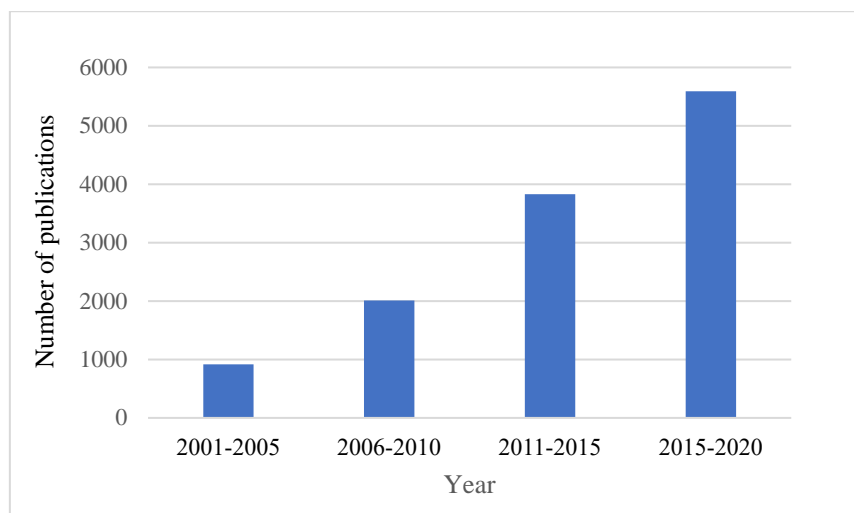
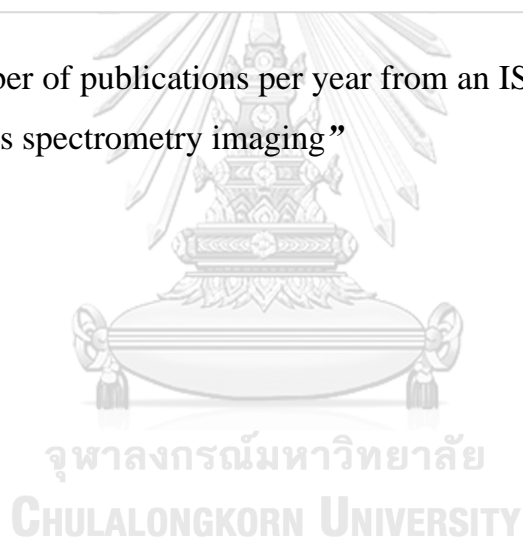


Figure 2.7 Number of publications per year from an ISI Web of Science search of the topic “mass spectrometry imaging”



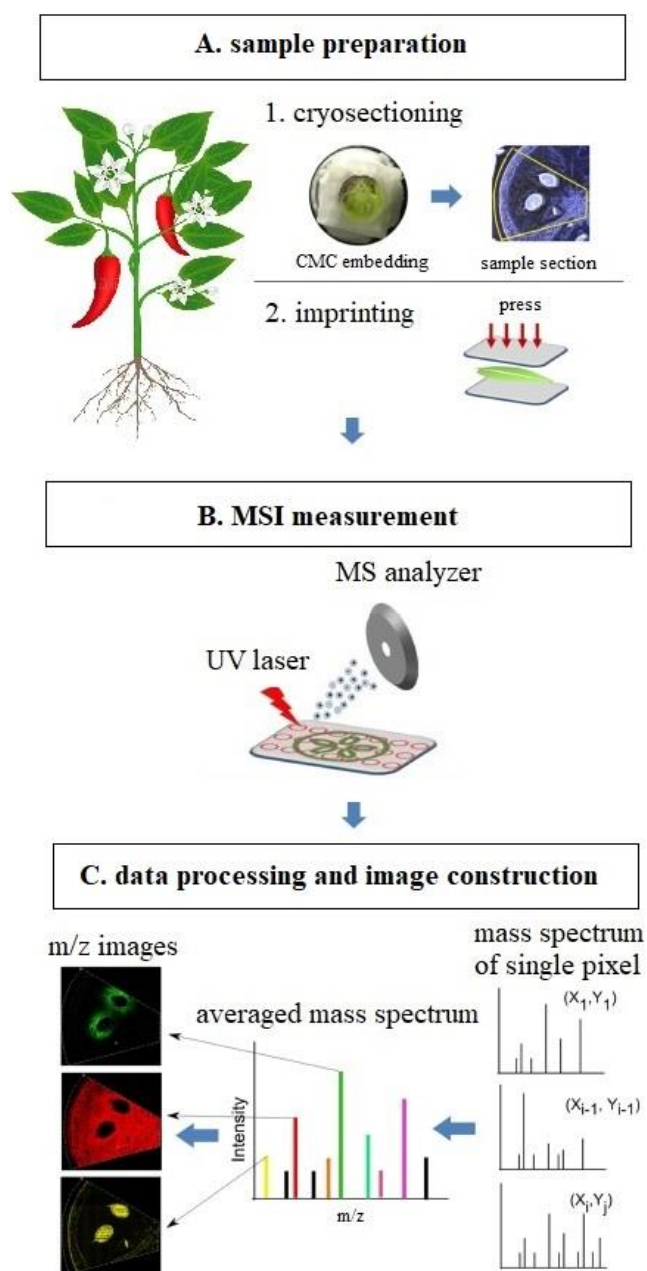


Figure 2.8 Experimental workflow for the MSI analysis (modified from the image of Dong et al. (10))

The typical workflow of a MSI experiment is shown in Figure 2.8. A basic concept of MSI experiment can be divided into three steps: (1) sample preparation, (2) MSI measurement, and (3) data processing and image construction. First, the tissue is removed in the form of thin section from the

interested material. Following the preparation step, the basic settings of an MSI experiment consist of defining a grid (x, y) over the sample surface and the user selects the grid region. Then the mass spectrometer ionizes the molecules on the sample surface and generates a mass spectrum at each pixel on the section resulting in the spatial resolution defined by the pixel size. The computer software will be used after spectrum collection to select an individual m/z value, and the m/z intensity is extracted from the spectrum of each pixel. These intensities are then integrated into a heat map image and it will display the relative distribution of the m/z value over the entire sample surface (11).

The core of MSI operation is similar to the common mass spectrometer which made up of three main parts: ion source, mass analyzer, and detector. Various ion sources are available for MSI, and different ion sources have their own advantages and disadvantages (Table 2.1). Thus, the use of ion sources is depending on the purpose of the experiment. Among several ionization techniques, MALDI is the most popular ion source for MSI because it can image a broad range of substances including metabolites and proteins. Moreover, MALDI provides resolutions down to 20 μm , and a wide selection of instruments is commercially available at prices comparable to other mass spectrometry analysis (12).

Compared to other imaging techniques, MSI presents a numerous advantage that are specifically obtained from modern mass spectrometers. MSI offers high molecular selectivity, high sensitivity, and a fast multiplexed acquisition in a single measurement of several ionizable compounds. MSI could give extremely high lateral imaging resolution that enables the molecular nature of fine morphological characteristics of tissue to be differentiated. When combined with appropriate mass analyzers, it can identify several substances in a profiling-type experiment simultaneously. Modern MSI instruments and software technologies provide fast data collection, enabling high-throughput analysis and screening approaches (13).

During the last ten years, MS imaging has taken a long way and its use in biological material studies has obviously been considerably more common in recent years. In the coming years, this technique would become much more important to the biological research community.



Table 2.1 List of ion sources used for MSI. Information about lateral resolutions, preparation steps required for MSI, sample considerations, and applications

Ionization source	Lateral resolution	Preparation steps	Sample type/limitations considerations	Applications
DESI (ambient)	50–200 μm	None for external surfaces; section and mount for internal tissues, imprint onto PTFE	Solid, frozen liquid	Small molecule metabolites, lipids
nano-DESI (ambient)	20 μm	No sample pre-treatment, section if needed	Solid, frozen liquid	Analysis of complex mixtures of soluble organic and biological molecules on substrates
LAESI (ambient)	300–500 μm	Section if needed, mount sections on flat surface, prevent condensation by using a chamber filled with inert gas	Fresh sample	Small molecule metabolites, lipids
MALDI (vacuum)	UV = 10–50 μm IR = 100–200 μm	Tissue section, drying and application of matrix	Dried sample in matrix/matrix signal interference	Small molecule metabolites, lipids, proteins and peptides, non-covalent complexes
SIMS (high vacuum)	50 nm–5 μm	Tissue section and drying. For matrix enhanced SIMS additional application of matrix	Dried sample/may ionize both inorganic and organic molecules which may complicate discovery efforts	Cellular biology, lipids and lipid fragments, elements, small fragments of large biomolecules
LESA (ambient)	1–2 mm	None for external surfaces, section and mount for internal tissues	Fresh sample/low resolution	Micro-liquid extraction of biomolecules

*Abbreviations: DESI - desorption electrospray ionization; LAESI - laser ablation electrospray ionization; MALDI – matrix assisted laser desorption/ionization; SIMS – secondary ion mass spectrometry; LESA – liquid extraction surface analysis

2.3 Applications of mass spectrometry for biological research

Mass spectrometry is the most widely used analytical techniques within multiple fields, including biological research. This usefulness derives from the fact of mass spectrometers offering qualitative and quantitative information about the elemental, isotopic and molecular structure of organic and inorganic specimens. In addition, all states of samples can be analyzed, and the analyzing mass vary from single atoms to protein (over 300,000 Da).

MS was first applied in biology in the 1940s when heavy stable isotopes were used as tracers for examining processes such as the production of CO₂ in animals (14). In 2002, the ongoing significance of MS to biological research is illustrated when the Nobel Prize in Chemistry was given to John Fenn and Koichi Tanaka, “for their development of soft desorption ionization methods for mass spectrometric analyses of biological macromolecules”.

There is a wide variety of MS applications for biology. Table 2.2 summarizes a list of applications that MS can achieve.

Table 2.2 Summary the common applications of mass spectrometry in various study fields in biological research

Field of study	Applications
Genomics	<ul style="list-style-type: none"> • analyze oligonucleotides and intact nucleic acids • characterize single nucleotide polymorphisms (SNPs)
Proteomics	<ul style="list-style-type: none"> • determine the molecular mass of peptides and proteins and the sequences • identify structure, function, folding, and interaction of protein • analyze differential expression of proteins in

Field of study	Applications
	<p>samples (quantitative proteomics)</p> <ul style="list-style-type: none"> • detect protein modifications and location of the modifying sites without a prior knowledge (post-translational modification analysis) • observe reaction of enzyme
Metabolomics	<ul style="list-style-type: none"> • identify and quantify the metabolites in a biological samples • investigate the effect on metabolite levels of drugs, toxins and multiple diseases • track the metabolic pathways
Clinical diagnosis	<ul style="list-style-type: none"> • identify disease biomarkers • determine cancer aggressiveness • monitor therapeutic drug • screening for newborn errors of metabolism • forensic drug testing • identify microbes in the clinical microbiology laboratory • identify bacterial toxins and antibiotic resistance type
Plant research	<ul style="list-style-type: none"> • characterize plant natural products • study plant-omics • profiling of plant hormones • analyze pesticide residues in fruits and vegetables

Apart from common mass spectrometry, MS imaging is another technique which have caught the attention of the biological society. MSI can

be used to localize wide variety of molecular species of interest including proteins, lipids, small molecules, drugs, and metals etc.

MSI was initially employed to locate proteins and other peptides in a sample. After the on-tissue digestion with trypsin has been developed, it expands the coverage of protein, not only by allowing higher molecular weight, but also by allowing more sensitive, higher resolution instrumental platforms for protein analysis to become accessible. There are many publications about the utilization of MS imaging technique to map proteins or peptides. For example, Gemperline et al. (15) studied the endogenous peptides and proteins in *Medicago truncatula* and hundreds of peptides and protein fragments were imaged. MSI was not used only in plant samples, it also widely used to localize proteins in animal tissues as the work of Piehowski et al. (16). In their work, they could analyze and generate the image of more than 2000 proteins from mouse uterine tissue sections preparing for blastocyst implantation.

Lipids are also gradually being targeted for MSI analysis due to its diagnostic power. For instance, distribution of folic acid tends to increase during the intravenous administration of prostate tumor tissue and the findings indicate that MSI technique could be utilized in the diagnosis of cancer. (17). Moreover, this approach can be used to identified new traumatic brain injury lipid related markers (acylcarnitines) which is significance in determining their fundamental function in the regeneration process and inflammatory response (18).

Drug is another popular target for the analyzation using MSI. The application of MSI in the drug development process consisting of drug distribution, drug metabolism, drug delivery and drug quantification (19). The study of Ntshangase et al. (20) illustrated the use of MSI for studying drug deposition and spatial distribution into the central nervous system (CNS). Their results revealed that MS imaging offer valuable knowledge about the spatial

distribution of the two common antiretroviral drugs (elvitegravir and tenofovir) and also demonstrated the ability of this technique for direct visualization of pharmaceutical drugs in situ.

2.4 Background of the study for the first part of thesis (Chapter 3: MALDI-mass spectrometry imaging for phytoalexins detection in Thai rice)

2.4.1 Importance of rice and blast disease

Rice (*Oryza sativa*) is one of the most important crops in the world. It provides the primary source of energy for more than half of the world's population (21). Rice consumption continues to increase as a result of population growth and improved living standards. Many studies have shown that the demand for rice is increasing every year, and as a result, production will have to be increased by more than 40% by 2030. Thailand is one of the largest rice export countries, comprising 26% of world rice export. However, the rate of increased rice production in the country has slowed disease outbreaks (22). Blast disease is one of the major diseases in rice caused by *Magnaporthe oryzae* (Fig 2.9). All parts of rice plant can be infected by this fungus, including roots (23). The disease cycle (Fig 2.9c) starting with the dispersion of conidia which attach to the host surface by producing spore tip mucilage. After that, the conidia will germinate and adhere to the host surface through the production of a hyphal filament which is covered in an extracellular matrix. The following step is formation of melanized appressorium. Lastly, a penetration peg from the appressorium penetrates the plant cuticle and cell wall by applying turgor pressure. Subsequent to penetration, fungus will invade the adjacent cell of host through pit fields which are the clusters of plasmodesmata. The lesion development begins around 4-5 days after infection (24).

It is estimated that each year blast disease causes between 10-30% of yield losses in the rice harvest (25). In Thailand, rice blast is common in all parts of the country (26). The disease is also distributed in about 85 countries on all continents where rice is cultivated (21). The symptoms of the disease which are usually examined in the infected rice plants including the blast at leaf, neck, and the panicle of the plant. Among these, rice production has been damaged the most by neck blast (21).

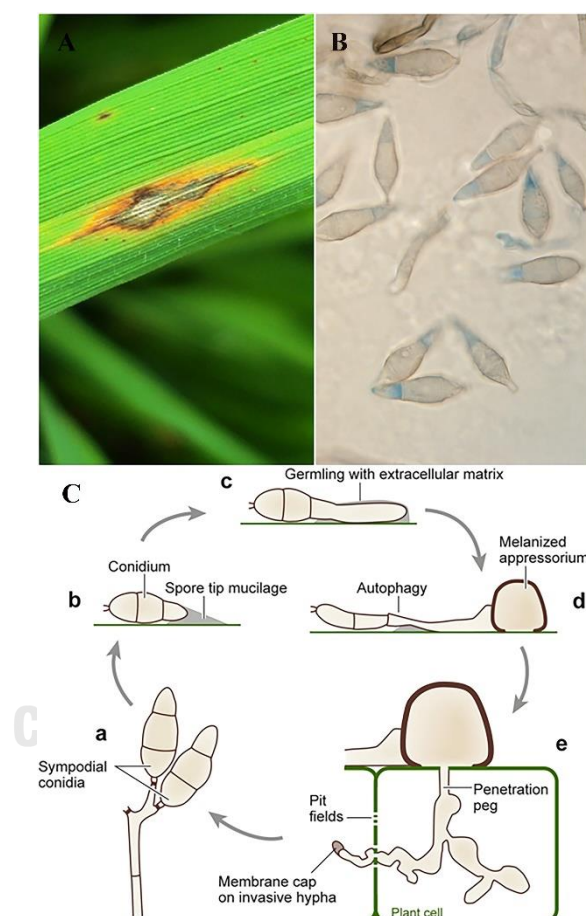


Figure 2.9 Rice blast disease caused by *Magnaporthe oryzae*. (A) Lesion on the leaf. (B) Conidia of *M. oryzae* under light microscope. (C) Blast disease cycle (24).

In recent years, many techniques have been developed to control rice fungal diseases, including chemical and biological methods. Even though using pesticides is a popular way to control the disease, it is expensive and has

negative effects to human health and the environment. Choosing rice varieties with the ability to resist the disease may represent an effective method for preventing crop yield loss (27). However, blast-resistant rice varieties rarely ever last more than a few years, since the pathogen mutates very quickly, ultimately overcoming the plant's resistance. Therefore, plant breeders have to develop new resistant rice varieties continuously, which are selected by means of extensive and time-consuming field trials. If there were simple chemical tests to determine whether a new rice variety is resistant, it would be much quicker and cheaper, such as determination of the phytoalexin response of newly developed genotypes (28).

2.4.2 Phytoalexins: role in disease resistance in rice plants

Phytoalexins are plant antimicrobial compounds that are both synthesized and accumulate in plants after exposure to microorganisms or abiotic agents (29). Consequently, phytoalexins can be used to indicate the resistance properties of plants to disease. Phytoalexins have been identified in multiple plant species but the role of phytoalexins was first described 80 years ago by Müller and Börger (30). They worked with potato (*Solanum tuberosum*) and oomycete *Phytophthora infestans*, the causative agent of potato rot. From their experiments, they found that potato tubers previously infected with an avirulent strain of pathogen induced resistance to a virulent strain. This finding strongly suggested that potato tubers produced substances (phytoalexins) to inhibit the growth of pathogens, protecting the tissue against subsequent infection by other virulent strains of the pathogen (31). In addition, phytoalexins have also been identified in rice. The diterpenoid phytoalexins of rice currently identified include momilactones A and B, oryzalexins A-F, oryzalexin S, phytocassanes A-E and ent-10-oxodepressin (Fig 2.10) (32). Rice varieties that produce these groups of metabolites tend to have the ability to resist blast disease. Moreover, resistant rice plants can produce phytoalexin

faster than susceptible rice plants, and the accumulation of phytoalexins in resistant rice is several times higher than in susceptible rice (33).

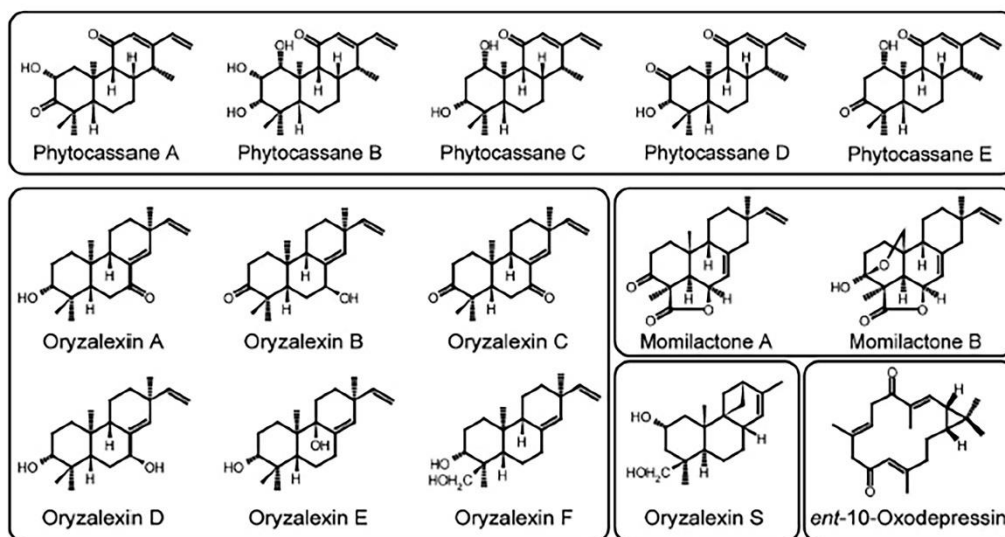


Figure 2.10 Diterpenoid phytoalexins in rice (34)

2.5 Background of the study for the second part of thesis (Chapter 4: Global analysis of protein expression of A549 cells after prolonged nicotine exposure by using label-free quantification)

2.5.1 Lung cancer

Lung cancer is one of the most common cancers and the leading cause of cancer death worldwide (35, 36). The International Agency for Research on Cancer (IARC) released the updated on 14th December 2020 that global cancer burden has risen to 19.3 million cases and 10 million cancer deaths. Over 2.2 million of newly lung cancer cases were reported worldwide (both sexes, all ages). Most importantly, lung cancer causes highest mortality rate among all new cancer cases in almost of the world's nations (Fig. 2.11) (37). In Thailand, lung cancer accounts for 12.4% of new cancer cases in 2020 which is the second highest percent among other cancer types. Although the diagnostic and treatment methods have been improved, the overall survival rate of lung cancer

patient remains disappointing at less than 15% of 5-year survival rate from the time of diagnosis (38).

Lung cancers can be divided into two main types called small cell lung cancer (SCLC) and non-small cell lung cancer (NSCLC). SCLC comprises about 20-25% of lung cancer cases. Cigarette smoke is the cause of nearly all cases of SCLC. This tumor grows very rapidly and spreads much quicker than other forms of lung cancer. The NSCLC are further classified into 3 main types: adenocarcinoma, squamous cell carcinoma, and large cell carcinoma. Adenocarcinoma is the most prevalent type of lung cancer, accounting for 30-40% of overall lung cancer cases. This type of cancer is the most common form of lung cancer among non-smoker and women. Adenocarcinomas are found in the outer edges of the lungs and appear to metastasize more than squamous cell carcinomas. Squamous cell carcinoma is responsible for 30% of lung cancers and is generally associated with smoking. This type of cancer is mostly found in the central part of the chest and most likely no metastasized. Large cell carcinoma usually responsible for 10-15% of all cases of lung cancers. This tumor may grow in a peripheral site and has high tendency to spread to the distant locations like adenocarcinomas (39). Figure 2.12 demonstrates various cancer cell types visualized under microscope.

Cell lines produce cells of identical genotypes and phenotypes nearly unlimited. Human cancer cell lines are the widely used as experimental models in many laboratories to study the biology of human cancer and to evaluate the therapeutic effectiveness of anticancer agents (40). Cell lines are selected based on the purpose of experiment. One commonly used model for NSCLC is A549 adenocarcinoma cell line. This cell line developed in 1972 by Giard et al. (41) from the type II pneumocyte lung tumor. A549 cells have been used to study the metabolic processing of lung tissue and possible mechanisms of drug delivery to the tissue (42). This cell line was also extensively used as a model to study metastasis process in lung cancer. The study of Shindo-Okada et al.

(43) has reported that A549 cell line is an excellent tool to examine lung cancer metastases.

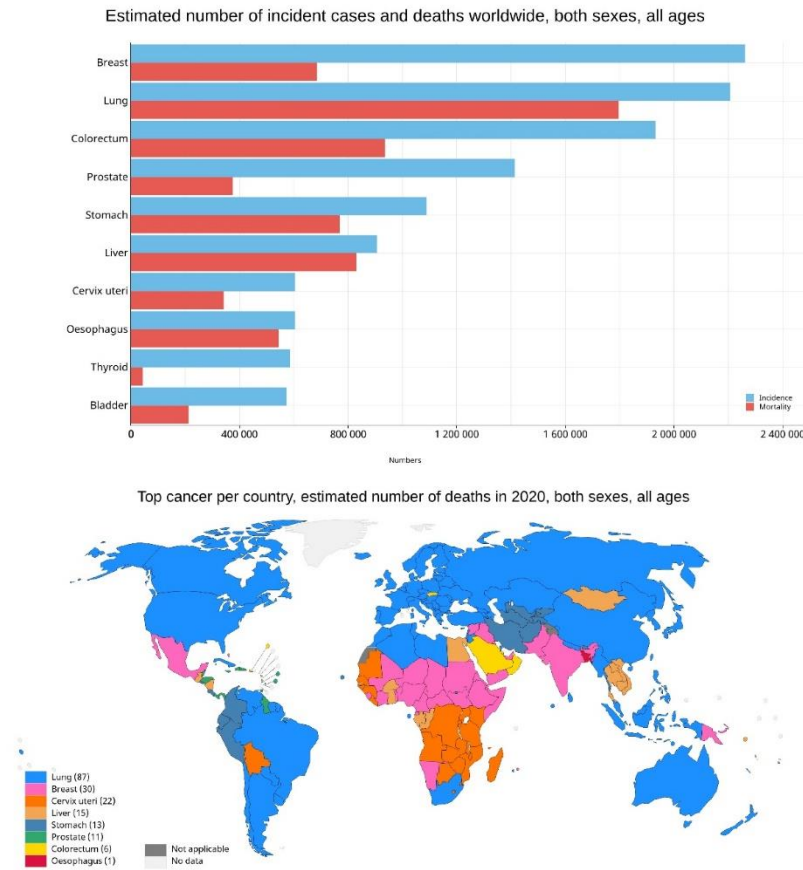


Figure 2.11 Global burden of new cases and deaths as reported by IARC in December 2020

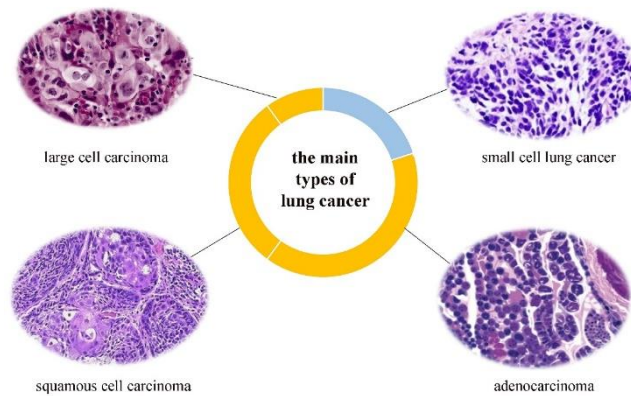


Figure 2.12 The main types of lung cancer under microscope

2.5.2 Nicotine

Cigarette smoke consists of over 5000 chemical constituents, including over 60 human carcinogens (44). Long term exposure to tobacco smoke toxins is not a matter of preference, but because of addiction to nicotine (45).

Nicotine is one of the major addictive components of cigarettes. It is a bicyclic compound with a pyridine cycle and a pyrrolidine cycle extracted from tobacco plants (Fig. 2.13) (46). The concentrations of nicotine in blood of smokers who smoke 25 cigarettes/day are in the range of 0.025-0.444 μM (47).

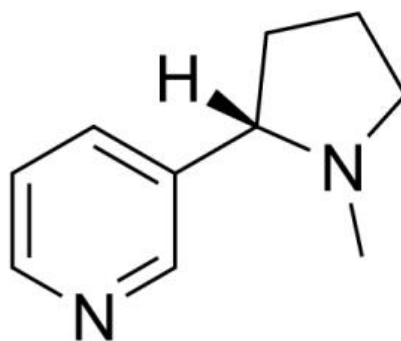


Figure 2.13 Structure of nicotine or 3-(1-methyl-2-pyrrolidiny) pyridine.

Nicotine performs its functions by activating the nicotinic acetylcholine receptors (nAChRs). nAChRs are ligand-gated ion channel proteins and are pentamers of various subunits combination. The opening of channels is mediated by ACh binding or by nicotinic agonists, for example nicotine, cotinine, and tobacco specific *N*-nitrosamines (TSNA) (48, 49). Product-containing nicotine can increase signaling via nAChRs since nicotine binds with a higher affinity than natural ligand ACh with these receptors (48). Initial effect of the binding nicotine to nAChR is implicated in the brain's rewarding effects of tobacco use by increasing the activity of the dopamine neurons. However, chronic exposure to nicotine activates neuroadaptation leading to desensitization of these receptors to even its natural agonist, which contributes to dependency and withdrawal responses (50-52).

Although nicotine itself is not carcinogenic, there are several studies showed that it enhances the development of cancer by stimulating various processes.

Promotes angiogenesis

A number of researches illustrated that nicotine has an impact on angiogenesis in several tumor cells, such as lung, breast and colon (53, 54). *In vitro* studies, nicotine stimulates migration, invasion, proliferation, development of new blood vessels, and production of nitric oxide (NO), immitating other angiogenic growth factors (55, 56). The study in *In vivo* mouse model of lung cancer also exhibited similar results that nicotine could built up the number and size of tumors within the lung, and promoted metastasis (57).

Reduces efficiency of cancer therapy

Nicotine has been shown to minimize the effects of radiotherapy (RT) and chemoradiotherapy (CRT). It has been demonstrated that the anti-proliferation or pro-apoptotic effetcts conducted by chemotherapy on various malignant cell lines were diminished at concentrations as low as 1 μ M based on many *in vitro* studies (58, 59). *In vivo* experiments also concern the effect of nicotine during chemotherapy. Warren et al. (60) examined the impact of nicotine in RT and CRT response by using male Foxn1^{nu} athymic nude mice. Mice were received human H460 lung cancer cell to generate xenografts in the right rear flank. Their study found that administration of nicotine in mice during fractionated RT or CRT has enhanced xenograft regrowth compared with RT or CRT alone.

Inhibits antitumor immune response

Dijk et al. (61) studied effects of nicotine on cytokine production *in vivo*. The results showed that the production of Interleukin 2 (IL-2) is lowered in mitogen-stimulated human peripheral blood mono-nuclear cells which indicates nicotine immunosuppressive effect. Nicotine toxicity has also been

described to adversely influence dendritic cells, which play a major role to detect and eliminate tumor cells (62).

Enhances tumor metastasis

Nicotine has been shown to promote invasion and migration of some human cancer cell lines (63-65) and metastasis of various cancer types (65, 66). For example, Dasgupta et al. (63) showed that nicotine increases proliferation, migration, invasion, and EMT in A549 lung cancer cells. Another study of Nair et al. (67) was done a microarray analysis on two NSCLC cell lines (A549 and H1650). The authors implied that nicotine and EGF enhance the proliferation, invasion, and migration of NSCLC by inducing genes such as STMN3 and GSPT1. However, these researches only study the role of nicotine in metastasis in short period.

Apart from dose of nicotine, timing of exposure also be an important factor associated with cancer metastasis. Fararjeh et al. (68) investigated the effect of long-term exposure to low-dose of nicotine and 4-(methylnitrosamino)-1-(3-pyridyl)-1-butanone (NNK) in HBL-100 breast non-tumorigenic cell line. Cells were repeatedly treated with nicotine and NNK for 23 cycles. The authors found that it can disturb cell growth control and increase a migratory and invasion ability in non-tumorigenic breast epithelial cells. The effect of long-term exposure to nicotine was also studied in lung cancer. Martínez-García et al. (69) observed that repetitive nicotine exposure increases a more malignant and metastasis properties in SCLC cell line.

2.5.3 Metastasis

Metastasis is the spread of cancer from where it originated to the distant areas of the body. It is the hallmark of cancer and causes the highest number of deaths connected to cancer. While metastasis being the major factor to the therapeutic failure and mortality of cancer patients, it is still incompletely known. The formation of metastases enables cancer cells to escape their

primary site, enter the bloodstream, extravasate from the circulation into the distance tissues and adhesion. The majority of the mortalities due to lung cancers are attributable to tumor metastases (70). Therefore, it is a great need to gain our knowledge in the molecular alterations underlying metastasis.

The metastatic cascade is a multi-step process as shown in Figure 2.14. It consists of 5 crucial steps; invasion, intravasation, circulation, extravasation, and colonization (71, 72).

1. Invasion: tumor cells leave their primary site by invading through basement membrane and migrate through the tumor stroma
2. Intravasation: tumor cells infiltrate into the wall of blood vessel and get into circulation
3. Circulation: circulate in the bloodstream, tolerate blood vessel's pressure, cope with shearing forces, and avoiding clearance by the immune system before arriving distant sites
4. Extravasation: extravasation from the vasculature
5. Colonization: tumor cells establish metastatic colonies at secondary tumor sites

Before traveling to a distant location in the body, tumor cells must first overcome containment. Tumor cells achieved this by a process called epithelial–mesenchymal transition (EMT). EMT is a biological mechanism where cells lose epithelial properties (immotile) and establish mesenchymal characteristics (motile). Diverse tumor mechanisms have been correlated with EMT such as tumor progression, tumor cell migration, intravasation, metastasis, and therapeutic resistance (73, 74). For an EMT initiation, several different molecular processes are involved such as transcription factors activation, specific cell-surface proteins expression, cytoskeletal proteins reorganization and expression, extracellular matrix (ECM)-degrading enzymes production, and specific microRNAs expression changes (75). Gain of mesenchymal characteristics is marked by reducing expression of the epithelial

marker E-cadherin and the overexpression of the mesenchymal marker vimentin (76).

Recently, a significant discussion has been conducted on whether EMT plays a key role in cancer metastases and chemotherapy resistance. Study in lung and pancreatic cancers has shown that although EMT may not be necessary for metastasis, the chemoresistance does contribute (77, 78). However, further evidence is needed to clarify the involvement of EMT in the progression of cancer and metastatic processes.

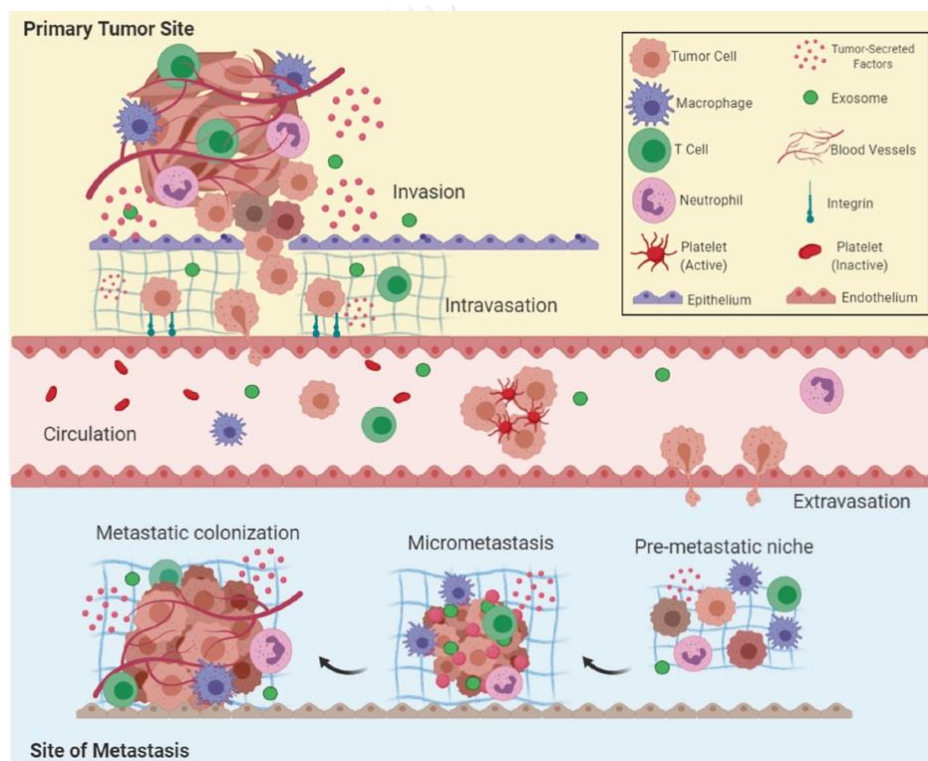


Figure 2.14 Overview key events in the metastatic cascade (71)

CHAPTER 3

MALDI-Mass Spectrometry Imaging for Phytoalexins Detection in Thai Rice

Over the last decade, MALDI-MSI has been gradually applied in plant research. It has been used for mapping various ranges of analytes, such as lipids, proteins, peptides, and other small molecule metabolites. This technique has been successfully used to directly image analytes from different organ tissue sections. In leaves, it was applied for imaging glucosinolates in *Arabidopsis thaliana* (79) and lipids in *Zea mays* (80). In stems, it was used for mapping low molecular weight compounds in *Allium sativum* (81) and urushiols in *Toxicodendron radicans* (82). In seeds, it has been applied for imaging of cyanogenic glucosides in *Linum usitatissimum* (83) and lipids in *Brassica napus* (84).

Many previous studies have highlighted MALDI-MSI applications in agriculture. It was used to study plant–pest interactions between rice–bacteria and soybean–aphid (85). From the experiments, they were able to visualize salicylic acid and isoflavone based resistance in soybean–aphid and antibiotic diterpenoids in rice–bacteria interactions. Recently, MALDI-MSI has been utilized to investigate the biological activity and distribution of cyclotides in Sweet Violet (*Viola odorata* L.) with respect to plant host defense system (86). MALDI-MSI is an alternative imaging technique with the potential to detect all cyclotides that ionize and are present in sufficiently high concentrations within a given sample. The distribution of cyO2, cyO3, and cyO19 was observed by MALDI-MSI, confirming their previously reported immunohistochemical findings.

This part of the study aimed to investigate the production and distribution of diterpenoid phytoalexins in Thai rice using MALDI-MSI, since

there are numerous studies about Thai rice but no reports concerning detection of phytoalexins in Thai rice using this technique. Results obtained from MALDI-MSI were confirmed by liquid extraction analysis. Additionally, this study has modified the fracturing method that is used for sample preparation. This method should be applicable for determining whether many other classes of metabolites are localized on plant leaves.



EXPERIMENTAL

3.1 Materials and Chemicals

Ethanol (Merck KGaA, Germany)

Gelatin (Sigma-Aldrich, USA)

Glucose (Ajax Finechem, New Zealand)

Iron (II, III) oxide nanopowder (Sigma-Aldrich, USA)

Methanol (Merck KGaA, Germany)

Sodium hypochlorite (Kao, Thailand)

3.2 Equipments

Airbrush (Iwata, Japan)

Autoclave (Tomy ES-315, Japan)

Autopipette (Gilson, USA)

Balance (Sartorius CP323S, Germany)

Hemocytometer (HBG, Germany)

Hotplate stirrer (IKA C-MAG HS7, Germany)

Incubator (Shel Lab 1565, USA)

ITO-coated glass slide (Sigma-Aldrich, USA)

Laminar flow (Safety Lab, Thailand)

MALDI-SpiralTOF mass spectrometry imaging (JEOL JMS-S3000, Japan)

Microcentrifuge (WiseSpin CF-10, Korea)

Scanning electron microscope (JEOL SEM- JSM-IT500HR, Japan)

Stereomicroscope (Olympus SZX7, Japan)

3.3 Methods

3.3.1 Plant materials

Five rice varieties (*O. sativa*) consisting of RD6, RD31, RD41, RD57 and Pathumthani1 were obtained from Pathumthani Rice Research Center, Thailand. Rice seeds were immersed in 70% ethanol for 5 min and 5.25% sodium hypochlorite for 45 min. Next, seeds were rinsed with sterile water 5 times for 5 min each. After surface sterilization, each type of rice seeds was planted in soil in 10 pots (5 seeds per pot). Five pots were used as a control set, while another 5 pots were inoculated with the blast fungus (*M. oryzae*). Soil was autoclaved at 121°C for 20 min. Rice plants were grown in a greenhouse at 30°C for 3 weeks. Finally, rice seedlings were inoculated with the blast fungus.

3.3.2 Blast fungus optimizing medium

M. oryzae came from the Plant Protection Research and Development office, Department of Agriculture, Thailand. To find out the suitable culture medium for the sporulation of blast fungus, fungus was initially cultured in 6 different agar media comprised of Rice Flour Agar (RFA), Rice Potato Carrots Agar (RPCA), Oat Meal Agar (OMA), Wheat Flour Agar (WFA), Glutinous Rice Flour Agar (GRFA) and Potato Dextrose Agar (PDA). The agars were sterilized by autoclaving at 15 psi at a temperature of 121°C for 15 min. Once the agar had cooled to less than 50 °C. Molten agars were then dispensed at a volume of around 15 ml in to 9 cm diameter sterile plastic Petri dishes (Grenier bio-one). Petri dishes were left to solidify at room temperature. Fungus was cut into 5 mm square pieces and placed onto agar plates. Fungus was incubated under fluorescent light at 27°C for 14 days. Lastly, spore production was determined under microscope and colony size was also measured by ruler.

3.3.3 Blast fungus cultivation

Oat Meal Agar was selected as a suitable culture medium from the previous experiment. Therefore, the fungus was grown on it under fluorescent light at 27°C for 14 days. To stimulate conidia production, the mycelial mat on agar plates were covered with 2 ml sterile water and scraped with an L-shaped glass rod. Excess water was decanted. Next, the agar plates were continually incubated for 5-7 days in an ultraviolet cabinet at 27°C to induce sporulation (87).

3.3.4 Blast fungus inoculation

On inoculation day, distilled water was added to the agar plate, the mycelial mat was scraped with an L-shaped glass rod and conidia were counted using a hemocytometer. Suspension concentration was adjusted to 1×10^4 conidia per ml (suspended in sterile water and 2% gelatin). The three week old rice plants were sprayed with *M. oryzae* conidia suspension (87). Inoculated rice plants were kept in the dark under high humidity for 24 h at 27°C for effective infection, and then the rice plants were moved to a greenhouse. After 7 days of inoculation, infected leaves were observed and harvested for analysis.

3.3.5 Analysis of phytoalexins on rice leaf tissues by MALDI-MSI

A modified fracturing method from Klein et al. (85) was used to prepare leaf tissue sections (Fig. 3.1). First, a fresh leaf was cut into a 2 cm piece and stuck to a transparent sealing tape before rolling the tape to enclose (Fig. 3.1A and 3.1B). The leaf sandwich was then rolled using a 5 ml glass bottle and continually pulled open, fracturing the leaf (Fig. 3.1C and 3.1D). Leaf tissue on the sealing tape was adhered to an ITO-coated glass slide with double-sided tape and was sprayed with 2 ml of Fe_3O_4 matrix (10 mg/ml in 70% methanol) using an airbrush. The sample was then applied to MALDI-SpiralTOF mass spectrometry imaging coupled with Nd:YLF 349 nm with 20-30 μm of laser diameter. The instrument was operated using msTornado control program in a

positive mode over a mass range 250-500 Da, 50 μm raster, 250 Hz laser repetition rate, 57% laser intensity and 100 ns of delay time. Finally, MSI data were obtained using msMicroImage and msMicroImage view programs. At the same time, the rice leaf (before and after using the modified fracturing method) surface was examined using a scanning electron microscope.

3.3.6 Analysis of phytoalexins in rice leaves by liquid extraction

To compare the production of phytoalexins between infected and uninfected leaves, both sets of rice leaves were extracted by methanol. For phytoalexin extraction, infected leaves were detached after indicated times and were cut into 5-mm lengths, and 0.15 g of each was frozen at -80°C until use. A leaf sample was mixed with 40 volumes of 70% methanol and heated for 5 min in a long glass tube with a screw cap. The extract was then transferred to a new tube, and the residue was re-extracted twice with 20 volumes of 70% methanol. The combined extracts were then concentrated to dryness. The residue was resuspended in 0.5 ml of methanol and was subjected to MALDI-SpiralTOF mass spectrometry equipped with an Nd:YLF laser at 349 nm (20-30 mm spot diameter). The instrument was operated under the msTornado program in a positive mode, 250 Hz laser repetition rate, 50-70% laser intensity and 100-180 ns of delay time to obtain MS spectra and MSMS spectra, which were acquired over a mass range of 250-400 Da and 5-400 Da respectively. High-energy collision-induced dissociation (HE-CID) was performed with helium gas to obtain fragmentation ions. Finally, the spectra of precursor and product ions were derived using the msTornado analysis program.

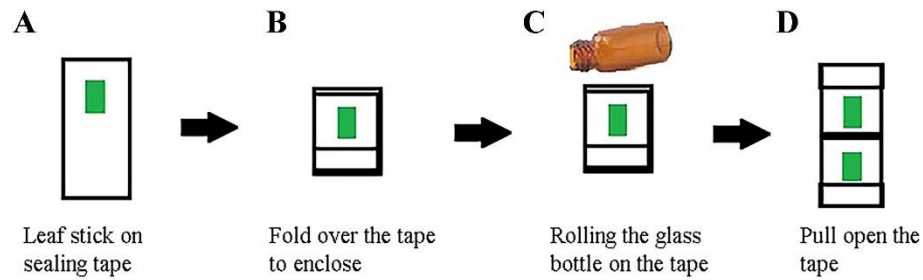


Figure 3.1 Steps of the modified fracturing method

3.4 Results

3.4.1 Optimization of medium for spore production of blast fungus

To investigate the optimum medium for the blast fungus to produce maximum spore, fungus was cultured on 6 different agar media as shown in Table 3.1. The results from the table showed that fungus can grow best on PDA according to colony diameter, following by RPCA, OMA, RFA, WFA, and GRFA respectively. Moreover, the colony morphology in Figure 3.2 showed the significantly different in sizes, shapes, and textures in all media.

However, the main purpose of selecting media is getting the maximum amount of spore. Consequently, the determination of spore production was observed under light microscope as shown in Table 3.2. The results exhibited that Oat Meal Agar (OMA) is an excellent medium that can induce the production of spore of *M. oryzae*. Therefore, this medium was chosen to cultivate fungus in the further experiment.

Table 3.1 Growth of fungus after 14 days of culture on various media

Type of medium	Diameter of colony (cm)					
	Replicate					Avg. \pm SD
	1	2	3	4	5	
Rice Flour Agar (RFA)	4.8	5.2	5.2	5.0	4.7	5.0 \pm 0.23
Rice Potato Carrot Agar (RPCA)	5.8	5.5	5.4	5.3	5.4	5.5 \pm 0.19
Oat Meal Agar (OMA)	5.5	5.4	4.8	4.9	4.8	5.1 \pm 0.34
Wheat Flour Agar (WFA)	4.7	4.7	4.8	4.9	4.9	4.8 \pm 0.10
Glutinous Rice Flour Agar (GRFA)	2.7	2.7	2.5	2.7	3.2	2.8 \pm 0.26
Potato Dextrose Agar (PDA)	5.7	5.6	5.5	5.5	5.7	5.6 \pm 0.10

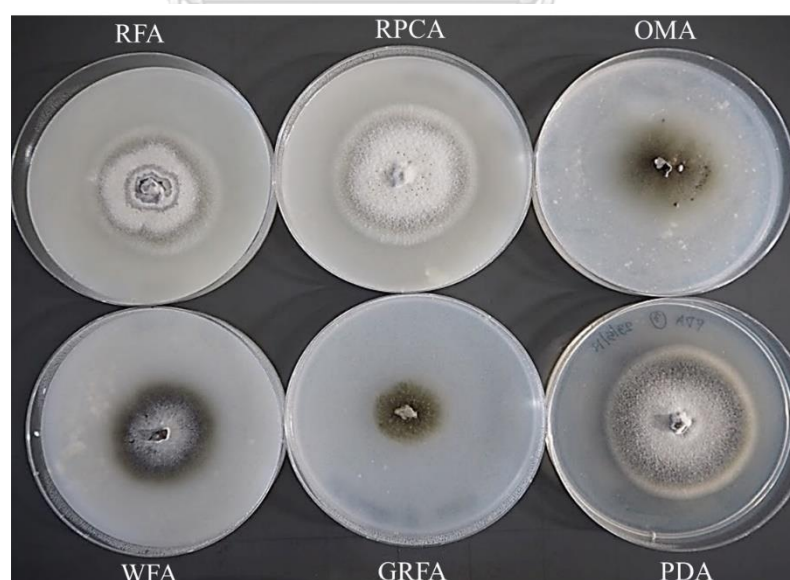

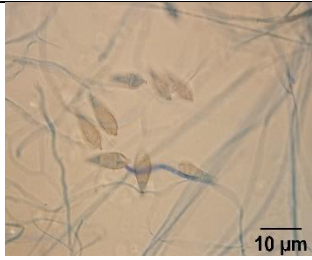

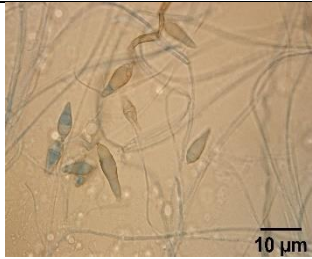

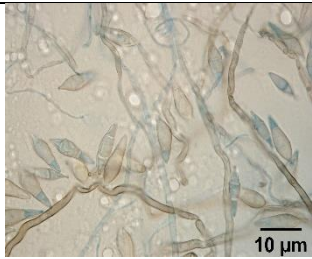
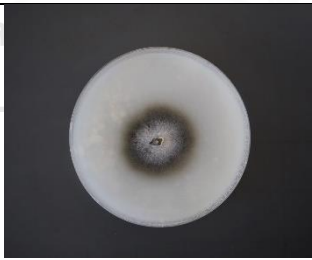
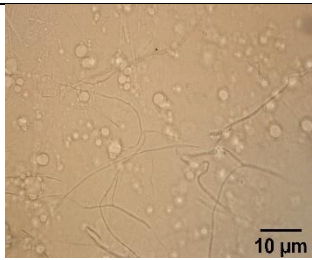

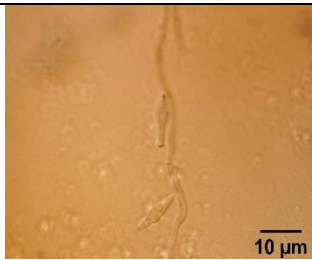


**Figure 3.2** Colony morphology of blast fungus on different media after 14 days of incubation

Table 3.2 Observation of spore production of blast fungus on various media under microscope

Type of medium	Colony morphology	Conidia under microscope
Rice Flour Agar (RFA)		
Rice Potato Carrot Agar (RPCA)		
Oat Meal Agar (OMA)		
Wheat Flour Agar (WFA)		
Glutinous Rice Flour Agar (GRFA)		

Type of medium	Colony morphology	Conidia under microscope
Potato Dextrose Agar (PDA)		

3.4.2 Observation of rice leaves infection by blast fungus at 7 days post-infection

Figure 3.3 illustrates the presence of infected areas on rice leaves. The leaves started having small brown spots and the lesion were enlarged causes diamond-shaped white to gray or brown lesions after 7 days of inoculation.



Figure 3.3 Infected rice leaves after 7 days of inoculation

3.4.3 Determination of phytoalexin production and distribution on a fractured rice leaf by MALDI-MSI

Sample preparation is one of the fundamental steps of MALDI-MSI analysis. In this research, a fracturing method which previously described by Klein et al. (85) were modified for leaf tissue preparation. The MALDI-MSI data obtained from this modified method displayed positive results. To evaluate the quality of tissue samples with the modified fracturing method before subjecting to MALDI-MSI, the intact and fractured leaves were observed by stereomicroscope (Fig. 3.4). Results showed slight differences between intact (Fig. 3.4A and 3.4B) and fractured leaves (Fig. 3.4C and 3.4D) and did not clearly present the detail of either leaf. As a result, SEM was applied to determine leaf surface and structure. SEM images of intact leaf (Fig. 3.5A and 3.5B) clearly show the veins, trichomes and surface bulges. The intact leaf was then fractured by the modified fracturing method and analyzed with SEM. Figure 3.5C and 3.5D show the fractured leaf with the disappearance of surface bulges, and though, fragile, the fractured leaf tissues maintained their primary structure. Consequently, it can be concluded that leaf tissue from the modified fracturing method was suitable for further MALDI-MSI analysis.

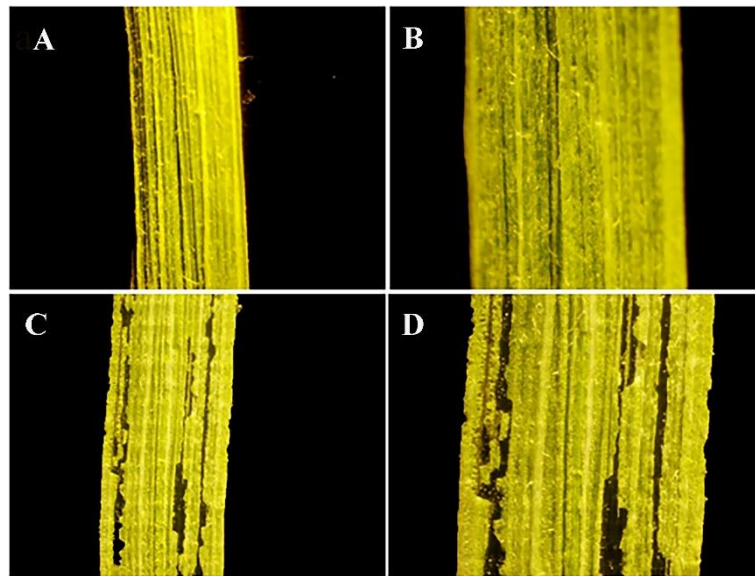


Figure 3.4 Stereo microscope images of rice leaf surface. (A, B) Surface of leaf tissue before fracture. (C, D) Surface of leaf tissue after fracture.

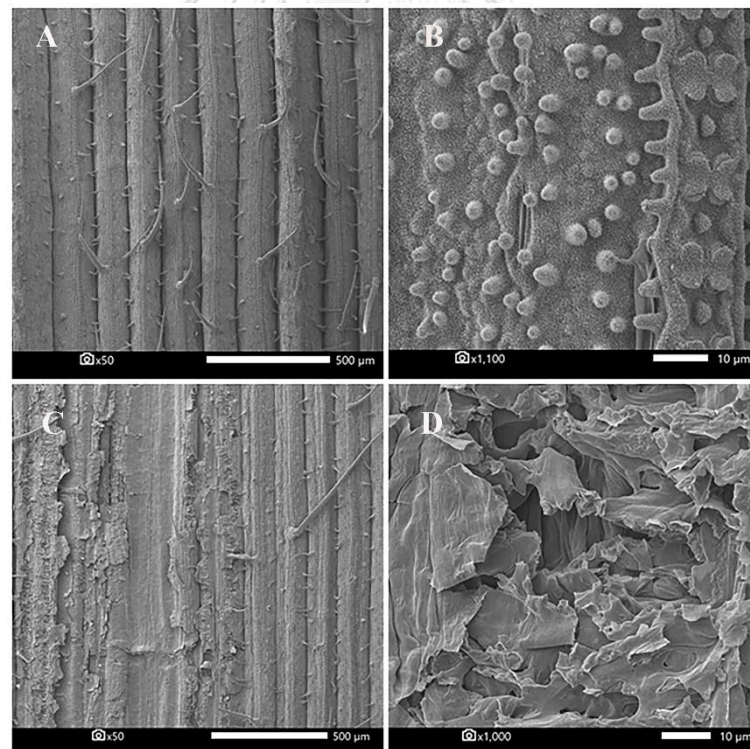


Figure 3.5 SEM images of rice leaf surface. (A, B) Surface of leaf tissue before using a modified fracturing method. (C, D) Surface of leaf tissue after using a modified fracturing method.

Production and accumulation of phytoalexins in *M. oryzae* infected rice plants has been previously reported by GC-MS and HPLC-ESI-MS/MS analysis of rice leaf extracts. However, localization of these antimicrobial compounds was not reported (33). This study is the first examined the production and distribution of diterpenoid phytoalexins in infected and uninfected Thai rice plants using MALDI-MSI.

Each rice plant varieties were divided into two sets. The first was inoculated with *M. oryzae*, while the other comprised non-infected leaves (control set). Both were grown in the same environment, described in the methods section. Subsequently, leaves from both groups were prepared by a modified fracturing method before analysis with MALDI-MSI. MALDI-MSI results from non-infected leaves of all rice varieties presented similar results as shown in Figure 3.6. The leaves contained common plant metabolites, such as sucrose and monogalactosyldiacylglycerol (MGDG) (88), but no phytoalexins were detected. Disaccharide, which was most likely sucrose, was distributed across the uninfected leaves, especially around the midrib where possessed the highest distribution. The midrib consists of vascular tissues that can transport sucrose to other organs to support growth and development (89). Accordingly, this is the likely reason for the present finding of high levels of sucrose distribution in this region. MGDG, a lipid which is found in thylakoid membrane of chloroplast is also visualized (Fig. 3.6C) across the leaves. However, the intensity is lower than sucrose.

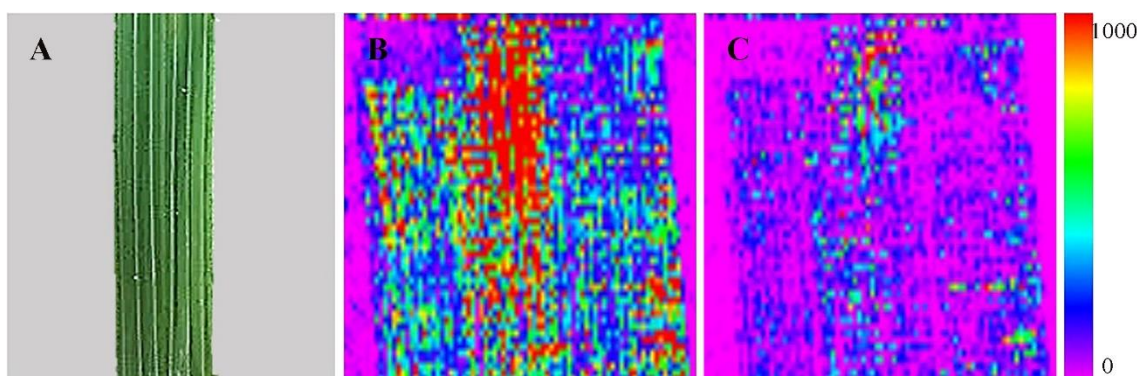


Figure 3.6 MALDI-MS images of uninfected rice leaf section. (A) An optical image of the rice leaf. MALDI-MS images of (B) disaccharide, most likely, sucrose (m/z 381.21) and (C) MGDG (m/z 813.74). Both compounds were detected as potassiatted ions ($[M + K]^+$).

In infected rice leaves of 5 rice varieties, only RD6 rice plant could produce diterpenoid phytoalexins. Interestingly, five types of diterpenoid phytoalexins, including momilactone-A (Fig. 3.7B), momilactone-B (Fig. 3.7E), phytocassane-A, D, or E (Fig. 3.7C), phytocassane-B (Fig. 3.7F) and phytocassane-C (Fig. 3.7D), were observed the distribution on the infected site of the leaf sample, corresponding to numerous previous studies on the induction of phytoalexin production in plants results from an invasion of organisms, such as bacteria, viruses, and fungi. Most studies have demonstrated that phytoalexins rapidly accumulate at areas of incompatible pathogen infection (85, 86, 90, 91). On the other hand, diterpenoid phytoalexins were absent in the healthy region of the leaves. Apart from phytoalexins, sucrose was found to be slightly distributed on the infected area, the data are shown in the appendix (Fig. A.1 and A.2).

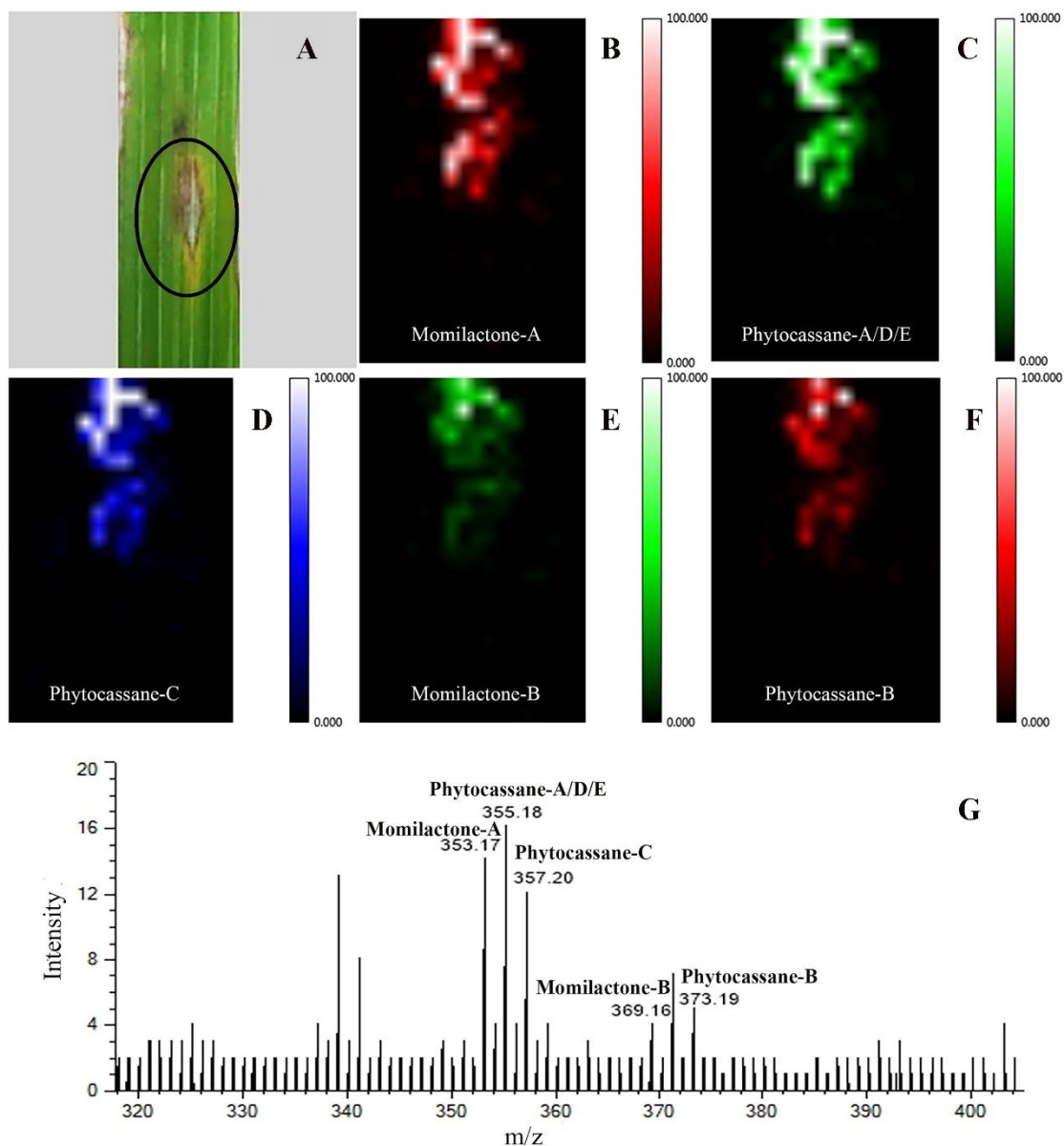


Figure 3.7 MALDI-MS images of infected rice leaf section. (A) An optical image of the rice leaf with a black circle representing the infected area. MALDI-MS images of (B) momilactone-A (m/z 353.17), (C) phytocassane-A, D, or E (m/z 355.18), (D) phytocassane-C (m/z 357.20), (E) momilactone-B (m/z 369.16), and (F) phytocassane-B (m/z 373.19). All compounds were detected as potassiumated ions ($[M + K]^+$). (G) MALDI mass spectrum of diterpenoid phytoalexins from infected rice leaf section.

3.4.4 Structural analysis of phytoalexins by tandem mass spectrometry

To confirm the results from MALDI-TOF localization of diterpenoid phytoalexins, a liquid extraction method was also used to analyze rice leaves of all rice varieties. Diterpenoid phytoalexins were extracted from infected and non-infected rice leaves before evaluating their structure using MALDI-MS. Results clearly corresponded to the MS spectrum obtained from MALDI-MS images (Fig. 3.7G). Among 5 rice varieties, only RD6 leaf extract presents diterpenoid phytoalexins after get invasion from blast fungus. Thus, this part will only display the results of RD6 leaf extract. However, the mass spectra of other rice varieties were placed into appendix B (Fig B.1, B.2).

Comparison of mass spectra between uninfected and infected RD6 rice leaf extracts is shown in Figure 3.8. The mass spectrum of uninfected rice leaf extracts (Fig. 3.8A) revealed common plant metabolites, such as sucrose (m/z 381.19) and MGDG (m/z 813.71), whereas the mass spectrum of infected rice leaf extracts (Fig. 3.8B) displayed the presence of five types of diterpenoid phytoalexins, including momilactone-A (m/z 353.16), momilactone-B (m/z 369.21), phytocassane-A, D, or E (m/z 355.17), phytocassane-B (m/z 373.19) and phytocassane-C (m/z 357.19). Identification of these compounds was primarily based on mass data and MS/MS spectra supported by available literature. The MS/MS spectra of some compounds, such as momilactone-A (Fig. 3.9A), phytocassane-A, D, or E (Fig. 3.9B), phytocassane-C (Fig. 3.9C) and sucrose (Fig. 3.9D) were obtained, even though phytocassane-A, D, or E are structural isomers that cannot be differentiated. However, this study were unable to obtain the MS/MS spectra of momilactone-B and phytocassane-B due to the limited amount of precursor ions and these compounds not being easily ionized.

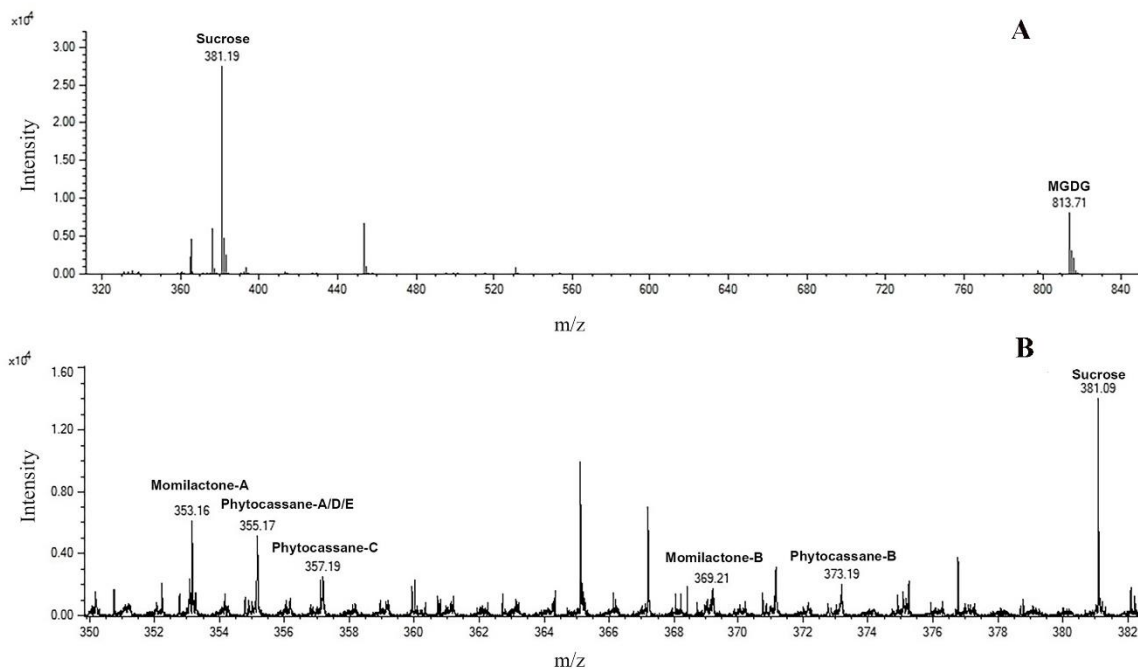


Figure 3.8 MALDI mass spectra obtained from RD6 rice leaf extract. (A) Uninfected rice leaf extract. (B) Infected rice leaf extract. Both mass spectra are shown, highlighting the m/z values of interest. All compounds were detected as potassiated ions ($[M + K]^+$).

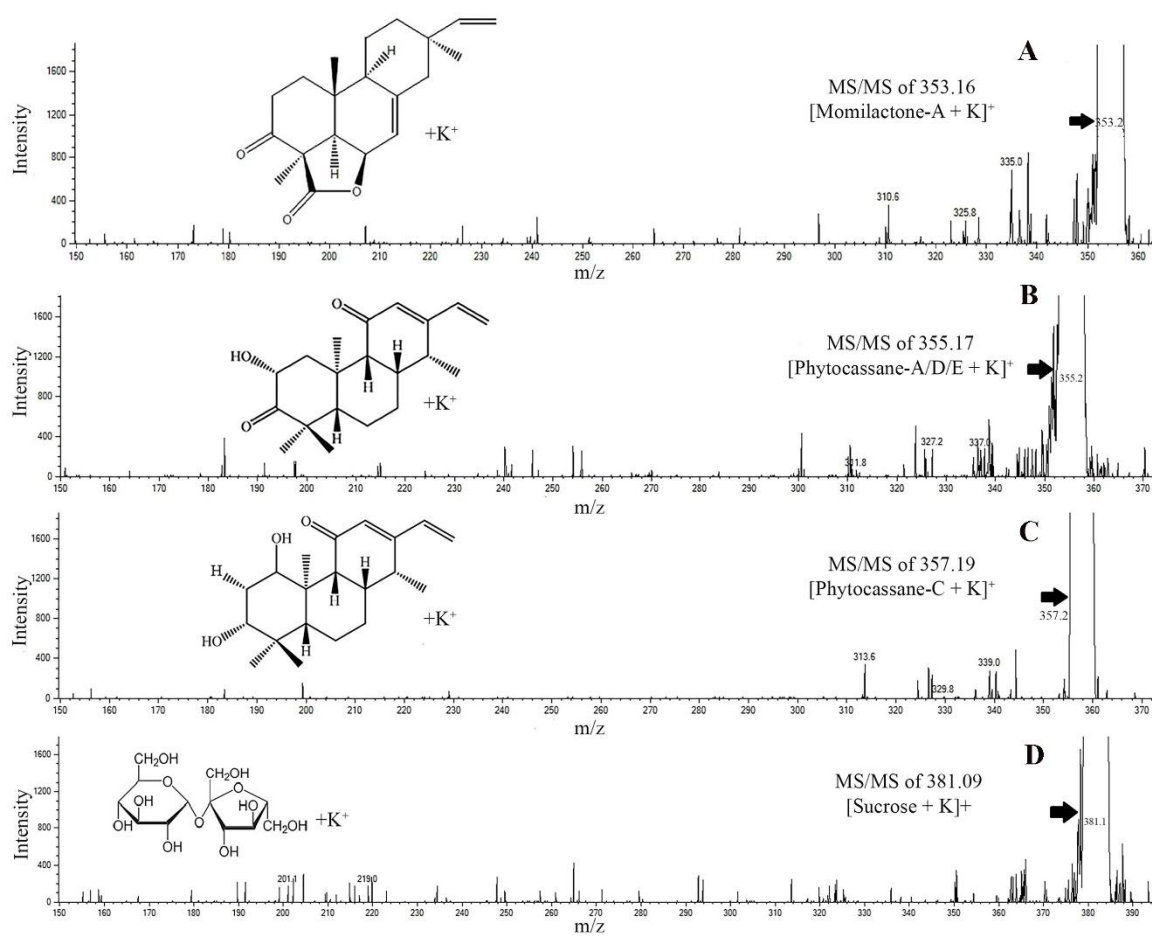


Figure 3.9 MALDI-MS/MS spectra obtained from rice leaf extract. (A) Momilactone-A. (B) Phytocassane-A/D/E. (C) Phytocassane-C. (D) Sucrose. The MS/MS spectra match the standard analysis of isolated diterpenes from rice leaves.

3.5 Discussion

Rice blast caused by *M. oryzae* is the most destructive disease in almost all rice-growing countries. Many factors are involved in the progression of the disease such as relative humidity, temperature, doses of nitrogen fertilizer, and rice development stages (92). Even though blast fungus can infect rice plant at any stage of growth and development, the infection results at each stage are somehow different. Therefore, rice development stage should be considered while evaluating blast resistance in cultivars (93, 94). In this study, 3 weeks old rice was chosen for inoculation with *M. oryzae* corresponded to previous studies (95, 96).

Phytoalexins are antimicrobial secondary metabolites synthesized by plants after exposure to microorganisms. Rice (*Oryza sativa*) produces various types of diterpene phytoalexins. Fourteen diterpenoids have been isolated and identified from rice, including phytocassanes A–E (97-99), oryzalexins A–F (100-102), oryzalexin S (103), and momilactones A and B (104, 105). Because production of phytoalexins constitutes an important system in rice to defend themselves against fungal pathogens, using this outstanding phytoalexin detection method may help researchers explore the ability of rice to combat blast disease.

The present study first reported on the production and distribution of diterpenoid phytoalexins in fungal infected Thai rice using MALDI-MSI. Sample preparation is one of the key steps of MALDI-MSI analysis. Even small mistakes in preparation can lead to many problems during analysis. Most methodologies of sample preparation in MSI were developed for animal tissues and cannot be used directly on plant samples due to the distinct structures and compositions between animal and plant tissues (12). This research modified a fracturing method previously described by Klein et al. (85) for leaf tissue preparation. The modified fracturing method can be performed in only one

hour because the vacuum drying step, which normally takes 4-5 h is removed. Furthermore, this method has many advantages, for example, cheap equipment used, no embedding step that could lead to ion suppression, no requirement for technical skill and relatively low cost compared to other preparation methods. However, the fracturing method has some limitations. This method is suitable with thin and small leaves, but thick and large leaves make it difficult to pull and open the packing tape without breaking some parts of the leaves. As a result, cryosectioning or imprinting methods might be required. For cryosectioning, leaves are embedded into embedding media, such as paraformaldehyde, gelatin or CMC, for sectioning. The embedding step increases sample preparation time, as well as ion suppression, on MSI. For imprinting methods, a thick leaf sample could be applied, but the delocalization of chemical substances on tissue surfaces can occur.

After the sample preparation step, the production and distribution of major diterpenoid phytoalexins were examined using MALDI-MSI. Results showed that only the RD6 rice plant could generate diterpenoid phytoalexins in inoculated rice leaves. When comparing these present results to a previous study by Klein et al. (85) that used bacterial blight in rice *Xanthomonas oryzae* pv. *oryzae* (Xoo) as a pathogen to invade rice plants and analyzed phytoalexin production with MALDI-MSI, it was found that similar types of phytoalexins were produced, but their abundance was different. In this work, momilactone-A, phytocassane-A, D, or E and phytocassane-C were at significantly higher abundance than other phytoalexins, and mass spectra results also showed high intensity (Fig. 2.7g). In contrast to this work, phytocassane-B had the highest abundance in results obtained by Klein et al. (85). This difference may be due to the sorts of pathogens that attack rice plants. Several reports have shown that the terpenoid phytoalexin momilactone A inhibits growth of the rice fungal pathogen *M. oryzae* (28, 33, 106), while its role in rice resistance to Xoo is not clear. This may explain the finding of high

abundance momilactone-A in the current experiment but not in the experiment that used Xoo as an agent to infect rice plants. Of course, the phytoalexin response of rice plants to fungus may be distinct from their response to bacteria. However, although the results of phytoalexin production after inoculation with *M. oryzae* and after inoculation with Xoo were not identical, they did show similar trends.

Hasegawa et al. (33) reported accumulation of major rice diterpenoid phytoalexins in resistant rice infected with blast fungus. In their work, they used rice leaf extracts to analyze the synthesis of phytoalexins. Their results showed that momilactones A and B and phytocassanes A through E were produced in fungal-infected resistant rice. However, their data provided no information on rice leaf extract localization of these compounds, which may be useful for studying the interaction between rice and blast fungus. Compared to the rice leaf extract method, the advantage of the MALDI-MSI used here is its convenient and fast track procedure for preparing samples, which does not require a complicated procedure of sample extraction before analysis by mass spectrometry. Furthermore, this technique can directly visualize the internal metabolite distribution from rice leaf tissues.

The successful detection technique described herein illustrates the use of MALDI-MSI in Thai rice research. MALDI-MS image results simultaneously revealed both localization and identification of target phytoalexins on a leaf tissue section. Detection and mapping of phytoalexins can considerably improve understanding of the defense mechanisms of rice plants against blast fungus. In addition, the MALDI-MSI technique demonstrated herein is expected to be further applied as an effective method to determine phytoalexin response for plant breeders who develop new varieties of resistant rice. Consequently, it should be noted that the MALDI-MSI technique has extremely high sensitivity and is suitable for metabolite imaging, providing new opportunities for agricultural applications in the future.

CHAPTER 4

Global Analysis of Protein Expression of A549 Cells after Prolonged Nicotine Exposure by using Label-Free Quantification

Proteins are the building blocks of the living thing which involved in all biological processes. Proteomics provides great promise in resolving the complex molecular events of tumorigenesis, as well as tumor behaviors such as metastases and invasion (107). Mass spectrometry-based techniques have been used during the last two decades to detect and quantify proteins in the biological sample in a confident and nearly comprehensive way. They contributed to cellular signaling networks being revealed, dynamics of protein-protein interactions being elucidated and gained diagnosis and molecular knowledge of mechanisms of disease (108). MS-based quantitative proteomics technology not only identify proteins, but quantifies the changes between normal and disease sample profiles so that classification models can be produced (109). The standard proteomics method begins with trypsin cleavage of protein into short peptides, and then separated by liquid chromatography. The peptides were eluted from the chromatography column and were sprayed into the mass spectrometer by electrospray ionization. In the mass spectrometer, two MS measurement levels are carried out in tandem. A mass analyzer determines the m/z ratio of molecular peptide ions in the first level (MS1), while the second level (MS2) measures the m/z values of fragmentation ions generated by the fragmentation of unique peptide ions. The specific fragment ion pattern and its value of m/z allow the confident identification of peptides in the sample. It is then possible to map the identified peptide sequences to proteins and use the signal intensities of either peptides or fragment ions to predict relative differences in abundance in samples (108).

Among several MS-based quantification strategies, label free quantitation is one of the methods which has gained popularity in recent years (110-113). This technique does not require a stable isotope containing compound to chemically bind to protein samples (114). It can be divided into two quantification approaches: peptide peak intensity based quantification and spectral counting quantification (115). Despite their power to analyze a large array of samples, they require less amount of protein sample compared to other proteomic techniques. Moreover, these approaches are simple and cost-effective (116). As the survival rate of lung cancer patients is very low, thus it is essential for researchers to discover prognostic markers to increase patient survival rate and for detecting the stage of cancer as early as we can (115).

This part of the study aimed to investigate the effect of prolonged exposure of nicotine on A549 non-small cell lung cancer cell line and its ability to induce invasion of cancer cell. Furthermore, label-free quantitative proteomic method was utilized to analyze the protein alterations of A549 lung cancer cell line upon treating with nicotine. Lastly, target proteins were validated by immunoblot.

EXPERIMENTAL

4.1 Materials and Chemicals

2-Mercaptoethanol (Sigma-Aldrich, USA)
Acetonitrile (Merck KGaA, Germany)
Acrylamide (Bio-Rad, USA)
Ammonium bicarbonate (Sigma-Aldrich, USA)
Ammonium persulfate (Sigma-Aldrich, USA)
Bovine serum albumin (Sigma-Aldrich, USA)
Bradford reagent (Bio-Rad, USA)
Bromophenol blue (Merck KGaA, Germany)
Coomassie brilliant blue (SERVA, Germany)
Dimethyl sulfoxide (Merck KGaA, Germany)
Dithiothreitol (Thermo Fisher Scientific, USA)
ECL Prime detection reagent (GE Healthcare, USA)
Ethanol (Merck KGaA, Germany)
Fetal bovine serum (Merck Millipore, USA)
Formic acid (Thermo Fisher Scientific, USA)
Glycerol (Thermo Fisher Scientific, USA)
Glycine (Calbiochem, USA)
Hydrochloric acid (Merck KGaA, Germany)
Iodoacetamide (Sigma-Aldrich, USA)
Matrigel (Corning, USA)
Methanol (Merck KGaA, Germany)
MTT (Sigma-Aldrich, USA)
N,N'-Methylenebisacrylamide (Bio-Rad, USA)
Nicotine (Sigma-Aldrich, USA)
Penicillin-streptomycin (Sigma-Aldrich, USA)
Primary antibodies (Abcam, UK and Cell Signaling Technology, USA)
RPMI 1640 medium (Gibco, USA)

Secondary antibodies (Dako, USA)
Sodium dodecyl sulfate (Calbiochem, USA)
Sodium chloride (Scharlab, Spain)
Tetramethylethylenediamine (AppliChem GmbH, Germany)
Trifluoroacetic acid (Thermo Fisher Scientific, USA)
Tris (Calbiochem, USA)
Trypsin (Promega, USA)
Tween 20 (Vivantis, Malaysia)

4.2 Equipments

Autopipette (Gilson, USA)
Balance (Mettler Toledo XS205DU, USA)
Biological safety cabinet (NuAire NU-543-400E, USA)
Cell culture flask (Thermo Fisher Scientific, USA)
Centrifuge (Hitachi CT15RE, Japan)
CO₂ incubator (Thermo Fisher Scientific 3111, USA)
Electrophoresis and blotting system (Bio-Rad, USA)
Glass pipette (HBG, Germany)
Hemocytometer (HBG, Germany)
HPLC separation system (Thermo Fisher Scientific Dionex UltiMate 3000, USA)
Inverted microscope (Nikon Eclipse TS100, Japan)
Luminescent image analyzer (GE Healthcare ImageQuant LAS4000 mini, USA)
Magnetic stirrer (Heidolph MR Hei-Mix L, Germany)
Mass spectrometer (Bruker amaZon speed ETD, USA)
Mini-centrifuge (Hercuvan TT-6000, UK)
Microplate reader (Molecular Devices SpectraMax M2, USA)
Nano HPLC column Acclaim PepMap RSLC C18 (Thermo Fisher Scientific, USA)

PVDF membranes (Pall Corp., USA)

Shaker (GFL 3017, Germany)

Thermomixer (Eppendorf ThermoMixer C, Germany)

Transwell (Corning cat.no. 3422 and 3428, USA)

Vortex mixer (Scientific Industries Vortex-Genie 2, USA)

Water bath (Julabo GmbH, Germany)

Well plate (Thermo Fisher Scientific, USA)



4.3 Methods

4.3.1 Cell culture

Human non-small cell lung cancer, A549 cells, were cultured in RPMI 1640 containing 10% fetal bovine serum and 1% penicillin-streptomycin. Cells were maintained in 37 °C incubator with 5% CO₂. Cell were passaged successively when achieving 80% confluency.

4.3.2 Cytotoxicity assay

A549 cells were used to determine the cytotoxic effect of nicotine using an MTT assay as described by Kuljittichanok et al. (117). Cells (5x10³ cells/well) were seeded to 96-well plates and then treated with various concentration of nicotine (1-40 mM) for 24, 48 and 72 h. After incubation, the culture medium with nicotine was removed and replaced with fresh culture medium consisting of 0.5 mg/mL MTT. The cells were then incubated for 2 h at 37 °C. Culture medium was removed and formazan products were dissolved by adding 100 µl of dimethyl sulfoxide (DMSO) to each well. The absorbance was measured at 550 nm using a 96 well microplate reader and background subtraction was adjusted with the absorbance readings at 650 nm.

4.3.3 Cell invasion assay

In vitro cell invasion assays were performed using a 6.5 mm Transwell chamber (8 µm pore size) as described by Weeraphan et al. (118). Briefly, the upper surface of membrane was coated with 30 µg of Matrigel. Transwell chambers were then incubated overnight at 37 °C. Then, 100 µl of fresh serum-free media was added to the upper chamber, incubated at 37 °C for 1 h, after which all the media in upper chamber was removed. Five thousand of A549 cells were suspended with serum-free media containing nicotine at various concentration (0.1, 1.0, 5.0 and 10.0 nM) and then plated into the upper chamber. Cells containing serum-free media with 0.5% (v/v) ethanol were used

as a vehicle control. Then 500 μ l of complete medium was added to the lower chamber and incubated overnight at 37 °C in a CO₂ incubator. On the next day, cells that migrated across the filter membrane were fixed with 25% methanol for 15 min, followed by staining with 0.1% crystal violet for 15 min. Five random phase contrast images of migrated cells were taken and counted under 100 \times magnification. All experiments were performed in biological triplicates.

4.3.4 Prolonged nicotine exposure of A549 cells

A549 cells were cultured in RPMI 1640 containing 10% fetal bovine serum, 1% penicillin-streptomycin and 5 nM of nicotine. Briefly, 1×10^6 of A549 cells were seeded and grown at 37 °C in an atmosphere of 5% CO₂. On the next day, cells were treated with 5 nM of nicotine and then passaged after an incubation period of 48 h. Cells containing media with 0.5% (v/v) ethanol were included as a vehicle control. The prolonged nicotine exposure of A549 was designated as A549-P5 and NicoA549-P5, respectively. Cells were then harvested and kept at -80 °C for further analysis. All experiment were done in biological triplicates.

4.3.5 Prolonged nicotine exposure on motile A549 cells

Subpopulations of A549 cells were selected according to their invasiveness capacity using 24 mm Transwell chamber. Briefly, the upper surface of membrane was coated with 400 μ g of Matrigel and incubated as mentioned previously. One million A549 cells were suspended with serum-free media containing 5 nM of nicotine and then plated into the upper chamber. Cells containing serum-free media with 0.5% (v/v) ethanol were included as a vehicle control. Then 2.6 mL of complete medium was added to the lower chamber and incubated for 48 h at 37 °C in CO₂ incubator. The cells that migrated across the membranes were aseptically harvested and expanded for the next round of selection. The subline of the first-round selection was designated as A549-L1 and NicoA549-L1. Similarly, the sublines from 2, 3,4,

and 5 rounds of selection were designated as A549- and NicoA549-L2, -L3, -L4, -L5, respectively. A549-L5 and NicoA549-L5 cells that migrated across the membranes were harvested and kept at -80 °C for further analysis. All experiments were done in biological triplicates.

4.3.6 Protein preparation for label free proteomic analysis

Ten micrograms of sample were resuspended in 50 mM ammonium bicarbonate (NH_4HCO_3) and protein concentration was determined using the Bradford assay. Samples were reduced with 10 mM DTT at 95°C for 5 min, alkylated with 1/10 volume of 200 mM iodoacetamide for 30 min at room temperature in the dark and then enzymatically digested with trypsin at a 1: 50 enzyme/protein ratio. Digestion was carried out overnight at 37°C. The reaction was stopped by adding formic acid at a final concentration of 1% and the samples were completely dried by Speed Vacuum.

4.3.7 Label free LC-MS/MS analysis

Samples were prepared for label-free LC-MS/MS quantification by dissolving the digested samples in 0.1% formic acid in H_2O and separated on a Nanoflow liquid chromatography system. All samples were run in triplicate. Samples were injected into a C18 Acclaim PepMap RSLC (75 μm i.d. x 150 mm) column at a flow rate of 300 nl/min and temperature of the column was maintained at 40 °C. The LC gradient was performed using 0.1% formic acid in 100% water (solution A) and 0.1% formic acid in 100% ACN (solution B) with the following conditions: 1-50% B in 70 min, 50-90% B in 5 min, followed by 15 min with 90% B. One microliter of sample (100 ng/ μL) was injected into the nano-LC system and then the separation was performed. The eluting peptides were analyzed directly via MS/MS on an amaZon speed ion trap mass spectrometer equipped with a captive-electrospray ion source. The positive mode was used with a spray voltage 1.3 kV and the capillary temperature was set at 150 °C. Mass spectra were acquired from 400-1,400 m/z using

parameters optimized at 922 m/z with a target of 500,000 set for ion charge control and a maximum acquisition time of 100 msec. The scan range was 50-3,000 m/z. MS/MS data were processed by Bruker Compass 1.4 software. The raw data obtained from LC-MS/MS was processed and calculated the significant changes by Progenesis label-free LC-MS software version 3.1 (Nonlinear Dynamics, Ltd., UK). Each replicated sample's retention time was aligned against a reference sample selected by the program itself, together with normalization of peak intensities. Protein identifications were performed by Mascot software version 2.4.0 (www.matrixscience.com). The search parameters were set up as follows: (1) data base, Swiss-Prot Fasta (which was released in October, 2018); (2) species, *Homo sapiens*; (3) digestion, trypsin; (4) instrument, ESI-TRAP; (5) fragment mass tolerance, 0.6 Da; (6) peptide mass tolerance, 1.2 Da; (7) maximum missed cleavages, 1. A false discovery rate (FDR) threshold of 1% was applied and identification of two or more unique peptides and two or more peptides were required for positive identification, respectively.

4.3.8 Western blot analysis

The proteins were extracted from the cells by homogenization in RIPA lysis buffer. The amount of protein in samples were quantified by Bradford assay. Ten micrograms of protein samples were separated by 10% SDS-PAGE and proteins were then transferred to PVDF membranes which were blocked with 3% Bovine Serum Albumin (BSA) in Tris buffered saline with tween-20 (TBST) for 1 h at room temperature with agitation. Subsequently, the membranes were incubated with primary antibodies, including legumain (1: 10,000 dilution; cat.no. ab183028; Abcam), HSP 90 (1:1,000 dilution; cat.no. 4874; Cell Signaling Technology), PDI (1: 3,000 dilution; cat.no. 3501; Cell Signaling Technology), HSP 70 (1:1,000 dilution; cat.no. 4872; Cell Signaling Technology), Profilin (1: 5,000 dilution; cat.no. ab124904; Abcam), Histone H3 (1: 10,000 dilution; cat.no. 9715; Cell Signaling Technology) and β -actin

(1: 10,000 dilution; cat.no. 3700; Cell Signaling Technology) in TBST buffer containing 3% BSA at 4 °C with agitation overnight. After washing 3 times with TBST buffer, the membranes were incubated with peroxidase-conjugated goat anti-mouse IgG and goat anti-rabbit IgG as secondary antibodies (1:5,000 dilution; Dako, CA, USA) in 3% non-fat dry milk for 1 h at room temperature with agitation. Membranes were then washed 3 times in TBST buffer. The immunoreactive bands were visualized using ECL Prime and detected by GE ImageQuant Las 4000 mini. All Western blot analyses were done in biological triplicates.

4.3.9 Bioinformatics

Various proteins from Progenesis QI software were further analyzed through bioinformatics platforms such as STRING (<https://string-db.org>) which is a database for predicted signaling networks and protein interactions. Ontological analysis of the dysregulated genes was analyzed using the UniProt database (<https://www.uniprot.org>) to classify functions.

4.3.10 Statistical analysis

Data were expressed as mean \pm SD (standard deviation) of three independent observations. Statistical significance was calculated using a two tailed unpaired Student's t-test. A P-value of 0.05 or less was considered significant in this study.

4.4 Results

4.4.1 Cytotoxic effect of nicotine on A549 lung cancer cells

To elucidate the cytotoxic effect of nicotine, A549 cells were treated with various concentrations of nicotine by the MTT assay (Fig. 4.1). According to the results of MTT cell viability assay, nicotine reduced cell viability in a time- and concentration-dependent manner. The IC₅₀ concentration of nicotine

was determined to be 16, 12 and 7 mM for incubation periods of 24, 48 and 72 h respectively. Non-cytotoxic concentrations were selected for further studies.

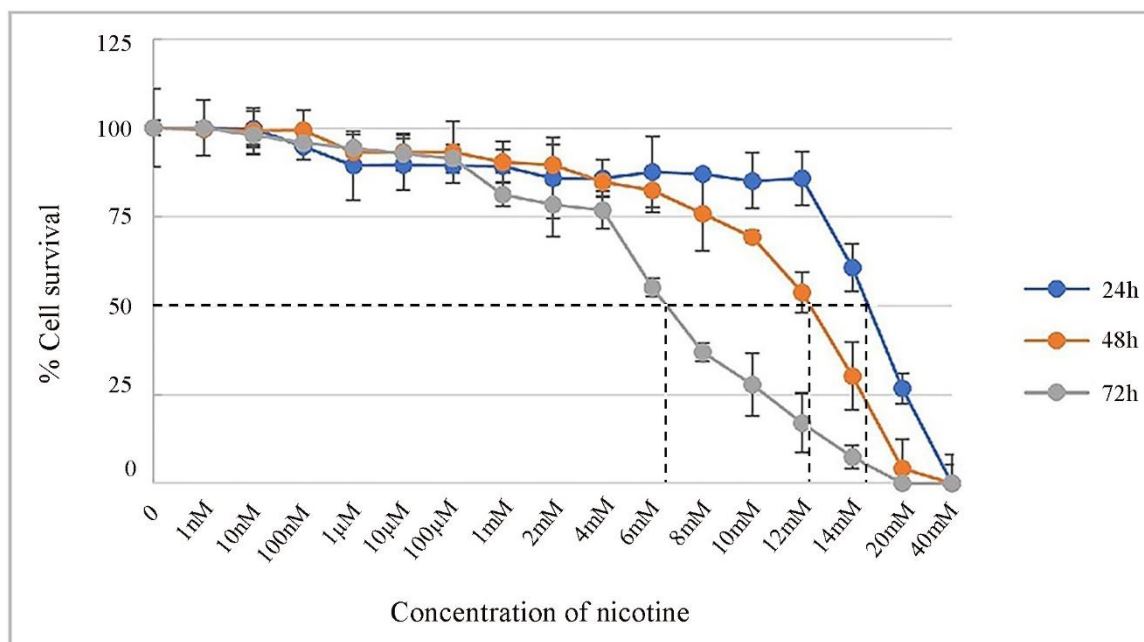


Figure 4.1 The cytotoxic effects of nicotine on A549 lung cancer cells by MTT assay. The results were expressed as mean \pm SD of three independent experiments.

4.4.2 Nicotine induces invasion of A549 lung cancer cells

Non-cytotoxicity concentrations were used to determine the invasive effect of nicotine on A549 cells using Boyden chambers assays. The invasive capacity of nicotine-treated A549 cells was significantly increased in a dose-dependent manner compared to those of untreated A549 cells (Fig. 4.2). Compared to untreated cells, the highest effect of nicotine was observed at 5 nM and 10 nM by 2-fold increase (Fig. 4.2B). 5 nM nicotine was chosen as a reference concentration to study the effect of prolonged nicotine exposure.

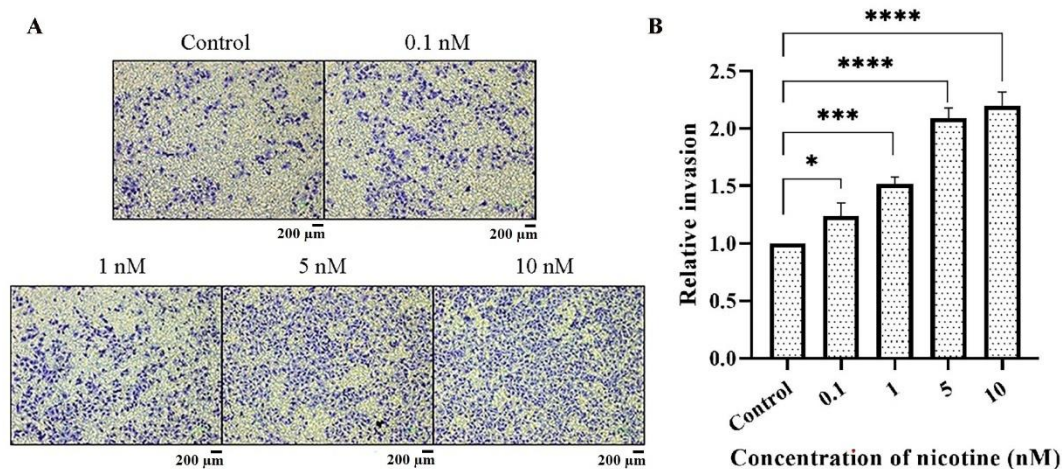


Figure 4.2 Nicotine induces invasion of A549 lung cancer cells. (A) Representative images of invasion assay from A549 cells treated with 0.1, 1.0, 5 and 10 nM of nicotine for 24 h. Scale bar, 200 μm. (B) Bar graph represents the relative invasion of A549 cells after treated with various concentrations of nicotine. Data points represent the mean ± SD. (* $P < 0.05$, *** $P < 0.001$, **** $P < 0.0001$).

4.4.3 Prolonged nicotine exposure enhances the invasive capability of A549 lung cancer cells

An invasive subpopulation of the A549 lung cancer cell line was selected to investigate the effect of prolonged nicotine exposure (Fig. 4.3). Results showed that the invasive subpopulation of A549 cells could be selected using Boyden chambers assays (Fig. 4.4A and 4.4B). The invasive capacity of sublines was gradually increased during subpopulation selection as compared to A549 parental cells by 1.25-fold to 2.6-folds (Fig. 4.4C and 4.4D). The invasive capacity of nicotine-treated subline (NicoA549-L5) was significantly increased by 2.6-fold as compared to A549 parental cells.

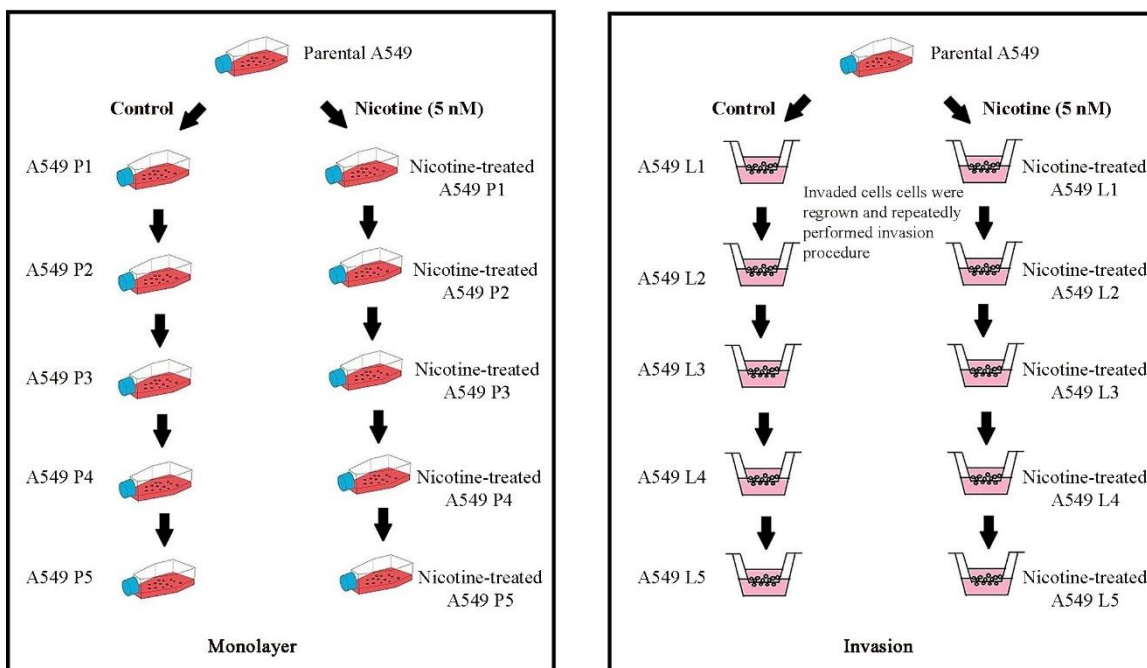


Figure 4.3 Experimental scheme of A549 cells continuous exposure to 5 nM nicotine. Samples were divided into 2 main groups, monolayer and invasion system. Each sample groups were subdivided into 2 conditions, control and nicotine treatment.

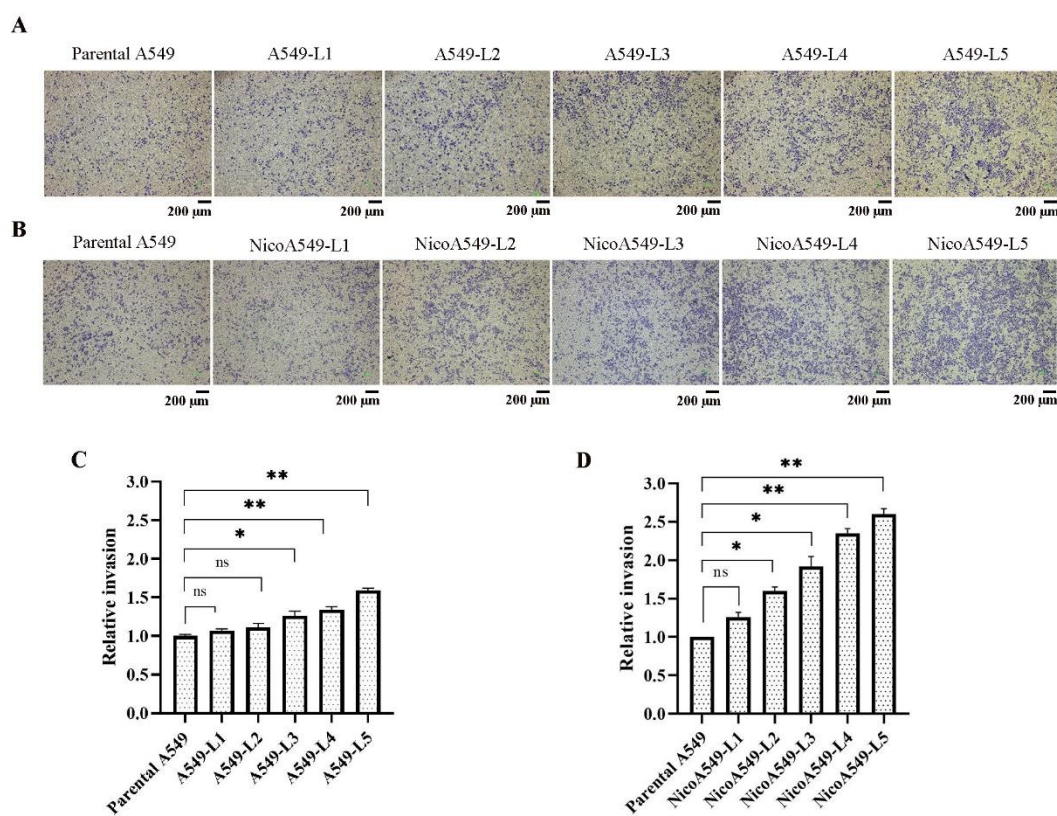


Figure 4.4 Prolonged nicotine exposure enhances the invasive capability of A549 lung cancer cells. Representative images of invasion assay from five sublines of A549 cells untreated (A) and treated (B) with 5 nM of nicotine. Scale bar, 200 μm . Bar graphs represent the relative invasion of sublines with (D) and without (C) nicotine treatment. Data points represent the mean \pm SD. (* $P < 0.05$, ** $P < 0.01$).

4.4.4 Label free quantitative proteomic analysis of untreated and nicotine treated A549 cells

To determine whether metastasis-related proteins were altered by nicotine treatment, the label free quantitative proteomics was employed. The differential effect of nicotine on the global proteins was performed by comparing the protein profiles between nicotine treated and untreated A549 cells. The study was performed by LC-MS/MS with three replicates to ensure reproducibility. Differential protein expression was determined by calculation

with Progenesis QI software version 3.1. The samples from monolayer system (parental and NicoA549-P5) were analyzed. Our investigation showed 55 proteins from the monolayer system which passed the cut off criteria of ANOVA $p\text{-value} \leq 0.05$ and fold change greater than 1.5. Out of the total identified proteins affected by nicotine treatment, 27 proteins were up-regulated and 28 proteins were down-regulated in nicotine-treated A549 P5 cells compared to untreated parental cells, as shown in Table 4.1 and Table 4.2. The protein with the greatest increase of 3.2 fold was lamina-associated polypeptide 2, isoforms beta/gamma (TMPO) while the protein with greatest decrease of 2.6 fold was arginine N-methyltransferase 2 (PRMT2). Heat shock-related 70 kDa protein 2 (HSPA2), cathepsin D (CTSD), heterogeneous nuclear ribonucleoproteins C1/C2 (HNRNPC), legumain (LGMN) and heat shock protein HSP 90-alpha (HSP90AA1) showed high increase of 2.02 to 2.99 fold, while 40S ribosomal protein S10 (RPS10), plasminogen activator inhibitor 1 RNA-binding protein (SERBP1), carbonic anhydrase 12 (CA12), putative high mobility group protein B1-like 1 (HMGB1P1), ras-related protein Rab-10 (RAB10) and serine/arginine-rich splicing factor 4 (SRSF4) showed lower increase of 2.02 to 2.47 fold. Legumain, heat shock-related 70 kDa protein 2, heat shock protein HSP 90-alpha, protein disulfide-isomerase A3 and profilin-1 were selected to validate expression using western blot analysis.

Table 4.1 List of up-regulated proteins from the monolayer system

No.	Accession	Gene	Protein name	Peptide count	Score	Mass	pI	Protein fold change	Protein function
1	LAP2B_HUMAN	TMPO	Lamina-associated polypeptide 2, isoforms beta/gamma	16	293.84	50639	9.39	3.2	Transcription
2	HSP72_HUMAN	HSPA2	Heat shock-related 70 kDa protein 2	12	604.77	69978	5.56	2.99	Response to stimulus
3	CATD_HUMAN	CTSD	Cathepsin D	12	196.1	44524	6.1	2.38	Proteolysis
4	HNRPC_HUMAN	HNRNPC	Heterogeneous nuclear ribonucleoproteins C1/C2	13	438.71	33650	4.95	2.22	mRNA processing
5	LGMN_HUMAN	LGMN	Legumain	9	108.48	49379	6.07	2.22	Proteolysis
6	HS90A_HUMAN	HSP90AA1	Heat shock protein HSP 90-alpha	28	43.41	84607	4.94	2.02	Response to stimulus
7	RL15_HUMAN	RPL15	60S ribosomal protein L15	7	159.84	24131	11.62	1.99	Translation
8	H4_HUMAN	HIST1H4F	Histone H4	7	307.19	11360	11.36	1.96	Nucleosome

No.	Accession	Gene	Protein name	Peptide count	Score	Mass	pI	Protein fold change	Protein function
9	ROA0_HUMAN	HNRNPA0	Heterogeneous nuclear ribonucleoprotein A0	11	113.08	30822	9.34	1.77	mRNA processing
10	RL37A_HUMAN	RPL37A	60S ribosomal protein L37a	9	208.66	10268	10.44	1.66	Translation
11	TBB5_HUMAN	TUBB	Tubulin beta chain	11	398.09	49639	4.78	1.63	Cell division
12	DDX5_HUMAN	DDX5	Probable ATP-dependent RNA helicase DDX5	17	512.82	69105	9.06	1.63	Transcription
13	SUMO2_HUMAN	SUMO2	Small ubiquitin-related modifier 2	3	147.63	10864	6.4	1.63	Metabolic process
14	DDX3Y_HUMAN	DDX3Y	ATP-dependent RNA helicase DDX3Y	26	230.47	73108	7.24	1.62	Transcription
15	LASPI_HUMAN	LASPI	LIM and SH3 domain protein 1	9	140.97	29698	6.61	1.61	Ion transport
16	PRDX5_HUMAN	PRDX5	Peroxisome oxidin-5, mitochondrial	11	168.35	22073	8.93	1.6	Response to stimulus

No.	Accession	Gene	Protein name	Peptide count	Score	Mass	pI	Protein fold change	Protein function
17	PDIA3_HUMAN	PDIA3	Protein disulfide-isomerase A3	14	349.25	56747	5.98	1.59	Response to stimulus
18	1433T_HUMAN	YWHAQ	14-3-3 protein theta	5	214.43	27747	4.68	1.58	Protein targeting
19	HMGAI_HUMAN	HMGAI	High mobility group protein HMG-I/HMG-Y	7	111.3	11669	10.32	1.57	Transcription
20	AKIBF_HUMAN	AKR1B15	Aldo-keto reductase family 1 member B15	9	285.66	36514	6.23	1.55	Metabolic process
21	PROF1_HUMAN	PFN1	Profilin-1	11	338.36	15045	8.44	1.54	Metabolic process
22	PTMA_HUMAN	PTMA	Prothymosin alpha	4	105.3	12196	3.69	1.54	Transcription
23	H31T_HUMAN	HIST3H3	Histone H3.1t	6	161.25	15499	11.13	1.54	Nucleosome assembly
24	PIR_HUMAN	PIR	Pirin	7	147.55	32093	6.42	1.53	Transcription
25	H2BFS_HUMAN	H2BFS	Histone H2B type F-S	5	148.61	13936	10.37	1.52	Nucleosome assembly
26	LDHB_HUMAN	LDHB	L-lactate dehydrogenase B chain	11	404.15	36615	5.71	1.51	Metabolic process

No.	Accession	Gene	Protein name	Peptide count	Score	Mass	pI	Protein fold change	Protein function
27	RAB15_HUMAN	RAB15	Ras-related protein Rab-15	5	149.32	24375	5.53	1.51	Protein transport



จุฬาลงกรณ์มหาวิทยาลัย
CHULALONGKORN UNIVERSITY

Table 4.2 List of down-regulated proteins from the monolayer system

No.	Accession	Gene	Protein name	Peptide count	Score	Mass	pI	Protein fold change	Protein function
1	ANM2_HUMAN	PRMT2	Protein arginine N-methyltransferase 2	5	42.97	49010	5.03	2.62	Transcription
2	RS10_HUMAN	RPS10	40S ribosomal protein S10	5	118.1	18886	10.15	2.47	Translation
3	PAIRB_HUMAN	SERBP1	Plasminogen activator inhibitor 1 RNA-binding protein	9	266.02	44938	8.66	2.17	Apoptotic process
4	CAH12_HUMAN	CA12	Carbonic anhydrase 12	6	92.2	39426	6.73	2.14	Ion transport
5	HGB1A_HUMAN	HMGBIPI	Putative high mobility group protein B1-like 1	5	99.7	24223	5.92	2.07	Transcription
6	RAB10_HUMAN	RAB10	Ras-related protein Rab-10	6	157.54	22527	8.59	2.07	Protein transport
7	SRSF4_HUMAN	SRSF4	Serine/arginine-rich splicing factor 4	10	118.09	56645	11.52	2.02	mRNA processing
8	TIF1B_HUMAN	TRIM28	Transcription intermediary factor 1-beta	11	176.84	88493	5.52	1.98	Transcription
9	1433G_HUMAN	YWHAG	14-3-3 protein gamma	8	132.67	28285	4.8	1.98	Protein targeting

No.	Accession	Gene	Protein name	Peptide count	Score	Mass	pI	Protein fold change	Protein function
10	RS15A_HUMAN	RPS15A	40S ribosomal protein S15a	5	131.82	14830	10.14	1.97	Translation
11	IQGAI_HUMAN	IQGAP1	Ras GTPase-activating-like protein IQGAP1	24	275.35	189134	6.08	1.96	Cell migration
12	ERO1A_HUMAN	ERO1L	ERO1-like protein alpha	4	30.94	54358	5.48	1.95	Apoptotic process
13	RAB1C_HUMAN	RAB1C	Putative Ras-related protein Rab-1C	10	282.58	22003	5.25	1.9	Protein transport
14	HMGB1_HUMAN	HMGB1	High mobility group protein B1	7	161.6	24878	5.62	1.84	Response to stimulus
15	PGK2_HUMAN	PGK2	Phosphoglycerate kinase 2	12	388.21	44767	8.74	1.79	Metabolic process
16	DDX39B_HUMAN	DDX39B	Spliceosome RNA helicase DDX39B	12	251.09	48960	5.44	1.76	Transcription
17	AL1B1_HUMAN	ALDH1B1	Aldehyde dehydrogenase X, mitochondrial	4	56.98	57170	6.36	1.73	Metabolic process
18	HSP76_HUMAN	HSPA6	Heat shock 70 kDa protein 6	17	444.92	70984	5.81	1.69	Response to stimulus
19	DESM_HUMAN	DES	Desmin	19	461.2	53503	5.21	1.65	Cytoskeleton

No.	Accession	Gene	Protein name	Peptide count	Score	Mass	pI	Protein fold change	Protein function
20	EF1B_HUMAN	EEF1B2	Elongation factor 1-beta	4	19.76	24748	4.5	1.63	Translation
21	COBA1_HUMAN	COL11A1	Collagen alpha-1(XI) chain	17	186.29	180954	5.06	1.6	Extracellular matrix organization
22	LACB2_HUMAN	LACTB2	Endoribonuclease LACTB2	3	78.69	32785	6.32	1.59	Endonucleolytic
23	SRP14_HUMAN	SRP14	Signal recognition particle 14 kDa protein	5	111.7	14561	10.05	1.55	Localization
24	RMXL2_HUMAN	RBMXL2	RNA-binding motif protein, X-linked-like-2	12	174.45	42788	10.33	1.54	mRNA processing
25	PSB3_HUMAN	PSMB3	Proteasome subunit beta type-3	20	192.97	22933	6.14	1.54	Metabolic process
26	RL19_HUMAN	RPL19	60S ribosomal protein L19	3	130.43	23451	11.48	1.53	Translation
27	CX6B1_HUMAN	COX6B1	Cytochrome c oxidase subunit 6B1	2	102.06	10186	6.54	1.52	Metabolic process
28	PSB1_HUMAN	PSMB1	Proteasome subunit beta type-1	8	85.08	26472	8.27	1.5	Metabolic process

4.4.5 Functional and interaction analysis

The up-regulated and down-regulated proteins from Table 4.1 and Table 4.2 were analyzed by UniProt database to classify functions as shown in Figure 4.5. Proteins were classified as follows: transcription, metabolic process, response to stimulus, translation, mRNA processing, protein transport, nucleosome assembly, ion transport, proteolysis, apoptotic process, protein targeting, and others, with the major group being involved in transcription at 18.18 %.

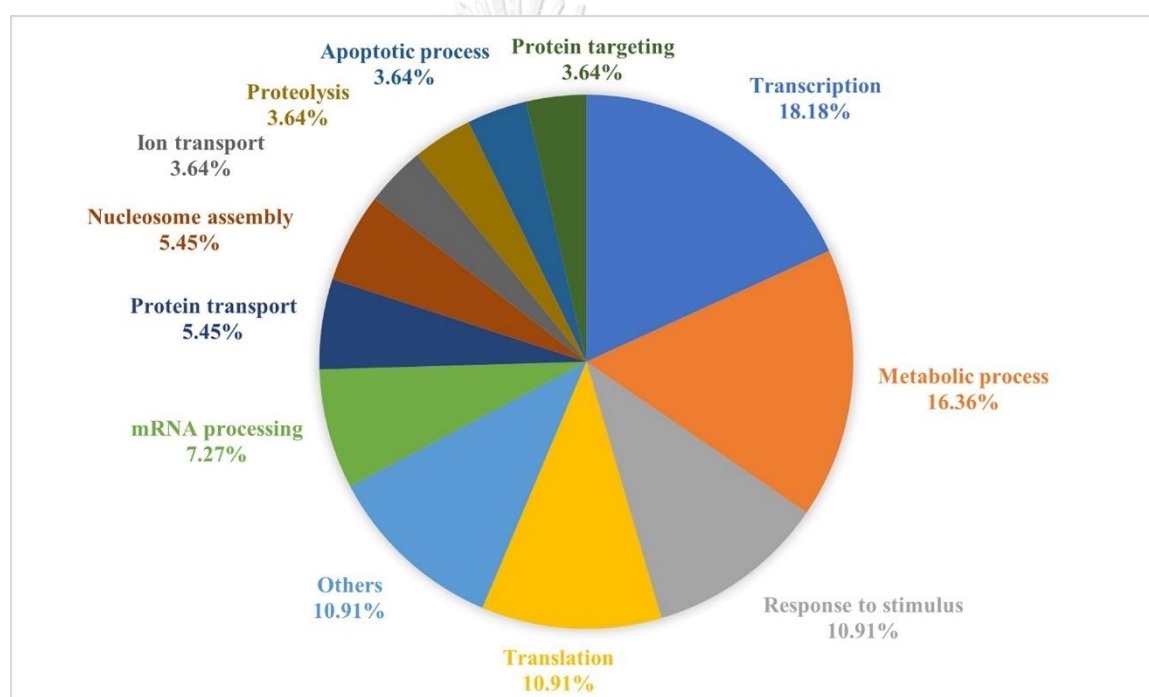


Figure 4.5 The differentially expressed proteins from the monolayer system were analyzed based on biological process.

The protein-protein interactions of 55 proteins with 1.5 up-and downregulation were analyzed by the STRING database and were used to predict functions using the GO pathway. Forty four out of 55 proteins showed good interaction as shown in Figure 4.6. Three interesting clusters were involved in regulation of metabolic process (24 proteins), regulation of gene expression (20 proteins), protein transport (22) and binding proteins (36 proteins). Some proteins were involved in many functions such as legumain

(LGMN), heat shock-related 70 kDa protein 2 (HSPA2), heat shock protein HSP 90-alpha (HSP90AA1), profilin-1 (PFN1), heterogeneous nuclear ribonucleoproteins C1/C2 (HNRNPC), 40S ribosomal protein S15a (RPS15A) and peroxiredoxin-5, mitochondrial (PRDX5).

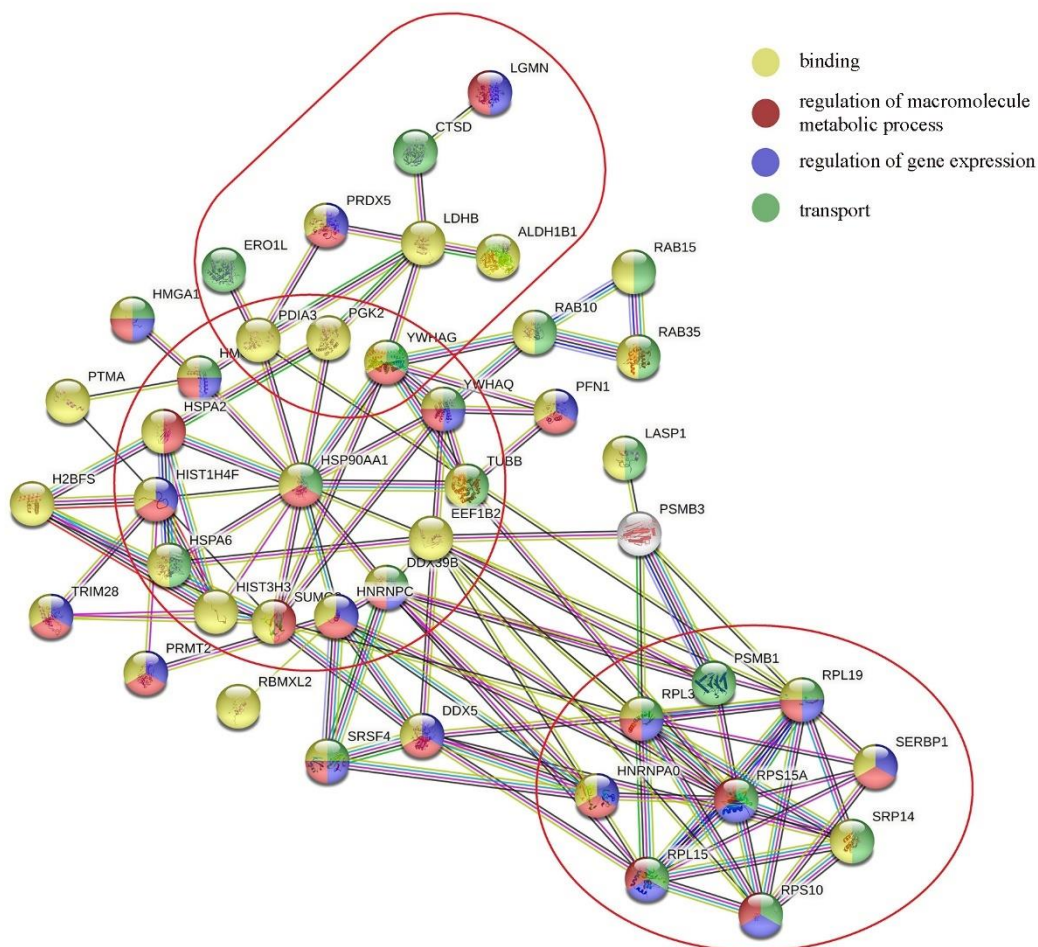


Figure 4.6 Nicotine induces differential protein expression in the A549 cells from monolayer culture (flask). The differentially expressed proteins were used to search the STRING database to predict their protein-protein interactions.

4.4.6 Validation of differential protein expression in untreated and nicotine treated A549 cells using western blot analysis

To confirm the expression of proteins from LC-MS/MS, legumain (LGMN), heat shock-related 70 kDa protein 2 (HSPA2), heat shock protein

HSP 90-alpha (HSP90AA1), protein disulfide-isomerase A3 (PDIA3) and profilin-1 (PFN1) were selected for western blot analysis. The results, shown in Figure 4.7, indicate that the expression level of all selected proteins was higher in nicotine treated A549 cells, when compared to untreated control cells, especially regarding legumain and profilin-1.

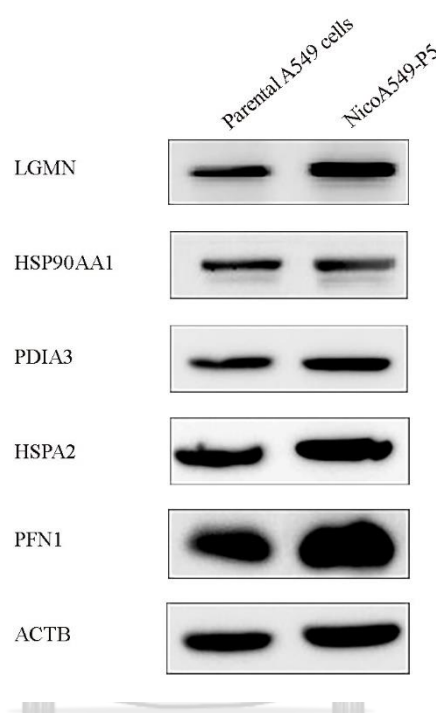


Figure 4.7 The expression levels of the dysregulated proteins from monolayer system were verified by western blot analysis. Western blot showing the expression of selected proteins in untreated and nicotine treated A549 cells.

4.4.7 Label free quantitative proteomic analysis of untreated and nicotine treated A549 cells in invasion system

Since label free quantitative mass spectrometry did not require large amounts of proteins, so we used the invaded cells from the Boyden transwell chambers to compare differential expression between cells treated with nicotine and untreated cells. Three replicated runs were performed using LC-MS/MS to increase the reproducibility of results, and differential protein expression was determined by calculating with Progenesis QI software version 3.1. Our results

showed that 100 proteins exhibited differential expression in the invasion system, using cut-off criteria of ANOVA p-value ≤ 0.05 , with fold change greater than 1.25. From the 100 identified proteins affected by nicotine treatment, 24 proteins were up-regulated and 76 proteins were down-regulated in nicotine treated A549-L5 cells, compared to untreated A549-L5 cells, as shown in Tables 4.3 and 4.4. The highest increase in expression level of up-regulated proteins was 2.03-fold found in Obg-like ATPase 1 (OLA1), while the lowest expression level in down-regulated proteins was 1.85-fold found in sarcoplasmic/endoplasmic reticulum calcium ATPase 2 (ATP2A2). The up-regulated and down-regulated proteins from Table 4.3 and 4.4 were then analyzed using the UniProt database to classify functions as shown in Figure 4.8. Proteins were classified as follows: translation, metabolic process, mRNA processing, transcription, cell division, response to stimulus, cytoskeleton, cell migration, protein targeting, nucleosome assembly, apoptotic process, and others. The major proteins involved in translation is 20.00% of the proteins.

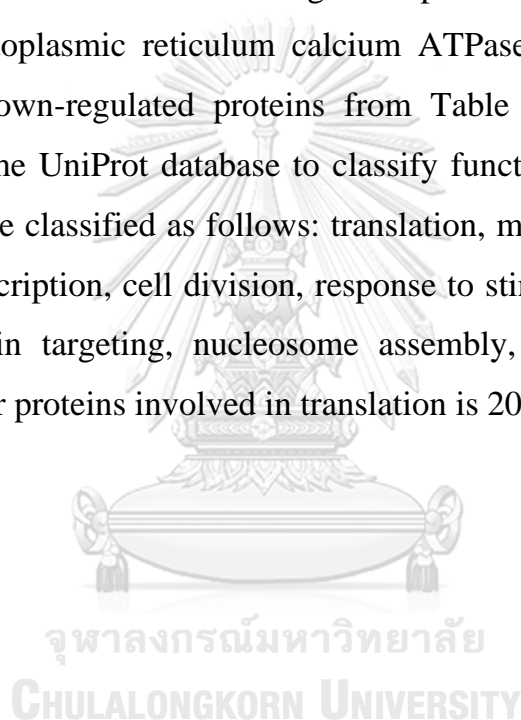


Table 4.3 List of up-regulated proteins from the invasion system

No.	Accession	Gene	Protein name	Peptide count	Score	Mass	pI	Protein fold change	Protein function
1	OLA1_HUMAN	OLA1	Obg-like ATPase 1	2	88.41	44715	7.64	2.03	Metabolic process
2	ETFB_HUMAN	ETFB	Electron transfer flavoprotein subunit beta	2	43.58	27826	8.24	1.92	Metabolic process
3	UCHL1_HUMAN	UCHL1	Ubiquitin carboxyl-terminal hydrolase isozyme L1	2	77.81	24808	5.33	1.86	Response to stimulus
4	ANXA5_HUMAN	ANXA5	Annexin A5	2	70.01	35914	4.94	1.79	Signal transduction
5	ATPB_HUMAN	ATP5B	ATP synthase subunit beta, mitochondrial	4	199.85	56525	5.26	1.71	Metabolic process
6	1433T_HUMAN	YWHAQ	14-3-3 protein theta	5	211.66	27747	4.68	1.65	Protein targeting
7	ALDOA_HUMAN	ALDOA	Fructose-bisphosphate aldolase A	6	107.82	39395	8.3	1.58	Metabolic process
8	RL6_HUMAN	RPL6	60S ribosomal protein L6	11	291.02	32708	10.59	1.50	Translation
9	IMA1_HUMAN	KPNA2	Importin subunit alpha-1	3	67.15	57826	5.25	1.40	Metabolic process
10	1433G_HUMAN	YWHAG	14-3-3 protein gamma	5	187.96	28285	4.8	1.37	Protein targeting
11	CISY_HUMAN	CS	Citrate synthase,	2	58.56	51680	8.45	1.33	Metabolic process

No.	Accession	Gene	Protein name	Peptide count	Score	Mass	pI	Protein fold change	Protein function
			mitochondrial						
12	SAHH_HUMAN	AHCY	Adenosylhomocysteinase	3	41.89	47685	5.92	1.33	Metabolic process
13	ASNS_HUMAN	ASNS	Asparagine synthetase [glutamine-hydrolyzing]	2	51.26	64329	6.39	1.32	Metabolic process
14	RS21_HUMAN	RPS21	40S ribosomal protein S21	2	41.98	9106	8.68	1.29	Translation
15	LGMN_HUMAN	LGMN	Legumain	1	55.43	49379	6.07	1.28	Proteolysis
16	NONO_HUMAN	NONO	Non-POU domain-containing octamer-binding protein	5	160.71	54197	9.01	1.28	mRNA processing
17	WDR36_HUMAN	WDR36	WD repeat-containing protein 36	2	34.02	105255	7.32	1.28	Response to stimulus
18	PUR9_HUMAN	ATIC	Bifunctional purine biosynthesis protein PURH	2	55.38	64616	6.27	1.28	Metabolic process
19	1433Z_HUMAN	YWHAZ	14-3-3 protein zeta/delta	4	311.6	27728	4.73	1.26	Protein targeting
20	ROA2_HUMAN	YWHAZ	Heterogeneous nuclear ribonucleoproteins A2/B1	25	946.49	37407	8.97	1.26	mRNA processing

No.	Accession	Gene	Protein name	Peptide count	Score	Mass	pI	Protein fold change	Protein function
21	K1C19_HUMAN	KRT19	Keratin, type I cytoskeletal 19	2	62.05	44079	5.04	1.26	Cytoskeleton
22	SAP_HUMAN	PSAP	Prosaposin	6	98.47	58074	5.06	1.25	Metabolic process
23	EIF3A_HUMAN	EIF3A	Eukaryotic translation initiation factor 3 subunit A	4	92.05	166468	6.38	1.25	Translation
24	ETFA_HUMAN	ETFA	Electron transfer flavoprotein subunit alpha, mitochondrial	6	142.12	35058	8.62	1.25	Metabolic process

Table 4.4 List of down-regulated proteins from the invasion system

No.	Accession	Gene	Protein name	Peptide count	Score	Mass	pI	Protein fold change	Protein function
1	AT2A2_HUMAN	ATP2A2	Sarcoplasmic/endoplasmic reticulum calcium ATPase 2	2	35.72	114683	5.23	1.85	Localization
2	MCM7_HUMAN	MCM7	DNA replication licensing factor MCM7	2	33.79	81257	6.08	1.74	DNA replication
3	LRC59_HUMAN	LRRC59	Leucine-rich repeat-containing protein 59	3	49.47	34909	9.61	1.74	Signal transduction
4	PA2G4_HUMAN	PA2G4	Proliferation-associated protein 2G4	4	61.65	43759	6.13	1.70	Translation
5	COR1C_HUMAN	CORO1C	Coronin-1C	2	37.73	53215	6.65	1.68	Cell division
6	RCC2_HUMAN	RCC2	Protein RCC2	4	128.44	56049	9.02	1.67	Cell division
7	DAZP1_HUMAN	DAZP1	DAZ-associated protein 1	3	59.83	43356	8.73	1.66	mRNA processing
8	MBB1A_HUMAN	MYBBP1A	Myb-binding protein 1A	2	32.41	148762	9.34	1.66	Transcription
9	ENOA_HUMAN	ENO1	Alpha-enolase	17	1201.93	47139	7.01	1.66	Transcription
10	RS26_HUMAN	RPS26	40S ribosomal protein S26	3	57	13007	11.01	1.62	Translation

No.	Accession	Gene	Protein name	Peptide count	Score	Mass	pI	Protein fold change	Protein function
11	EF1B_HUMAN	EEF1B2	Elongation factor 1-beta	3	95.39	24748	4.5	1.61	Translation
12	HMGB2_HUMAN	HMGB2	High mobility group protein B2	3	51.06	24019	7.62	1.60	Transcription
13	DSRAD_HUMAN	ADAR	Double-stranded RNA-specific adenosine deaminase	3	62.37	135981	8.86	1.54	mRNA processing
14	RS16_HUMAN	RPS16	40S ribosomal protein S16	3	67.2	16435	10.21	1.52	Translation
15	H2AV_HUMAN	H2AFV	Histone H2A.V	7	193.91	13501	10.58	1.52	Nucleosome assembly
16	H4_HUMAN	HIST1H4F	Histone H4	16	482.92	11360	11.36	1.51	Nucleosome assembly
17	RPN1_HUMAN	RPN1	Dolichyl-diphosphooligosaccharide--protein glycosyltransferase subunit 1	3	82.55	68527	5.96	1.50	Protein glycosylation
18	THOC4_HUMAN	ALYREF	THO complex subunit 4	4	98.35	26872	11.15	1.48	mRNA processing

No.	Accession	Gene	Protein name	Peptide count	Score	Mass	pI	Protein fold change	Protein function
19	RL23_HUMAN	RPL23	60S ribosomal protein L23	2	97.64	14856	10.51	1.46	Translation
20	HNRL1_HUMAN	HNRNPUL1	Heterogeneous nuclear ribonucleoprotein U-like protein 1	3	114.27	95679	6.49	1.45	mRNA processing
21	XRCC6_HUMAN	XRCC6	X-ray repair cross-complementing protein 6	14	373.74	69799	6.23	1.45	Transcription
22	PTBP1_HUMAN	PTBP1	Polypyrimidine tract-binding protein 1	10	265.16	57186	9.22	1.45	mRNA processing
23	RL24_HUMAN	RPL24	60S ribosomal protein L24	2	50.82	17768	11.26	1.40	Translation
24	RRP5_HUMAN	PDCD11	Protein RRP5 homolog	2	47.33	208570	8.99	1.40	mRNA processing
25	TXD17_HUMAN	TXNDC17	Thioredoxin domain-containing protein 17	2	72.27	13932	5.4	1.39	Metabolic process
26	SND1_HUMAN	SND1	Staphylococcal nuclease domain-containing protein 1	3	43.17	101934	6.74	1.39	Transcription
27	API5_HUMAN	API5	Apoptosis inhibitor 5	3	86.99	58968	6.99	1.39	Apoptotic process

No.	Accession	Gene	Protein name	Peptide count	Score	Mass	pI	Protein fold change	Protein function
28	G3P_HUMAN	GAPDH	Glyceraldehyde-3-phosphate dehydrogenase	20	802.92	36030	8.57	1.37	Translation
29	TAGL2_HUMAN	TAGLN2	Transgelin-2	6	202.4	22377	8.41	1.37	Epithelial cell differentiation
30	ICAL_HUMAN	CAST	Calpastatin	2	36.4	76526	4.97	1.37	Protease inhibitor
31	PARP1_HUMAN	PARP1	Poly [ADP-ribose] polymerase 1	5	198.26	113012	8.99	1.37	Transcription
32	LAP2A_HUMAN	TMPO	Lamina-associated polypeptide 2, isoform alpha	7	102.07	75446	7.56	1.37	Transcription
33	TOP1_HUMAN	TOP1	DNA topoisomerase 1	2	35.76	90669	9.33	1.37	DNA replication
34	RS6_HUMAN	RPS6	40S ribosomal protein S6	2	56.56	28663	10.85	1.37	Translation
35	U2AF2_HUMAN	U2AF2	Splicing factor U2AF 65 kDa subunit	3	43.95	53467	9.19	1.36	mRNA processing
36	IF4A1_HUMAN	EIF4A1	Eukaryotic initiation factor 4A-I	4	98.46	46125	5.32	1.35	Translation

No.	Accession	Gene	Protein name	Peptide count	Score	Mass	pI	Protein fold change	Protein function
37	RBM14_HUMAN	RBM14	RNA-binding protein 14	4	86.34	69449	9.68	1.35	Transcription
38	PEBP1_HUMAN	PEBP1	Phosphatidylethanolamine-binding protein 1	8	272.83	21044	7.01	1.35	Protease inhibitor
39	RSSA_HUMAN	RPSA	40S ribosomal protein SA	9	249.39	32833	4.79	1.35	Translation
40	TOP2A_HUMAN	TOP2A	DNA topoisomerase 2-alpha	6	250.02	174276	8.82	1.35	Apoptotic process
41	K2C7_HUMAN	KRT7	Keratin, type II cytoskeletal 7	20	1372.11	51354	5.4	1.34	Cytoskeleton
42	HNRH1_HUMAN	HNRNPH1	Heterogeneous nuclear ribonucleoprotein H	11	389.81	49198	5.89	1.34	mRNA processing
43	EFTU_HUMAN	TUFM	Elongation factor Tu, mitochondrial	7	204.84	49510	7.26	1.34	Translation
44	PCBP1_HUMAN	PCBP1	Poly(rC)-binding protein 1	7	206.6	37474	6.66	1.34	mRNA processing
45	CAVN1_HUMAN	PTRF	Caveolae-associated protein 1	2	43.86	43450	5.51	1.34	Transcription
46	ANXA1_HUMAN	ANXA1	Annexin A1	24	779.9	38690	6.57	1.34	Cell migration

No.	Accession	Gene	Protein name	Peptide count	Score	Mass	pI	Protein fold change	Protein function
47	RUVB1_HUMAN	RUVBL1	RuvB-like 1	2	43.96	50196	6.02	1.33	Cell division
48	PAIRB_HUMAN	SERBP1	Plasminogen activator inhibitor 1 RNA-binding protein	6	187.57	44938	8.66	1.33	Apoptotic process
49	PRDX1_HUMAN	PRDX1	Peroxiredoxin-1	2	64.8	22096	8.27	1.32	Response to stimulus
50	NUCL_HUMAN	NCL	Nucleolin	4	39.86	76568	4.6	1.32	Transcription
51	BUB3_HUMAN	BUB3	Mitotic checkpoint protein BUB3	4	96.17	37131	6.36	1.32	Cell division
52	K2C8_HUMAN	KRT8	Keratin, type II cytoskeletal 8	17	979.99	53671	5.52	1.31	Cytoskeleton
53	LMNA_HUMAN	LMNA	Prelamin-A/C	12	735.27	74095	6.57	1.31	Cell migration
54	RL19_HUMAN	RPL19	60S ribosomal protein L19	3	130.86	23451	11.48	1.31	Translation
55	TBB5_HUMAN	TUBB	Tubulin beta chain	10	397	49639	4.78	1.31	Cell division
56	H2A2B_HUMAN	ST2H2AB	Histone H2A type 2-B	5	104.73	13987	10.88	1.31	Nucleosome assembly
57	S10A4_HUMAN	S100A4	Protein S100-A4	2	44.71	11721	5.85	1.31	Cell migration

No.	Accession	Gene	Protein name	Peptide count	Score	Mass	pI	Protein fold change	Protein function
58	UBA1_HUMAN	UBA1	Ubiquitin-like modifier-activating enzyme 1	4	108.03	117774	5.49	1.31	Response to stimulus
59	K1C18_HUMAN	KRT18	Keratin, type I cytoskeletal 18	25	817.92	48029	5.34	1.30	Cytoskeleton
60	PRS6A_HUMAN	PSMC3	26S proteasome regulatory subunit 6A	3	77.22	49172	5.13	1.30	Transcription
61	EWS_HUMAN	EWSR1	RNA-binding protein EWS	4	87.32	68436	9.37	1.29	Transcription
62	PRP8_HUMAN	PRPF8	Pre-mRNA-processing-splicing factor 8	3	83.55	273427	8.95	1.28	mRNA processing
63	SRP09_HUMAN	SRP9	Signal recognition particle 9 kDa protein	2	50.6	10105	7.76	1.28	Translation
64	STIP1_HUMAN	STIP1	Stress-induced-phosphoprotein 1	3	96.86	62599	6.4	1.28	Response to stimulus
65	HNRL2_HUMAN	HNRNPUL2	Heterogeneous nuclear ribonucleoprotein U-like protein 2	2	50.33	85052	4.85	1.28	mRNA processing

No.	Accession	Gene	Protein name	Peptide count	Score	Mass	pI	Protein fold change	Protein function
66	LA_HUMAN	SSB	Lupus La protein	2	40.48	46808	6.68	1.27	tRNA processing
67	NOP56_HUMAN	NOP56	Nucleolar protein 56	4	97.52	66009	9.24	1.27	rRNA processing
68	GLU2B_HUMAN	PRKCSH	Glucosidase 2 subunit beta	3	54.97	59388	4.33	1.26	Metabolic process
69	MDHC_HUMAN	MDHI	Malate dehydrogenase, cytoplasmic	2	67.37	36403	6.91	1.26	Metabolic process
70	PADI1_HUMAN	PADI1	Protein-arginine deiminase type-1	2	41.54	74618	6.07	1.26	Chromatin organization
71	HNRPF_HUMAN	HNRNPF	Heterogeneous nuclear ribonucleoprotein F	6	174.75	45643	5.38	1.26	mRNA processing
72	RL3_HUMAN	RPL3	60S ribosomal protein L3	3	65.62	46080	10.19	1.25	Translation
73	RS5_HUMAN	RPS5	40S ribosomal protein S5	4	176.77	22862	9.73	1.25	Translation
74	RLA0_HUMAN	RPLP0	60S acidic ribosomal protein P0	2	51.81	34252	5.71	1.25	Translation
75	RAB7A_HUMAN	RAB7A	Ras-related protein Rab-7a	2	58.11	23475	6.4	1.25	Protein transport
76	RS28_HUMAN	RPS28	40S ribosomal protein S28	2	86.98	7836	10.7	1.25	Translation

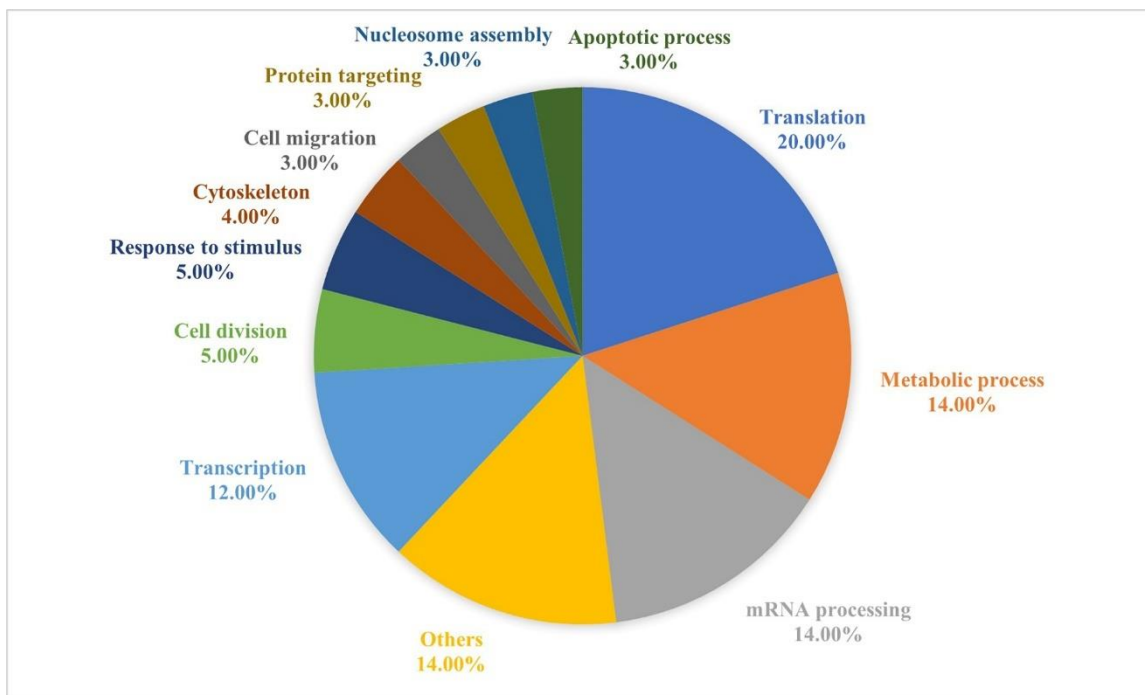


Figure 4.8 The differentially expressed proteins from invasion system were analyzed based for biological process.

4.4.8 Validation of the identified proteins from LC-MS/MS from invasion system

To validate the expression level of proteins from LC-MS/MS, legumain (LGMN), heat shock-related 70 kDa protein 2 (HSPA2), heat shock protein HSP 90-alpha (HSP90AA1), protein disulfide-isomerase A3 (PDIA3) and profilin-1 (PFN1) were selected for western blot analysis. The results, shown in Figure 4.9, indicate that the expression level of all selected proteins was increased in nicotine treated A549 cells, when compared to untreated control cells.

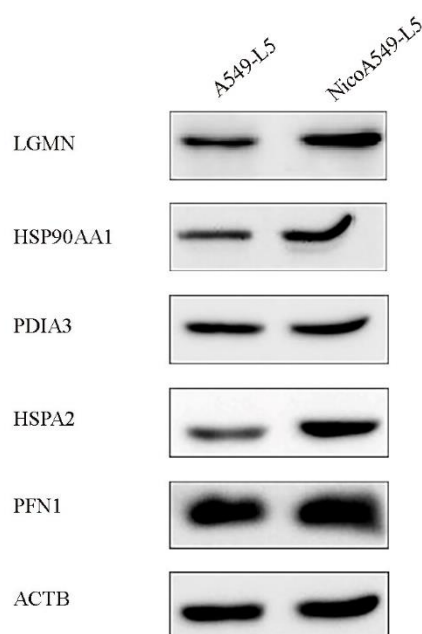


Figure 4.9 The expression levels of the dysregulated proteins from invasion system were verified by western blot analysis. Western blot showing the expression of selected proteins in untreated A549-L5 and nicotine treated A549-L5 cells.

4.5 Discussion

The aim of the studies was to investigate the effect of prolonged exposure of nicotine on non-small cell lung cancer using the A549 cell line as a model. Thus, the effect of nicotine on cytotoxicity and invasion was studied in the A549 cell line, and proteomic techniques were used to analyze differential protein expression in A549 cells treated and not treated with nicotine. The label-free quantitative proteomic technique was adapted to ensure that small amounts of protein, such as 100 ng, would be sufficient to show changes in the level of expression. First, the expressed proteins from nicotine-treated and untreated cells in the monolayer system. Then, results were confirmed by studying the proteins collected from the cells invading through the Boyden

chamber. Since the A549 cells were highly invasive, sufficient proteins could be obtained from the invaded cells to show differences in expression with and without nicotine treatment. The advantage of using the Boyden chamber in our work was that there was no interference by cell proliferation, and any changes found should only involve cell motility.

Based on the results of MTT cell viability assay, the IC_{50} concentration of nicotine was determined to be 16, 12 and 7 mM with incubation periods of 24 h, 48 h and 72 h, respectively. In agreement with Tao Gao et al. (119), nicotine did not show any significant effect on the A549 cell line at the dose of 0.01 μ M. The invasive property of A549 cells was studied using Boyden chamber assays at non-cytotoxic concentrations. In agreement with the reports of Dasgupta et al. (63) and Sun et al. (120), these results indicated that nicotine induced A549 cell invasion in a dose-dependent manner. To gain insight into the molecular events resulting from prolonged nicotine exposure on cell invasion, an invasive subpopulation of A549 lung cancer cell line was selected. In comparison with A549 parental cells, the invasive capacity was gradually increased during the subpopulation selection by 1.25-fold to 2.6-fold. Yi et al. (121) found that five sublines from the human lung cancer cell line CL1 showed 4-fold to 6-fold higher invasive capability through the basement membrane matrix, as compared to the parental cells. The results of present study agree with those of Amaro et al. (122), who isolated an invading subpopulation of the breast cancer MDA-MB-231 cells by repeated selection, which showed greater invasive potential as compared to parental cells. Interestingly, these findings indicated that the invasive capacity of NicoA549-L5 was significantly increased by 2.6-fold, as compared to parental cells. In agreement with previous studies, the effect of prolonged exposure to nicotine enhances more invasive and metastatic properties in numerous types of cancer cells, such as breast, lung, and oral cancers (123, 124).

Label-free mass spectrometry has now become a powerful technique in a variety of biological and life science areas. As a result, a high-throughput software program is necessary to process massive proteomic data obtained from LC-MS/MS analysis (125). There are several software programs available to convert raw MS data into quantified protein abundances. Progenesis QI software is one proteomic software that performed very well based on the evaluation of previous research (126). This software allows researchers to quantify and identify proteins that are changing significantly in the samples.

In this study, the label-free quantitative mass spectrometry technique was used to compare the proteins from nicotine-treated and untreated A549 cells in the monolayer system. Data analysis was performed using Progenesis QI software. The results showed 55 up-regulated and down-regulated proteins, which could be linked into 3 interesting clusters by protein-protein interaction analysis. LGMN, HSP90AA1, PDIA3, HSPA2 and PFN1 were selected for validation by immunodetection and the results of all 5 proteins showed up-regulated expression when treated with nicotine, in agreement with the mass spectrometry results. The functions of these five proteins are proteolysis for LGMN, response to stimulus for HSP90AA1, PDIA3 and HSPA2 and metabolic process for PFN1. The results were further confirmed our results by label-free quantitative LC/MS/MS of nicotine-treated and untreated cells, by collecting proteins from the cells which invaded through the Boyden chamber. One hundred proteins were identified from the invasion system and found the same up-regulated proteins for validation.

Legumain (LGMN) or asparagine endopeptidase plays a role in the cell invasion and migration (127). There have been several studies on legumain expression in cancer cells, but the expression of legumain in A549 NSCLC treated with nicotine has never been investigated. The result demonstrated in this study is the first report showing higher expression of legumain in A549 cells when treated with nicotine, both in monolayer system and in the invasion

system. Legumain has been found in plants, invertebrate parasites, and mammals (128). It is known to be expressed in various human tissues such as placenta, kidney, liver, spleen, and testis (129). Legumain could directly degrade fibronectin, the main component of extracellular matrix protein (130). It has also been found to cleave pro-gelatinase A into gelatinase A in HT1080 fibrosarcoma cell line and plays a role in the extracellular matrix remodeling and degradation to make cell invasion and migration (127). Emerging evidence indicated that overexpression of legumain is associated with several types of human solid tumor, including breast and colorectal cancers (131-133). Tumor cells overexpressing legumain possess increased migratory activity *in vitro* and present invasive and metastatic phenotypes *in vivo*. Thus, legumain may be involved in tumor invasion and metastasis by degradation of extracellular matrix proteins (132).

Heat shock proteins (HSPs) are molecular chaperone proteins found in the cells of organisms. They are vital for the newly formed proteins and also lead to the repair or degradation of denatured proteins after stress or injury. In a wide variety of human cancers, HSPs are overexpressed and involved in the proliferation, differentiation, invasion, and metastasis of tumor cells. This family of proteins are induced by a variety of stresses including nicotine (134). The results herein showed higher expression of HSPA2 and HSP90AA1 in A549 cells, when treated with nicotine in both the monolayer system and in the invasion system.

Heat shock protein HSP 90- α (HSP90AA1) is a member of the heat shock protein 90 family which is present in most mammalian cells and seems to be important to cancer cells survival. There are many studies that disclose the role of HSP90AA1 in cancer invasion and metastasis. It is involved in the migration of neuronal cells, melanoma cells, and lung cancer cells (135-137). Wu et al. (138) reported the involvement of nicotine and HSP90AA1. They found that nicotine can induce the higher expression level of HSP90AA1

protein. Furthermore, HSP90AA1 has been found to form a complex with prolegumain which promotes its intracellular stability and secretion. Disrupting the interaction between HSP90AA1 and prolegumain allowed the secretion of prolegumain to be decreased, and thus tumor growth was positively impacted by reduced metastasis (128). These information may explain the findings in a current study that both legumain and HSP90AA1 are overexpressed after the treatment of cells with nicotine.

Heat shock-related 70 kDa protein 2 (HSPA2) is another heat shock protein member required for the development of numerous cancers (139). Jagadish et al. (140) could observe the overexpression of HSP70 in breast cancer patients and four different breast cancer cell lines. They also suggested that HSP70 play an important role for cellular motility, migration, and invasion. Increased expression of HSP70 was also found in A549 cells to protect them from hypoxic injury and to respond to zinc oxide nanoparticles exposure (141, 142). The exposure of cigarette smoke has been reported as another cause for inducing the up-regulated expression of HSP70 in rat brain (143).

Protein disulfide isomerase (PDI) is a molecular chaperone which has a role in maintaining cellular homeostasis through oxidative protein folding mediation. Increasing data indicates that PDI promotes various cancers' survival and progression (144). The effect of nicotine exposure on PDI expression were reported in some research (145, 146). The current study showed that treatment of A549 cells with nicotine led to increased expression of PDIA3 in both the monolayer and invasion systems. The protein disulfide isomerase A3 (PDIA3) known as ERp57 is a thiol-oxidoreductase chaperone. The overexpression of it has been observed in different types of cancers, including ovarian, mammary, uterine, pulmonary, gastric cancers, and hepatocellular carcinoma (147). The findings of present study were consistent

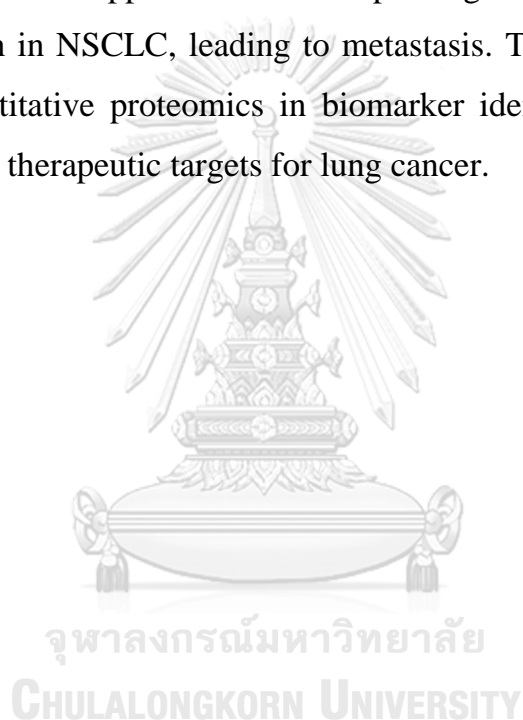
with several previous studies that considered PDIA3 to be involved in the induction of cancer cell migration and invasion. (148, 149).

Actin rearrangement is fundamental in cell motility, which is also significant the metastatic cascade. Actin filament elasticity is a determining point for an efficient metastasis. The cycle of generating and decomposition of actin microfilaments is controlled by actin-binding proteins. One of the important actin-binding proteins is profilin-1.

Profilin-1 (PFN1) is a small actin-binding protein that regulates actin remodeling and facilitate cancer cell metastases. Recent study has demonstrated changes in the expression of profilin-1 in multiple types of cancer such as breast, pancreatic, hepatic, gastric and lung cancer (150). The investigation here showed higher expression of profilin-1 in A549 cells when treated with nicotine in both the monolayer system and in the invasion system. Moreover, the expression of profilin-1 is significantly higher when cells were treated with nicotine in monolayer system. The increased expression of profilin-1 in A549 was previously observed in the study of Ali et al. (151). The authors provided the evidence that the high expression of profilin-1 regulates metastatic property of cancer cell. The role of nicotine treatment among cancer cell types has been investigated previously as well. Paulo et al. (152) compared the proteomic alterations induced by nicotine treatment in pancreatic cells. They found the significantly different relative abundance of profilin-1 when comparing nicotine-treated and untreated cells. The result of the present study, together with these previous reports, suggest that nicotine can induce the expression of profilin-1 and lead to metastasis in A549 cells.

These studies indicate that nicotine is correlated with the metastasis of lung cancer, which can be further studied by label-free quantitative proteomics to identify the precise targets of action. In addition, studies also exhibit that the changes in protein expression may alter cancer in several pathways depending

on the function of that protein such as cell metabolism, proliferation, migration, and apoptosis. For the first time, the studies show high expression of legumain in A549 cells when treated with nicotine. Legumain expression appears to be associated with nicotine treatment and increased tumor invasion. These findings suggest that legumain, heat shock protein HSP 90-alpha, heat shock-related 70 kDa protein 2, protein disulfide isomerase A3 and profilin-1 could be significant biomarkers for lung cancer therapy. Taken together, these results provide strong data to support the idea that prolonged exposure of nicotine can promote invasion in NSCLC, leading to metastasis. This study testifies to the strength of quantitative proteomics in biomarker identification, allowing the discovery of new therapeutic targets for lung cancer.



CHAPTER 5

CONCLUSIONS

From two main parts of the study, it is concluded that mass spectrometry is a powerful technique which can be used for both quantitative and qualitative applications.

The first part of the study investigated the production and distribution of diterpenoid phytoalexins in Thai rice using MALDI-MSI. Results revealed both localization and identification of target phytoalexins on a leaf tissue section. Five types of diterpenoid phytoalexins were successfully detected on RD6 rice leaf tissue, including momilactone-A (m/z 353.17), momilactone-B (m/z 369.16), phytocassane-A, D, or E (m/z 355.18), phytocassane-B (m/z 373.19) and phytocassane-C (m/z 357.20). MSI data correlated with the results from the MALDI-MS of rice leaf extraction. Moreover, the structure of momilactone-A, phytocassane-A, D, or E and phytocassane-C was also determined using the MS/MS technique.

The second part of the study investigated the protein alterations in human non-small cell lung cancer cell line A549 upon treating with nicotine using label-free quantitative proteomic method. Fifty five proteins from monolayer system and 100 proteins from invasion system were identified with a change in expression level after prolonged nicotine treatment. The candidate proteins were chosen and confirmed their expression level by western blot analysis. Results from western blot experiment revealed the higher expression of legumain in A549 cells when treated with nicotine. Its expression appears to be associated with nicotine treatment and the increased tumor invasion. Other proteins such as heat shock proteins, protein disulfide isomerase A3 and profilin also showed higher expression in nicotine treated A549 cells.

Overall, mass spectrometry is a useful and reliable technique for biological molecule detection, representing new possibilities for diverse applications in the future.



REFERENCES

1. El-Aneed A, Cohen A, Banoub J. Mass spectrometry, review of the basics: electrospray, MALDI, and commonly used mass analyzers. *Appl Spectrosc Rev.* 2009;44(3):210-30.
2. Muddiman DC. Jürgen H. Gross: Mass spectrometry: a textbook, 3rd ed. *Anal Bioanal Chem.* 2018;410(8):2051-2.
3. Laiko VV, Baldwin MA, Burlingame AL. Atmospheric pressure matrix-assisted laser desorption/ionization mass spectrometry. *Anal Chem.* 2000;72(4):652-7.
4. Dole M, Mack LL, Hines RL, Mobley RC, Ferguson LD, Alice MB. Molecular beams of macroions. *J Chem Phys.* 1968;49(5):2240-9.
5. Pramanik BN, Ganguly AK, Gross ML. Applied electrospray mass spectrometry: practical spectroscopy series volume 32: CRC Press; 2002.
6. Banerjee S, Mazumdar S. Electrospray ionization mass spectrometry: a technique to access the information beyond the molecular weight of the analyte. *Int J Anal Chem.* 2012;2012:282574.
7. Wolff M, Stephens W. A pulsed mass spectrometer with time dispersion. *Rev Sci Instrum.* 1953;24(8):616-7.
8. Gross JH. Mass spectrometry: a textbook: Springer Science & Business Media; 2006.
9. Thomas SN. Chapter 10 - Mass spectrometry. In: Clarke W, Marzinke MA, editors. *Contemporary practice in clinical chemistry* 4th ed: Academic Press; 2019. p. 171-85.
10. Dong Y, Li B, Malitsky S, Rogachev I, Aharoni A, Kaftan F, et al. Sample preparation for mass spectrometry imaging of plant tissues: a review. *Front Plant Sci.* 2016;7:60.
11. Buchberger AR, DeLaney K, Johnson J, Li L. Mass spectrometry imaging: a review of emerging advancements and future insights. *Anal Chem.*

- 2018;90(1):240-65.
12. Bjarnholt N, Li B, D'Alvise J, Janfelt C. Mass spectrometry imaging of plant metabolites—principles and possibilities. *Nat Prod Rep*. 2014;31(6):818-37.
 13. Boughton BA, Thinagaran D, Sarabia D, Bacic A, Roessner U. Mass spectrometry imaging for plant biology: a review. *Phytochem Rev*. 2016;15(3):445-88.
 14. De Laeter JR. Applications of inorganic mass spectrometry: John Wiley & Sons; 2001.
 15. Gemperline E, Keller C, Jayaraman D, Maeda J, Sussman MR, Ané J-M, et al. Examination of endogenous peptides in *Medicago truncatula* using mass spectrometry imaging. *J Proteome Res*. 2016;15(12):4403-11.
 16. Piehowski PD, Zhu Y, Bramer LM, Stratton KG, Zhao R, Orton DJ, et al. Automated mass spectrometry imaging of over 2000 proteins from tissue sections at 100- μ m spatial resolution. *Nat Commun*. 2020;11(1):8.
 17. Lu Q, Hu Y, Chen J, Jin S. Laser desorption postionization mass spectrometry imaging of folic acid molecules in tumor tissue. *Anal Chem*. 2017;89(16):8238-43.
 18. Mallah K, Quanico J, Raffo-Romero A, Cardon T, Aboulouard S, Devos D, et al. Matrix-assisted laser desorption/ionization-mass spectrometry imaging of lipids in experimental model of traumatic brain injury detecting acylcarnitines as injury related markers. *Anal Chem*. 2019;91(18):11879-87.
 19. Schulz S, Becker M, Groseclose MR, Schadt S, Hopf C. Advanced MALDI mass spectrometry imaging in pharmaceutical research and drug development. *Curr Opin Biotechnol*. 2019;55:51-9.
 20. Ntshangase S, Mdanda S, Naicker T, Kruger HG, Baijnath S, Govender T. Spatial distribution of elvitegravir and tenofovir in rat brain tissue: Application of matrix-assisted laser desorption/ionization mass

- spectrometry imaging and liquid chromatography/tandem mass spectrometry. *Rapid Commun Mass Spectrom.* 2019;33(21):1643-51.
21. Gnanamanickam SS. Rice and its importance to human life. *Biological control of rice diseases*. 8. Dordrecht, Netherlands: Springer; 2009. p. 1-11.
 22. Khush GS. What it will take to feed 5.0 billion rice consumers in 2030. *Plant Mol Biol.* 2005;59(1):1-6.
 23. Sesma A, Osbourn A. The rice leaf blast pathogen undergoes developmental processes typical of root-infecting fungi. *Nature.* 2004;431:582-6.
 24. Ebbole DJ. *Magnaporthe* as a model for understanding host-pathogen interactions. *Annu Rev Phytopathol.* 2007;45(1):437-56.
 25. Talbot NJ. On the trail of a cereal killer: exploring the biology of *Magnaporthe grisea*. *Annu Rev Microbiol.* 2003;57(1):177-202.
 26. Disthaporn S. Current rice blast epidemics and their management in Thailand. In: Zeigler RS, Leong SA, Teng PS, editors. *Rice Blast Disease*. Los Banos, Philippines: IRRI; 1994. p. 321-32.
 27. Hammerschmidt R. Phytoalexins: what have we learned after 60 years? *Annu Rev Microbiol.* 1999;37(1):285-306.
 28. Grayer RJ, Kokubun T. Plant–fungal interactions: the search for phytoalexins and other antifungal compounds from higher plants. *Phytochemistry.* 2001;56(3):253-63.
 29. VanEtten HD, Mansfield JW, Bailey JA, Farmer EE. Two classes of plant antibiotics: phytoalexins versus "phytoanticipins". *Plant cell.* 1994;6(9):1191-2.
 30. Müller KO, Borger H. Experimentelle untersuchungen über die *Phytophthora* -resistenz der kartoffel. *Arb Biol Reichsanst Land Forstwirtschaft* 1940;23:189-231.
 31. Ahuja I, Kissen R, Bones AM. Phytoalexins in defense against pathogens. *Trends Plant Sci* 2012;17(2):73-90.

32. Schmelz EA, Huffaker A, Sims JW, Christensen SA, Lu X, Okada K, et al. Biosynthesis, elicitation and roles of monocot terpenoid phytoalexins. *Plant J*. 2014;79(4):659-78.
33. Hasegawa M, Mitsuhara I, Seo S, Imai T, Koga J, Okada K, et al. Phytoalexin accumulation in the interaction between rice and the blast fungus. *Mol Plant Microbe Interact*. 2010;23(8):1000-11.
34. Miyamoto K, Shimizu T, Okada K. Transcriptional regulation of the biosynthesis of phytoalexin: a lesson from specialized metabolites in rice. *Plant Biotechnol*. 2014;31(5):377-88.
35. Bray F, Ferlay J, Soerjomataram I, Siegel RL, Torre LA, Jemal A. Global cancer statistics 2018: GLOBOCAN estimates of incidence and mortality worldwide for 36 cancers in 185 countries. *CA Cancer J Clin*. 2018;68(6):394-424.
36. Siegel RL, Miller KD, Jemal A. Cancer statistics, 2020. *CA Cancer J Clin*. 2020;70(1):7-30.
37. IARC. Number of new cases in 2020, both sexes, all ages Lyon: The Global Cancer Observatory; 2020 [updated 2020 December 14th; cited 2021 January 19th]. Available from: <https://gco.iarc.fr/today/data/factsheets/cancers/15-Lung-fact-sheet.pdf>.
38. Crino L, Weder W, Van Meerbeeck J, Felip E. Early stage and locally advanced (non-metastatic) non-small-cell lung cancer: ESMO clinical practice guidelines for diagnosis, treatment and follow-up. *Ann Oncol*. 2010;21(S5):103-15.
39. Cersosimo RJ. Lung cancer: a review. *Am J Health Syst Pharm*. 2002;59(7):611-42.
40. Gillet J-P, Varma S, Gottesman MM. The clinical relevance of cancer cell lines. *J Natl Cancer Inst*. 2013;105(7):452-8.
41. Giard DJ, Aaronson SA, Todaro GJ, Arnstein P, Kersey JH, Dosik H, et al. In vitro cultivation of human tumors: establishment of cell lines derived

- from series of solid tumors. *J Natl Cancer Inst.* 1973;51(5):1417-23.
42. Foster KA, Oster CG, Mayer MM, Avery ML, Audus KL. Characterization of the A549 cell line as a type II pulmonary epithelial cell model for drug metabolism. *Exp Cell Res.* 1998;243(2):359-66.
 43. Shindo-Okada N, Takeuchi K, Han B-S, Nagamachi Y. Establishment of cell lines with high and low metastatic potential from A549 human lung adenocarcinoma. *Jpn J Cancer Res.* 2002;93(1):50-60.
 44. Talhout R, Schulz T, Florek E, van Benthem J, Wester P, Opperhuizen A. Hazardous compounds in tobacco smoke. *Int J Environ Res Public Health.* 2011;8(2):613-28.
 45. Warren GW, Cummings KM. Tobacco and lung cancer: risks, trends, and outcomes in patients with cancer. *Am Soc Clin Oncol Educ Book.* 2013:359-64.
 46. Bharti M, Yashila G. Lung cancer and nicotine. *J Chromatogr Sep Tech.* 2016;7(319):2.
 47. Russell MA, Jarvis M, Iyer R, Feyerabend C. Relation of nicotine yield of cigarettes to blood nicotine concentrations in smokers. *BMJ.* 1980;280(6219):972.
 48. Grando SA. Connections of nicotine to cancer. *Nat Rev Cancer.* 2014;14(6):419-29.
 49. O'Leary K, Parameswaran N, McIntosh JM, Quik M. Cotinine selectively activates a subpopulation of alpha3/alpha6beta2 nicotinic receptors in monkey striatum. *J Pharmacol Exp Ther.* 2008;325(2):646-54.
 50. Benowitz NL, Hukkanen J, Jacob P. Nicotine chemistry, metabolism, kinetics and biomarkers. In: Henningfield JE, London ED, Pogun S, editors. *Nicotine psychopharmacology: Handbook of experimental pharmacology.* 192. Berlin, Heidelberg: Springer; 2009. p. 29-60.
 51. De Biasi M, Dani JA. Reward, addiction, withdrawal to nicotine. *Annu Rev Neurosci.* 2011;34:105-30.

52. Pidoplichko VI, DeBiasi M, Williams JT, Dani JA. Nicotine activates and desensitizes midbrain dopamine neurons. *Nature*. 1997;390(6658):401-4.
53. Heeschen C, Weis M, Aicher A, Dimmeler S, Cooke JP. A novel angiogenic pathway mediated by non-neuronal nicotinic acetylcholine receptors. *J Clin Invest*. 2002;110(4):527-36.
54. Mousa S, Mousa SA. Cellular and molecular mechanisms of nicotine's pro-angiogenesis activity and its potential impact on cancer. *J Cell Biochem*. 2006;97(6):1370-8.
55. Cardinale A, Nastrucci C, Cesario A, Russo P. Nicotine: specific role in angiogenesis, proliferation and apoptosis. *Crit Rev Toxicol*. 2012;42(1):68-89.
56. Lee J, Cooke JP. Nicotine and pathological angiogenesis. *Life Sci*. 2012;91(21):1058-64.
57. Davis R, Rizwani W, Banerjee S, Kovacs M, Haura E, Coppola D, et al. Nicotine promotes tumor growth and metastasis in mouse models of lung cancer. *PLoS One*. 2009;4(10):e7524.
58. Shen T, Le W, Yee A, Kamdar O, Hwang PH, Upadhyay D. Nicotine induces resistance to chemotherapy in nasal epithelial cancer. *Am J Rhinol Allergy*. 2010;24(2):e73-7.
59. Zhang J, Kamdar O, Le W, Rosen GD, Upadhyay D. Nicotine induces resistance to chemotherapy by modulating mitochondrial signaling in lung cancer. *Am J Respir Cell Mol Biol*. 2009;40(2):135-46.
60. Warren GW, Romano MA, Kudrimoti MR, Randall ME, McGarry RC, Singh AK, et al. Nicotinic modulation of therapeutic response in vitro and in vivo. *Int J Cancer*. 2012;131(11):2519-27.
61. Dijk V, Meijssen, Brouwer, Hop, Bergeijk V, Feyereabend, et al. Transdermal nicotine inhibits interleukin 2 synthesis by mononuclear cells derived from healthy volunteers. *Eur J Clin Invest*. 1998;28(8):664-71.
62. Töpfer K, Kempe S, Müller N, Schmitz M, Bachmann M, Cartellieri M, et

- al. Tumor evasion from T cell surveillance. *J Biomed Biotechnol.* 2011;2011:918471.
63. Dasgupta P, Rizwani W, Pillai S, Kinkade R, Kovacs M, Rastogi S, et al. Nicotine induces cell proliferation, invasion and epithelial-mesenchymal transition in a variety of human cancer cell lines. *Int J Cancer.* 2009;124(1):36-45.
64. Dinicola S, Masiello MG, Proietti S, Coluccia P, Fabrizi G, Catizone A, et al. Nicotine increases colon cancer cell migration and invasion through epithelial to mesenchymal transition (EMT): COX-2 involvement. *J Cell Physiol.* 2018;233(6):4935-48.
65. Schaal C, Chellappan SP. Nicotine-mediated cell proliferation and tumor progression in smoking-related cancers. *Mol Cancer Res.* 2014;12(1):14-23.
66. Momi N, Ponnusamy MP, Kaur S, Rachagani S, Kunigal SS, Chellappan S, et al. Nicotine/cigarette smoke promotes metastasis of pancreatic cancer through $\alpha 7$ nAChR-mediated MUC4 upregulation. *Oncogene.* 2013;32(11):1384-95.
67. Nair S, Bora-Singhal N, Perumal D, Chellappan S. Nicotine-mediated invasion and migration of non-small cell lung carcinoma cells by modulating STMN3 and GSPT1 genes in an ID1-dependent manner. *Mol Cancer Res.* 2014;13(1):173.
68. Fararjeh A-FS, Tu S-H, Chen L-C, Cheng T-C, Liu Y-R, Chang H-L, et al. Long-term exposure to extremely low-dose of nicotine and 4-(methylnitrosamino)-1-(3-pyridyl)-1-butanone (NNK) induce non-malignant breast epithelial cell transformation through activation of the $\alpha 9$ -nicotinic acetylcholine receptor-mediated signaling pathway. *Environ Toxicol.* 2019;34(1):73-82.
69. Martínez-García E, Irigoyen M, González-Moreno O, Corrales L, Teijeira A, Salvo E, et al. Repetitive nicotine exposure leads to a more malignant and metastasis-prone phenotype of SCLC: a molecular insight into the

- importance of quitting smoking during treatment. *Toxicol Sci.* 2010;116(2):467-76.
70. Hanahan D, Weinberg RA. Hallmarks of cancer: the next generation. *Cell.* 2011;144(5):646-74.
 71. Fares J, Fares MY, Khachfe HH, Salhab HA, Fares Y. Molecular principles of metastasis: a hallmark of cancer revisited. *Signal Transduct Target Ther.* 2020;5(1):28.
 72. Hapach LA, Mosier JA, Wang W, Reinhart-King CA. Engineered models to parse apart the metastatic cascade. *NPJ Precis Oncol.* 2019;3(1):20.
 73. Brabletz T. To differentiate or not — routes towards metastasis. *Nat Rev Cancer.* 2012;12(6):425-36.
 74. Nieto MA, Huang Ruby Y-J, Jackson Rebecca A, Thiery Jean P. EMT: 2016. *Cell.* 2016;166(1):21-45.
 75. Kalluri R, Weinberg RA. The basics of epithelial-mesenchymal transition. *J Clin Invest.* 2009;119(6):1420-8.
 76. Pastushenko I, Blanpain C. EMT transition states during tumor progression and metastasis. *Trends Cell Biol.* 2019;29(3):212-26.
 77. Fischer KR, Durrans A, Lee S, Sheng J, Li F, Wong STC, et al. Epithelial-to-mesenchymal transition is not required for lung metastasis but contributes to chemoresistance. *Nature.* 2015;527(7579):472-6.
 78. Zheng X, Carstens JL, Kim J, Scheible M, Kaye J, Sugimoto H, et al. Epithelial-to-mesenchymal transition is dispensable for metastasis but induces chemoresistance in pancreatic cancer. *Nature.* 2015;527(7579):525-30.
 79. Shroff R, Schramm K, Jeschke V, Nemes P, Vertes A, Gershenzon J, et al. Quantification of plant surface metabolites by matrix-assisted laser desorption–ionization mass spectrometry imaging: glucosinolates on *Arabidopsis thaliana* leaves. *Plant J.* 2015;81(6):961-72.
 80. Dueñas ME, Klein AT, Alexander LE, Yandea-Nelson MD, Nikolau BJ,

- Lee YJ. High spatial resolution mass spectrometry imaging reveals the genetically programmed, developmental modification of the distribution of thylakoid membrane lipids among individual cells of maize leaf. *Plant J.* 2017;89(4):825-38.
81. Misiorek M, Sekuła J, Ruman T. Mass spectrometry imaging of low molecular weight compounds in garlic (*Allium sativum* L.) with gold nanoparticle enhanced target. *Phytochem Anal* 2017;28(6):479-86.
82. Aziz M, Sturtevant D, Winston J, Collakova E, Jelesko JG, Chapman KD. MALDI-MS imaging of urushiols in poison ivy stem. *Molecules.* 2017;22(5):711.
83. Dalisay DS, Kim KW, Lee C, Yang H, Rübel O, Bowen BP, et al. Dirigent protein-mediated lignan and cyanogenic glucoside formation in flax seed: integrated omics and MALDI mass spectrometry imaging. *J Nat Prod.* 2015;78(6):1231-42.
84. Woodfield HK, Sturtevant D, Borisjuk L, Munz E, Guschina IA, Chapman K, et al. Spatial and temporal mapping of key lipid species in *Brassica napus* seeds. *Plant Physiol.* 2017;173(4):1998-2009.
85. Klein AT, Yagnik GB, Hohenstein JD, Ji Z, Zi J, Reichert MD, et al. Investigation of the chemical interface in the soybean–aphid and rice–bacteria interactions using MALDI-mass spectrometry imaging. *Anal Chem.* 2015;87(10):5294-301.
86. Slazak B, Kapusta M, Strömstedt AA, Słomka A, Krychowiak M, Shariatgorji M, et al. How does the sweet violet (*Viola odorata* L.) fight pathogens and pests – cyclotides as a comprehensive plant host defense system. *Front Plant Sci.* 2018;9(1296).
87. Sirithunya P, Tragoonrung S, Vanavichit A, Pa-In N, Vongsaprom C, Toojinda T. Quantitative trait loci associated with leaf and neck blast resistance in recombinant inbred line population of rice (*Oryza sativa*). *DNA Res.* 2002;9(3):79-88.

88. Wang S, Uddin MI, Tanaka K, Yin L, Shi Z, Qi Y, et al. Maintenance of chloroplast structure and function by overexpression of the rice MONOGALACTOSYLDIACYLGLYCEROL SYNTHASE gene leads to enhanced salt tolerance in tobacco. *Plant Physiol.* 2014;165(3):1144-55.
89. Katifori E. The transport network of a leaf. *C R Phys.* 2018;19(4):244-52.
90. Becker L, Carré V, Poutaraud A, Merdinoglu D, Chaimbault P. MALDI mass spectrometry imaging for the simultaneous location of resveratrol, pterostilbene and viniferins on grapevine leaves. *Molecules.* 2014;19(7):10587-600.
91. Seneviratne HK, Dalisay DS, Kim K-W, Moinuddin SG, Yang H, Hartshorn CM, et al. Non-host disease resistance response in pea (*Pisum sativum*) pods: biochemical function of DRR206 and phytoalexin pathway localization. *Phytochemistry.* 2015;113:140-8.
92. Shahriar SA, Imtiaz AA, Hossain MB, Husna A, Eaty MNK. Rice blast disease. *Annu Res Rev Biol.* 2020:50-64.
93. Chen X, Jia Y, Wu BM. Evaluation of rice responses to the blast fungus *Magnaporthe oryzae* at different growth stages. *Plant Dis.* 2019;103(1):132-6.
94. Du Y, Qi Z, Yu J, Yu M, Cao H, Zhang R, et al. Effects of panicle development stage and temperature on rice panicle blast infection by *Magnaporthe oryzae* and visualization of its infection process. *Plant Pathol* 2021;70(6):1436-44.
95. Sallaud C, Lorieux M, Roumen E, Tharreau D, Berruyer R, Svestasrani P, et al. Identification of five new blast resistance genes in the highly blast-resistant rice variety IR64 using a QTL mapping strategy. *Theor Appl Genet.* 2003;106(5):794-803.
96. Yara A, Yaeno T, Hasegawa M, Seto H, Montillet J-L, Kusumi K, et al. Disease resistance against *Magnaporthe grisea* is enhanced in transgenic rice with suppression of ω -3 fatty acid desaturases. *Plant Cell Physiol.*

- 2007;48(9):1263-74.
97. Koga J, Ogawa N, Yamauchi T, Kikuchi M, Ogasawara N, Shimura M. Functional moiety for the antifungal activity of phytocassane E, a diterpene phytoalexin from rice. *Phytochemistry*. 1997;44(2):249-53.
 98. Koga J, Shimura M, Oshima K, Ogawa N, Yamauchi T, Ogasawara N. Phytocassanes A, B, C and D, novel diterpene phytoalexins from rice, *Oryza sativa* L. *Tetrahedron*. 1995;51(29):7907-18.
 99. Yajima A, Mori K. Synthesis and absolute configuration of (-)-phytocassane D, a diterpene phytoalexin isolated from the rice plant, *Oryza sativa*. *Eur J Org Chem*. 2000;2000(24):4079-91.
 100. Akatsuka T, Kodama O, Sekido H, Kono Y, Takeuchi S. Novel phytoalexins (oryzalexins A, B and C) isolated from rice blast leaves infected with *Pyricularia oryzae*. *Agric Biol Chem*. 1985;49(6):1689-701.
 101. Kato H, Kodama O, Akatsuka T. Oryzalexin E, A diterpene phytoalexin from UV-irradiated rice leaves. *Phytochemistry*. 1993;33(1):79-81.
 102. Kato H, Kodama O, Akatsuka T. Oryzalexin F, a diterpene phytoalexin from UV-irradiated rice leaves. *Phytochemistry*. 1994;36(2):299-301.
 103. Tamogani S, Mitani M, Kodama O, Akatsuka T. Oryzalexin S structure: a new stemarane-type rice plant phytoalexin and its biogenesis. *Tetrahedron*. 1993;49(10):2025-32.
 104. Cartwright DW, Langcake P, Pryce RJ, Leworthy DP, Ride JP. Isolation and characterization of two phytoalexins from rice as momilactones A and B. *Phytochemistry*. 1981;20(3):535-7.
 105. Kato T, Kabuto C, Sasaki N, Tsunagawa M, Aizawa H, Fujita K, et al. Momilactones, growth inhibitors from rice, *Oryza sativa* L. *Tetrahedron Lett*. 1973;14(39):3861-4.
 106. Dillon VM, Overton J, Grayer RJ, Harborne JB. Differences in phytoalexin response among rice cultivars of different resistance to blast. *Phytochemistry*. 1997;44(4):599-603.

107. Yarbrough WG, Slebos RJC, Liebler D. Proteomics: Clinical applications for head and neck squamous cell carcinoma. *Head Neck*. 2006;28(6):549-58.
108. Schubert OT, Röst HL, Collins BC, Rosenberger G, Aebersold R. Quantitative proteomics: challenges and opportunities in basic and applied research. *Nat Protoc*. 2017;12(7):1289-94.
109. Cifani P, Kentsis A. Towards comprehensive and quantitative proteomics for diagnosis and therapy of human disease. *Proteomics*. 2017;17(1-2):1600079.
110. Fang R, Elias DA, Monroe ME, Shen Y, McIntosh M, Wang P, et al. Differential label-free quantitative proteomic analysis of *Shewanella oneidensis* cultured under aerobic and suboxic conditions by accurate mass and time tag approach. *Mol Cell Proteomics*. 2006;5(4):714-25.
111. Gravett MG, Thomas A, Schneider KA, Reddy AP, Dasari S, Jacob T, et al. Proteomic analysis of cervical-vaginal fluid: identification of novel biomarkers for detection of intra-amniotic infection. *J Proteome Res*. 2007;6(1):89-96.
112. Le Bihan T, Goh T, Stewart II, Salter AM, Bukhman YV, Dharsee M, et al. Differential analysis of membrane proteins in mouse fore- and hindbrain using a label-free approach. *J Proteome Res*. 2006;5(10):2701-10.
113. Wienkoop S, Larrainzar E, Niemann M, Gonzalez EM, Lehmann U, Weckwerth W. Stable isotope-free quantitative shotgun proteomics combined with sample pattern recognition for rapid diagnostics. *J Sep Sci*. 2006;29(18):2793-801.
114. Bantscheff M, Schirle M, Sweetman G, Rick J, Kuster B. Quantitative mass spectrometry in proteomics: a critical review. *Anal Bioanal Chem*. 2007;389(4):1017-31.
115. Cheung CHY, Juan H-F. Quantitative proteomics in lung cancer. *J Biomed Sci*. 2017;24(1):37.

116. Wang M, You J, Bemis KG, Tegeler TJ, Brown DPG. Label-free mass spectrometry-based protein quantification technologies in proteomic analysis. *Brief Funct Genomics*. 2008;7(5):329-39.
117. Kuljittichanok D, Diskul-Na-Ayudthaya P, Weeraphan C, Chokchaichamnankit D, Chiablaem K, Lirdprapamongkol K, et al. Effect of *Derris scandens* extract on a human hepatocellular carcinoma cell line. *Oncol Lett*. 2018;16(2):1943-52.
118. Weeraphan C, Phongdara A, Chaiyawat P, Diskul-Na-Ayudthaya P, Chokchaichamnankit D, Verathamjamras C, et al. Phosphoproteome profiling of isogenic cancer cell-derived exosome reveals HSP90 as a potential marker for human cholangiocarcinoma. *Proteomics*. 2019;19(12):1800159.
119. Gao T, Zhou X-L, Liu S, Rao C-X, Shi W, Liu J-C. In vitro effects of nicotine on the non-small-cell lung cancer line A549. *J Pak Med Assoc*. 2016;66(4):368-72.
120. Sun H, Ma X. α 5-nAChR modulates nicotine-induced cell migration and invasion in A549 lung cancer cells. *Exp Toxicol Pathol*. 2015;67(9):477-82.
121. Yi WC, Pan CY, Shuenn CY, Yu CS, Hendrix MJC, Wu R, et al. Selection of invasive and metastatic subpopulations from a human lung adenocarcinoma cell line. *Am J Respir Cell Mol Biol*. 1997;17(3):353-60.
122. Amaro A, Angelini G, Mirisola V, Esposito AI, Reverberi D, Matis S, et al. A highly invasive subpopulation of MDA-MB-231 breast cancer cells shows accelerated growth, differential chemoresistance, features of apocrine tumors and reduced tumorigenicity in vivo. *Oncotarget*. 2016;7(42):68803-20.
123. Cheng CY, Yu CC. Enhancement of cancer stem-like and epithelial-mesenchymal transdifferentiation property in oral epithelial cells with long-term nicotine exposure: Reversal by targeting SNAIL. *Toxicol Appl Pharmacol*. 2013;266(3):459-69.

124. Martínez-García E, Irigoyen M, González-Moreno O, Corrales L, Teixeira A, Salvo E, et al. Repetitive nicotine exposure leads to a more malignant and metastasis-prone phenotype of SCLC: a molecular insight into the importance of quitting smoking during treatment. *Toxicol Sci.* 2010;116(2):467-76.
125. Mueller LN, Brusniak M-Y, Mani DR, Aebersold R. An assessment of software solutions for the analysis of mass spectrometry based quantitative proteomics data. *J Proteome Res.* 2008;7(1):51-61.
126. Välikangas T, Suomi T, Elo LL. A comprehensive evaluation of popular proteomics software workflows for label-free proteome quantification and imputation. *Brief Bioinform.* 2017;19(6):1344-55.
127. Chen JM, Fortunato M, Stevens RA, Barrett AJ. Activation of progelatinase A by mammalian legumain, a recently discovered cysteine proteinase. *Biol Chem.* 2001;382(5):777-84.
128. Dall E, Brandstetter H. Structure and function of legumain in health and disease. *Biochimie.* 2016;122:126-50.
129. Chen JM, Dando PM, Stevens RA, Fortunato M, Barrett AJ. Cloning and expression of mouse legumain, a lysosomal endopeptidase. *Biochem J.* 1998;335(1):111-7.
130. Morita Y, Araki H, Sugimoto T, Takeuchi K, Yamane T, Maeda T, et al. Legumain/asparaginyl endopeptidase controls extracellular matrix remodeling through the degradation of fibronectin in mouse renal proximal tubular cells. *FEBS Lett.* 2007;581(7):1417-24.
131. Gawenda J, Traub F, Lück HJ, Kreipe H, von Wasielewski R. Legumain expression as a prognostic factor in breast cancer patients. *Breast Cancer Res Treat.* 2007;102(1):1-6.
132. Liu C, Sun C, Huang H, Janda K, Edgington T. Overexpression of legumain in tumors is significant for invasion/metastasis and a candidate enzymatic target for prodrug therapy. *Cancer Res.* 2003;63(11):2957-64.

133. Murthy RV, Arberman G, Gao J, Roodman GD, Sun X-F. Legumain expression in relation to clinicopathologic and biological variables in colorectal cancer. *Clin Cancer Res.* 2005;11(6):2293-9.
134. Whitley D, Goldberg SP, Jordan WD. Heat shock proteins: A review of the molecular chaperones. *J Vasc Surg.* 1999;29(4):748-51.
135. Becker B, Multhoff G, Farkas B, Wild P-J, Landthaler M, Stolz W, et al. Induction of Hsp90 protein expression in malignant melanomas and melanoma metastases. *Exp Dermatol.* 2004;13(1):27-32.
136. Pan J, Jiang F, Zhou J, Wu D, Sheng Z, Li M. HSP90: a novel target gene of miRNA-628-3p in A549 cells. *Biomed Res Int.* 2018;2018:4149707.
137. Sidera K, Samiotaki M, Yfanti E, Panayotou G, Patsavoudi E. Involvement of cell surface HSP90 in cell migration reveals a novel role in the developing nervous system*. *J Biol Chem.* 2004;279(44):45379-88.
138. Wu Yp, Kita K, Suzuki N. Involvement of human heat shock protein 90 α in nicotine-induced apoptosis. *Int J Cancer.* 2002;100(1):37-42.
139. Ciocca DR, Calderwood SK. Heat shock proteins in cancer: diagnostic, prognostic, predictive, and treatment implications. *Cell Stress Chaperones.* 2005;10(2):86-103.
140. Jagadish N, Agarwal S, Gupta N, Fatima R, Devi S, Kumar V, et al. Heat shock protein 70-2 (HSP70-2) overexpression in breast cancer. *J Exp Clin Cancer Res.* 2016;35(1):150.
141. Wong HR, Menendez IY, Ryan MA, Denenberg AG, Wispé JR. Increased expression of heat shock protein-70 protects A549 cells against hyperoxia. *Am J Physiol.* 1998;275(4):L836-L41.
142. Singh A, Jain K, Ranjan R, Prasad D, Chauhan A, Singh S, et al. Protein profile of human lung epithelial cells (A549) revealing deviation in cytoskeleton proteins in response to zinc oxide nanoparticles exposure. *Def Life Sci J.* 2020;5:163-72.
143. Anbarasi K, Kathirvel G, Vani G, Jayaraman G, Shyamala Devi CS.

- Cigarette smoking induces heat shock protein 70 kDa expression and apoptosis in rat brain: modulation by bacoside A. *Neuroscience*. 2006;138(4):1127-35.
144. Xu S, Sankar S, Neamati N. Protein disulfide isomerase: a promising target for cancer therapy. *Drug Discov Today*. 2014;19(3):222-40.
145. Barra NG, Lisyansky M, Vanduzer TA, Raha S, Holloway AC, Hardy DB. Maternal nicotine exposure leads to decreased cardiac protein disulfide isomerase and impaired mitochondrial function in male rat offspring. *J Appl Toxicol*. 2017;37(12):1517-26.
146. Wong MK, Nicholson CJ, Holloway AC, Hardy DB. Maternal nicotine exposure leads to impaired disulfide bond formation and augmented endoplasmic reticulum stress in the rat placenta. *PLoS One*. 2015;10(3):e0122295.
147. Chen J, Doroudi M, Cheung J, Grozier AL, Schwartz Z, Boyan BD. Plasma membrane Pdia3 and VDR interact to elicit rapid responses to $1\alpha,25(\text{OH})_2\text{D}_3$. *Cell Signal*. 2013;25(12):2362-73.
148. Ye Q, Fu P, Dou J, Wang N. Downregulation of PDIA3 inhibits proliferation and invasion of human acute myeloid leukemia cells. *Oncotargets Ther*. 2018;11:2925-35.
149. Wang C, Zhu Y, Wu D, Wang Z, Xu X, Shi Y, et al. The role of PDIA3 in myogenesis during muscle regeneration. *Exp Mol Med*. 2020;52(1):105-17.
150. Coumans JV, Gau D, Poljak A, Wasinger V, Roy P, Moens PD. Profilin-1 overexpression in MDA-MB-231 breast cancer cells is associated with alterations in proteomics biomarkers of cell proliferation, survival, and motility as revealed by global proteomics analyses. *Omics*. 2014;18(12):778-91.
151. Ali M, Heyob K, Jacob NK, Rogers LK. Alternative expression and localization of profilin 1/VASPPs157 and cofilin 1/VASPPs239 regulates metastatic growth and is modified by DHA supplementation. *Mol Cancer*

Ther. 2016;15(9):2220-31.

152. Paulo JA, Urrutia R, Kadiyala V, Banks P, Conwell DL, Steen H. Cross-species analysis of nicotine-induced proteomic alterations in pancreatic cells. *Proteomics*. 2013;13(9):1499-512.





APPENDICES

จุฬาลงกรณ์มหาวิทยาลัย
CHULALONGKORN UNIVERSITY

APPENDIX A

MALDI-MS Images of Infected RD6 Rice Leaf Section

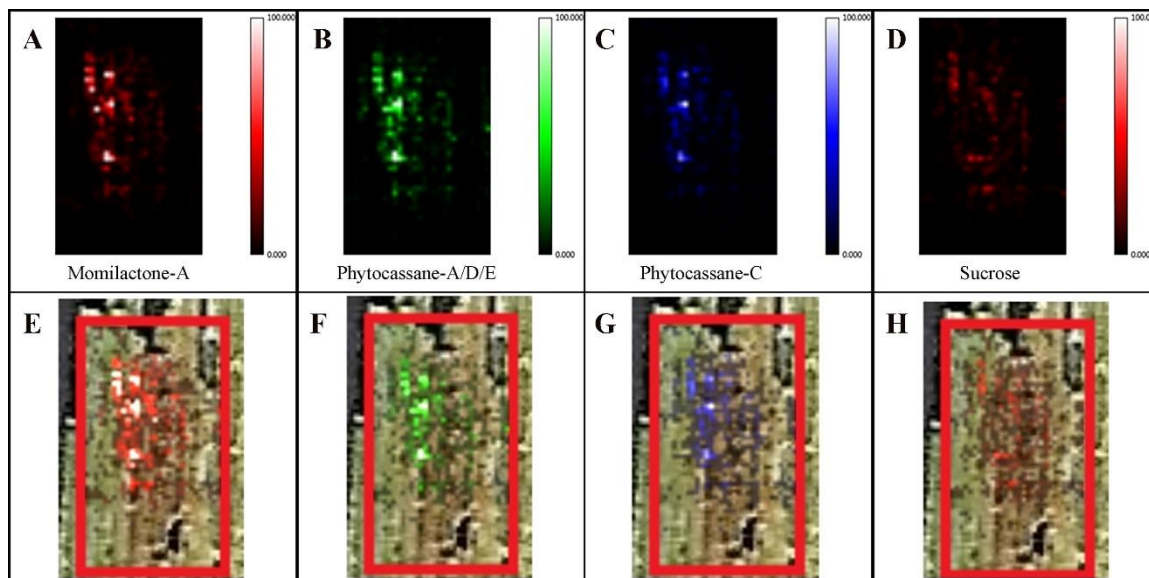


Figure A.1 MALDI-MS images of infected RD6 rice leaf section (2nd repeated experiment). (A) momilactone-A (m/z 353.24), (B) phytocassane-A, D, or E (m/z 355.24), (C) phytocassane-C (m/z 357.25), (D) sucrose (m/z 381.23) All compounds were detected as potassiated ions ($[M + K]^+$). The overlapping images between phytoalexins and infected leaf sections have been included to highlight that the phytoalexins were found at the infected areas only. (E) overlapping image of momilactone-A, (F) overlapping image of phytocassane-A, D, or E, (G) overlapping image of phytocassane-C, (H) overlapping image of sucrose.

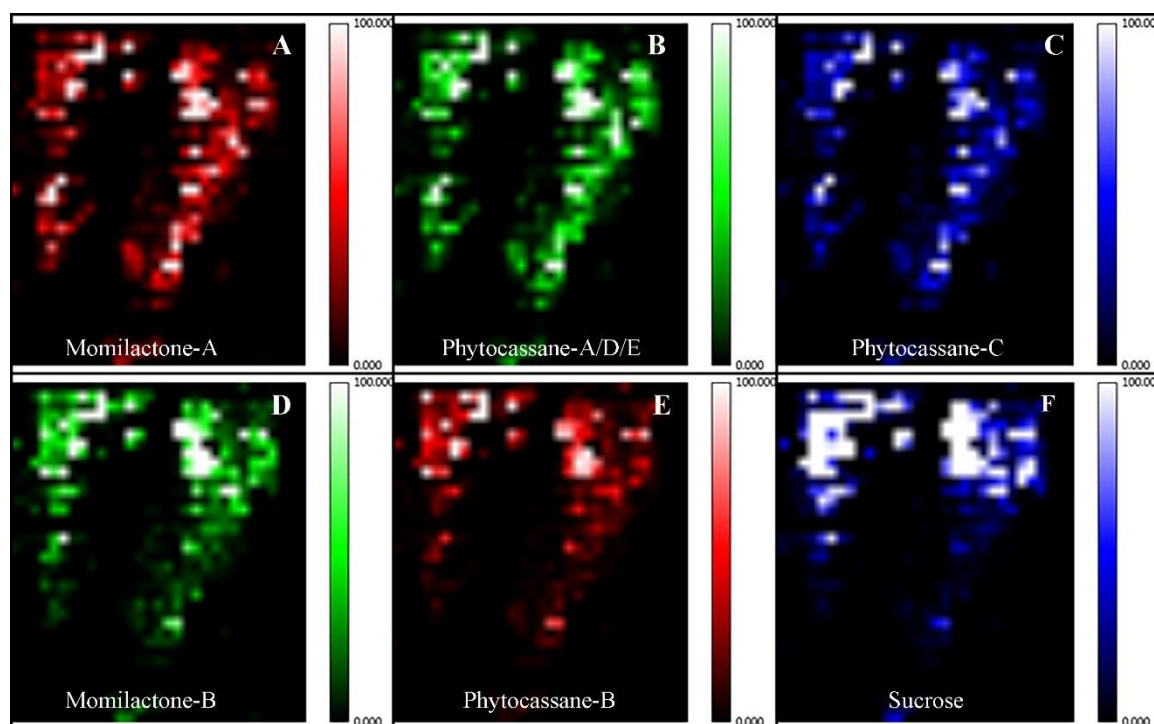


Figure A.2 MALDI-MS images of infected RD6 rice leaf section (3rd repeated experiment). (A) momilactone-A (m/z 353.41), (B) phytocassane-A, D, or E (m/z 355.41), (C) phytocassane-C (m/z 357.40), (D) momilactone-B (m/z 369.34), (E) phytocassane-B (m/z 373.33), (F) sucrose (m/z 381.35). All compounds were detected as potassiated ions ($[M + K]^+$).

APPENDIX B

MALDI Mass Spectra of Rice Leaf Extract

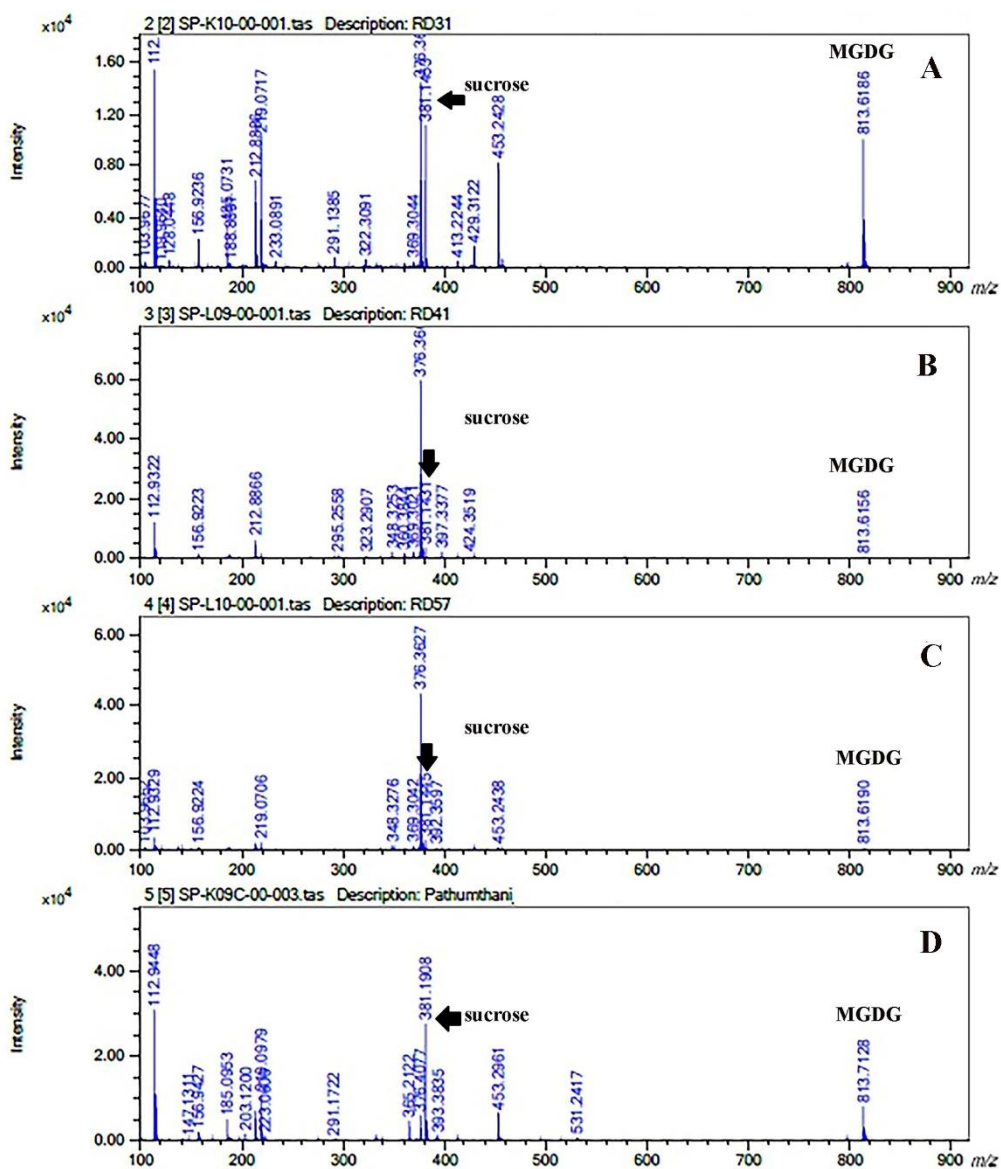


Figure B.1 MALDI mass spectra obtained from uninfected rice leaf extract. (A) Uninfected rice leaf extract of RD31. (B) Uninfected rice leaf extract of RD41. (C) Uninfected rice leaf extract of RD57. (D) Uninfected rice leaf extract of Pathumthani1.

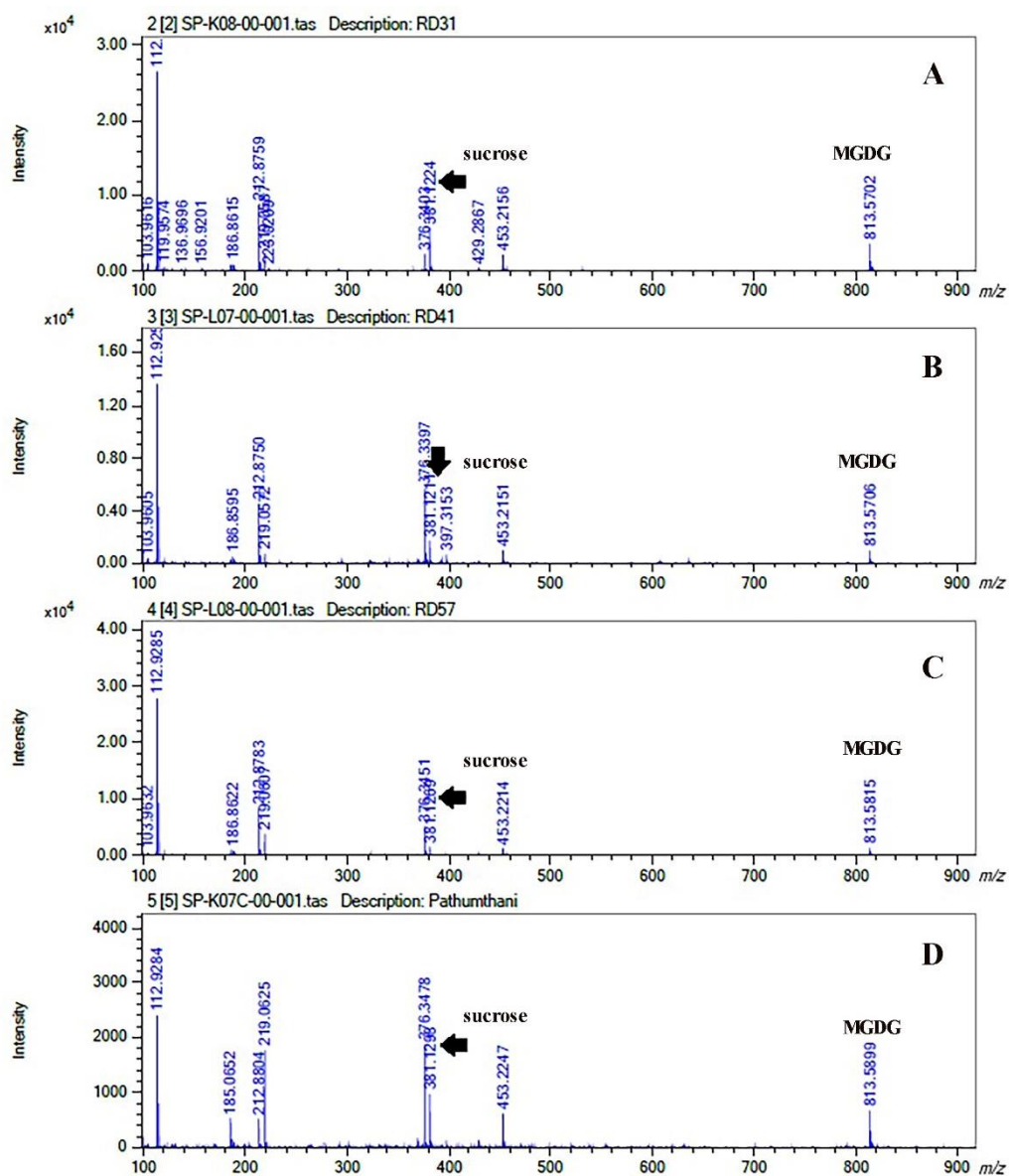


Figure B.2 MALDI mass spectra obtained from infected rice leaf extract. (A) Infected rice leaf extract of RD31. (B) Infected rice leaf extract of RD41. (C) Infected rice leaf extract of RD57. (D) Infected rice leaf extract of Pathumthani1.

APPENDIX C

Fungal Media Compositions from Chapter 3

1. Rice Flour Agar (RFA)

Rice flour	20	g
Yeast extract	2	g
Agar	15	g
Distilled water	1,000	ml

Mix the ingredients and boil to dissolve. Sterilization in an autoclave for 15 min at 121°C. Then aseptically transfer to Petri dishes.

2. Rice Potato Carrot Agar (RPCA)

Rice flour	20	g
Potato	20	g
Carrot	20	g
Agar	15	g
Distilled water	1,000	ml

Dice potato and carrot and boil them with rice flour in distilled water for 30 min. Filter through cheesecloth, saving effluent. Add agar and autoclave for 15 min at 121°C. Then aseptically transfer to Petri dishes.

3. Oat Meal Agar (OMA)

Rolled oats	40	g
Agar	15	g
Distilled water	1,000	ml

Boil oatmeal in distilled water for 30 min. Filter through cheesecloth, saving effluent, which is oatmeal infusion. Add agar and autoclave for 15 min at 121°C. Then aseptically transfer to Petri dishes.

4. Wheat Flour Agar (WFA)

Wheat flour	20	g
Yeast extract	2	g
Agar	15	g
Distilled water	1,000	ml

Mix the ingredients and boil to dissolve. Sterilization in an autoclave for 15 min at 121°C. Then aseptically transfer to Petri dishes.

5. Glutinous Rice Flour Agar (GRFA)

Glutinous rice flour agar	20	g
Yeast extract	2	g
Agar	15	g
Distilled water	1,000	ml

Mix the ingredients and boil to dissolve. Sterilization in an autoclave for 15 min at 121°C. Then aseptically transfer to Petri dishes.

6. Potato Dextrose Agar (PDA)

Potato	200	g
Dextrose	20	g
Agar	15	g
Distilled water	1,000	ml

To prepare potato infusion, boil 200 g sliced, unpeeled potatoes in 1,000 ml distilled water for 30 min. Filter through cheesecloth, saving effluent, which is potato infusion (or use commercial dehydrated form). Mix in other ingredients and boil to dissolve. Sterilization in an autoclave for 15 min at 121°C. Then aseptically transfer to Petri dishes.



APPENDIX D

Western Blot Analysis

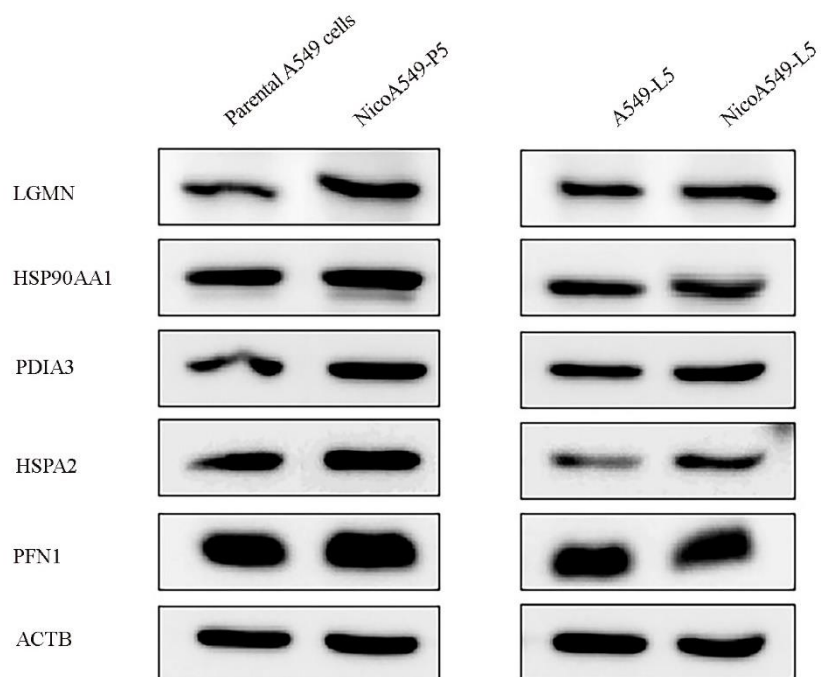


Figure D.1 Western blot showing the expression of selected proteins in untreated and nicotine treated A549 cells. (2nd repeated experiment).

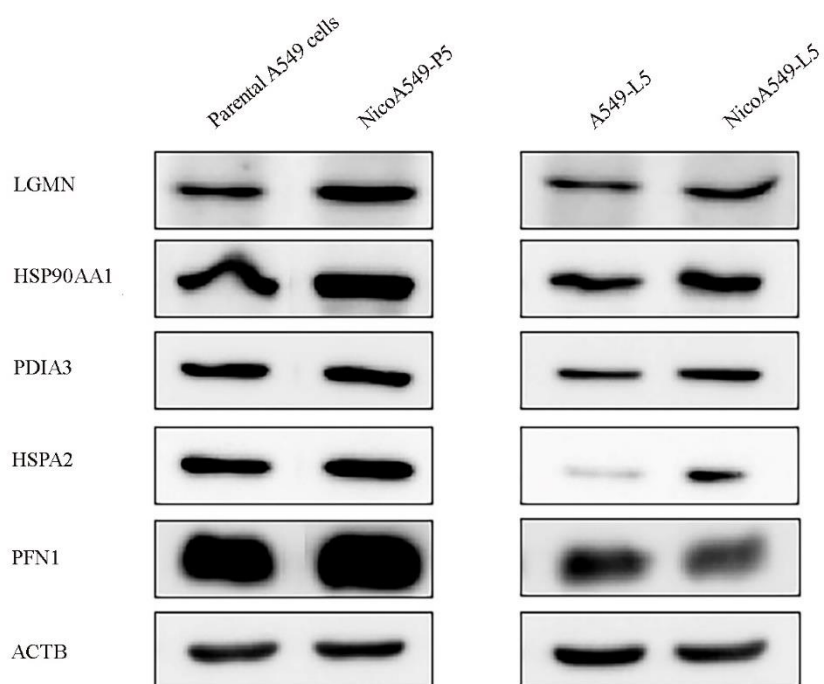


Figure D.2 Western blot showing the expression of selected proteins in untreated and nicotine treated A549 cells. (3rd repeated experiment).

APPENDIX E

Recipes of All Reagents from Chapter 4

1. 5X sample buffer (reducing condition-SDS-PAGE)

Milli Q water	3.80 ml
0.5 M Tris-HCl, pH 6.8	1.00 ml
Glycerol	0.80 ml
10% (w/v) SDS	1.60 ml
2-Mercaptoethanol	0.40 ml
0.05% (w/v) Bromophenol blue	0.40 ml

2. 30% (w/v) Acrylamide/ 0.8% N,N'-Methylenebisacrylamide

Acrylamide	30.00 g
N,N'-Methylenebisacrylamide	0.80 g

These chemicals were dissolved in Milli Q water and adjusted the final volume to 100 ml. After that, this solution was sterilized by filtration with Whatman Qualitative Grade 4 Filter paper and kept at 4 °C in the dark.

3. 10% (w/v) SDS

Ten grams of sodium dodecyl sulfate (SDS) was dissolved with gentle stirring and adjusted the final volume to 100 ml with Milli Q water.

4. 10% (w/v) APS

One gram of ammonium persulfate (APS) was dissolved in Milli Q water and adjusted the final volume to 10 ml.

5. 1.5 M Tris-HCl, pH 8.8

Tris	54.45 g
------	---------

This chemical was dissolved in 150 ml Milli Q water and adjusted pH to 8.8 using 6N HCl and made up the final volume to 300 ml with Milli Q water and stored at 4 °C.

6. 0.5 M Tris-HCl, pH 6.8

Tris 6.00 g

This chemical was dissolved in 60 ml Milli Q water and adjusted pH to 6.8 using 6N HCl and made up the final volume to 100 ml with Milli Q water and stored at 4 °C.

7. 10% Separating gel

Milli Q water	4.07 ml
1.5 M Tris-HCl, pH 8.8	2.50 ml
10% (w/v) SDS	0.10 ml
30% (w/v) Acrylamide/ 0.8% N,N'-methylenebisacrylamide	3.33 ml
10% (w/v) APS	50.00 µl
TEMED*	5.00 µl

*TEMED must be the last ingredient added

8. 4% Stacking gel

Milli Q water	3.05 ml
0.5 M Tris-HCl, pH 6.8	1.23 ml
10% (w/v) SDS	0.10 ml
30% (w/v) Acrylamide/ 0.8% N,N'-methylenebisacrylamide	0.65 ml
10% (w/v) APS	50.00 µl
TEMED*	5.00 µl

*TEMED must be the last ingredient added

9. 5X Running buffer

Glycine 72.00 g

Tris 15.00 g

SDS 5.00 g

Dissolved in Milli Q water and adjusted the volume to 1000 ml

10. 5X Blotting buffer

Glycine 72.00 g

Tris 15.00 g

Dissolved in Milli Q water and adjusted the volume to 1000 ml

11. 10X TBS, pH 7.6

Tris 24.20 g

NaCl 80.00 g

These chemicals were dissolved in Milli Q water, adjusted to pH 7.6 and made up the final volume to 1000 ml.

12. 1X TBST

10X TBS 100.00 ml

Tween 20 1.00 ml

Milli Q water 899.00 ml

13. 200 mM NH_4HCO_3

Ammonium bicarbonate (NH_4HCO_3) 0.7906 g

Milli Q water 50.00 ml

14. 100 mM DTT

Dithiothreitol (DTT)	1.54 mg
Milli Q water	100.00 μ l

15. 200 mM IAA

Iodoacetamide (IAA)	3.699 mg
Milli Q water	100.00 μ l

16. 0.1% TFA in Milli Q water

Trifluoroacetic acid (TFA)	10.00 μ l
Milli Q water	9.99 ml

17. 0.1% TFA in 50% ACN

Trifluoroacetic acid (TFA)	10.00 μ l
Acetonitrile (ACN)	5.00 ml
Milli Q water	4.99 ml

18. 0.1% TFA in 80% ACN

Trifluoroacetic acid (TFA)	10.00 μ l
Acetonitrile (ACN)	8.00 ml
Milli Q water	1.99 ml

19. Solution A (0.1% Formic acid in Milli Q water)

Formic acid	1.00 ml
Milli Q water	990.00 ml

20. Solution B (0.1% Formic acid in ACN)

Formic acid	1.00 ml
-------------	---------

Acetonitrile (ACN)

990.00 ml



จุฬาลงกรณ์มหาวิทยาลัย
CHULALONGKORN UNIVERSITY

VITA

NAME Sasikarn Komkleow

DATE OF BIRTH 24 February 1989

PLACE OF BIRTH Rayong

INSTITUTIONS ATTENDED Bachelor Degree of Science, Faculty of Science, Chulalongkorn University, 2011
Master Degree of Science, Faculty of Science, Chulalongkorn University, 2015

HOME ADDRESS 20/1522 The Trust Resident, Nonsi Road, Chongnonsi, Yannawa, Bangkok 10120

PUBLICATION

1. Maldi-mass Spectrometry Imaging for Phytoalexins Detection in RD6 Thai Rice (Applied Biochemistry and Microbiology, 2021, Volume 57, Issue 4, Page 533–541)
2. Global Analysis of Protein Expression in A549 Cells After Prolonged Nicotine Exposure by Using Label-free Quantification (Anticancer Research, 2021, Volume 41, Issue 8, Page 3833-3842)